

UNIVERSITY OF YAOUNDÉ I
UNIVERSITÉ DE YAOUNDÉ I



FACULTY OF SCIENCE
FACULTÉ DES SCIENCES

DEPARTMENT OF PHYSICS
DÉPARTEMENT DE PHYSIQUE

LABORATORY OF MODELLING AND SIMULATION IN
ENGINEERING, BIOMIMETICS AND PROTOTYPES
*LABORATOIRE DE MODÉLISATION ET SIMULATION EN
INGÉNIERIE, BIOMIMÉTISME ET PROTOTYPES*

**A model of artificial heart based on ferromagnetic mass
actuated by an electromagnet.**

Thesis

Submitted and defended for the award of
Doctorat/ PhD in Physics

Speciality: Mechanics and materials

Option: Mechanics

ABOBDA Théodore Lejuste

Registration Number: 02U077

DEA in Physics

WOAFO Paul

Professor

Year 2015

To the **Almighty God**, the Father of Beauties, the Beloved Son and the Holy One, always loving, living and labouring

Acknowledgements

This thesis is the fruit of the efforts of those who participated to its accomplishment. Therefore I would like to pay a tribute and thank :

- The **Almighty Father** for all his marvellous and over-abundant gifts, the always living **Lord Jesus** for his precious teachings, the **Holy Spirit** for his unspeakable power
- **Pr WOAFU Paul** for his urging follow-up during my research studies with this other work as fruit. May his professionalization efforts of our training be crowned with patience and collaboration
- **Pr KOFANE Timoléon Crépin** for his motivating teachings throughout my training in the University of Yaoundé I and for his collaborative support when I needed. May his efforts for the nation be transformed into economic development
- All the jury members not yet mentioned, **Pr ESSIMBI ZOBO Bernard**, **Pr ZEKENG Serges Sylvain**, **Pr FOTSIN Hilaire**, **Pr MOHAMADOU Alidou** for rendering this work with all their remarks.
- **Pr TCHAWOUA Clément** for the challenge he is by now, for most student in the Department of Physics. May his principles and rigour open to him new horizon and major prospects.
- All the teaching staff and personnel of the Department of Physics, Faculty of Science, Postgraduate School of Science, Technology and Geosciences, University of Yaoundé I, for their teachings and help since my first year in this institution
- **Pr TAKONGMO Samuel** of the Centre Hospitalier et Universitaire, Yaoundé, specialist in surgery, for its most precious contacts. Receive my gratitude
- **Dr GUELA-WAWO Yonta Edvine** of the Centre Médical de l’Hippodrome, Yaoundé, specialist in cardiology, for her appreciations, corrections and most valuable exchanges and advice. Thanks a lot.
- **Dr MBA Sébastien** of the General Hospital of Yaoundé, for his teaching on pacemakers and cardiac electrical activity. Thanks a lot.
- **Dr NANA Bonaventure** of the University of Bamenda, for the valuable exchanges and advices. Receive my gratitude
- **Dr NANA Nbandjo** of the University of Yaoundé I, for discreet follow-up, thank you
- **Dr MBOUSSI Aïssatou** of the University of Yaoundé I, for the warm welcome in the lab. Once more thank you

- **Dr TCHEUTCHOUA Omer, Dr KOL Guy, Dr TALLA Mbe**, receive my gratitude for your inspiring life experiences
- My elders in the lab, for your fruitful exchanges during my stay. One more time thank you **Dr TOGUE Fulbert, Dr NGUEUTEU Mbouna**
- My pairs, labmates and friends **Dr TAKOUGANG Kingni, Dr SIMO Hervé, NUBISSIE Achille, DJORWE Philippe, NANHA Armand, NOTUE Kadjie, TCHAWOU Tchuisseu, TALLA Alain, CHAMGOUE Cheague** and all the others, thank for your trust
- My friends, **Dr TOGUEU Alain, Dr ATOCK à Nwatchock, MAMBOU Luc, TANDJA Tchahatche, TOKO Donatien, NANTCHO Wandjou, ESENGUE Francis**, for the laborious moments at University
- My Family, my late father **SIMO TAGNE Norbert**, my mother **NONO marcelline**, sisters and brothers **SIMO Tagne Amélie, CIMOTAGNE Eric Martial**, late **MEBOUSIMOTAGNE Alida, KININSIMO Josiane, TANI Christian Brel** with their full love
- The families **TADJOMFAIN, SOUOP KAMTO, TEMI TEKAMDJO, TADO, TASUKAM, KAMOGNE Gabriel, TAFEN Maurice, SIMO Emmanuel, DJOUKAM Raphaël, TAGNET Victorien**, Pastor **NGNINTEDEM Félicité, SALE Hamidou**, Brother **EVAIN Marcel** and late Father **EVAIN Joseph**, for their unvaluable support
- Late **KAPCHE Florence**, the one who guided my first steps at school at 2 years old
- **KAMMOGNE FOM Martial, TAKOUTSING Eric** for their printing support and their unforgettable help
- My teachers of Ecole catholique St Jean-Baptiste de la Salle Foumban, former CES (Lycée) de Foumban, Lycée Bilingue Sultan Ibrahim NJOYA de Foumban for the fruit of their efforts that leads me here
- All my relatives, friends, uncles, aunts, nephews, nieces, brothers, sisters in Christ or not, of the Catholic Charismatic Renewal or not, those whose names have not been mentioned here, those reading this work for their active support and fruitful prayers.

Please, receive all of you moreover, my gratefulness for this achievement, your achievement; for you guide me unconditionally with love and I will respond also with unconditional and pure love.

Contents

Faculty List	i
Dedications	xv
Acknowledgements	xvii
Contents	xxii
List of Abbreviations	xxiii
List of Figures	xxvii
List of Tables	xxviii
Abstract	xxix
Résumé	xxx
General Introduction	1
I Literature Review	4
I-1- Introduction	5
I-2- Generalities on biological organs	5
I-2-1- Functional groups, systems and organs in the human body	5
I-2-2- Effects of organs failures and remedies	7
I-3- Generalities on artificial organs	9
I-3-1- Motivation of artificial organs	9
I-3-2- Artificial organs	9
I-3-3- Some technical, ethical, moral and religious issues related to artificial organs	11

I-3-4-	Common moral principle in artificial device	12
I-4-	Artificial heart	13
I-4-1-	Motivation of choice of the study of an artificial heart	13
I-4-2-	Anatomy and physiology of native heart	15
I-4-3-	Historical view of research on artificial heart	18
I-4-4-	Typical Profile of Patient in need of an total artificial heart and cardiac assist device	18
I-4-5-	Specifications of cardiac assist device and artificial heart	20
I-4-6-	Some approach carried out in artificial heart and cardiac assist de- vice research	21
I-5-	Approach of the cardiac assist device and total artificial heart	29
I-6-	Conclusion	30
II	Methodology	31
II-1-	Introduction	32
II-2-	Analytical Methods	32
II-2-1-	Principle of harmonic balance	32
II-2-2-	Principle of Cardano's Method	32
II-3-	Numerical methods	33
II-3-1-	Fourth-order Runge-Kutta method for first-order differential equation	33
II-3-2-	Fourth-order Runge-Kutta method for m-order differential equation	34
II-4-	Experimental procedure and devices	35
II-4-1-	Materials	35
II-4-2-	Declinations	35
II-5-	Conclusion	38
III	Results and discussions	40
III-1-	Introduction	41
III-2-	Basic cardiac assist device with ferromagnetic mass actuated by an elec- tromagnet with its servo-control	41
III-2-1-	Description of the device and mathematical model	41
III-2-2-	Dynamical behaviour of the device	46
III-3-	Optimized cardiac assist device	50

III-3-1-Heartbeat like induced dynamics: bursting dynamics	50
III-3-2-Description of fluid flow frequency servo control, mathematical model and dynamical behaviour	57
III-3-3-Description of fluid flow frequency and pull-in servo-control, math- ematical model and dynamical behaviour	62
III-3-4-Excitation by the Van der Pol oscillator	63
III-3-5-Excitation by the Hindmarsh-Rose oscillator	71
III-3-6-Analogical simulation of Van der Pol oscillator at low frequencies for pacemaking applications	77
III-3-7-Other applications of the device	82
III-4-Biventricular heart based on ferromagnetic masses actuated by an electro- magnet	82
III-4-1-Description of the device and mathematical model	82
III-4-2-Dynamical behaviour of the device	87
III-4-3-Dynamical behaviour of the device in the presence of square wave voltage	97
III-4-4-Other applications of the device	99
III-5-Conclusion	99
General Conclusion	100
List of Publications	111

List of Abbreviations

AC: Alternative Current
AHA: American Heart Association
BIVAD: Biventricular Assist Device
BTR: Bridge To Recovery
BTT: Bridge To Transplantation
CAD: Cardiac assist device
CVD(s): Cardiovascular Disease(s)
DC: Direct Current
DT: Destination Therapy
ECG: Electrocardiogram
FN: Fitzhugh-Nagumo
HH: Hodgking-Huxley
HR: Hindmarsh-Rose
LVAD: Left Ventricular Assist Device
NHLBI: National Heart, Lungs and Blood Institute
NODE: Nonlinear Ordinary Differential Equation
NYHA: New York Heart Association
ODE(s): Ordinary Differential Equation(s)
pH: Potential of Hydrogen
PS: Permanent Support
RK4: Fourth-Order Runge-Kutta
rpm: revolutions per minute
RVAD: Right Ventricular Assist Device
TAH: Total Artificial Heart
VDP: Van der Pol

List of Figures

1	Cardiovascular system	16
2	Internal heart and anterior view of exterior heart anatomy	17
3	Electrocardiogram	18
4	Decision Flow chart for different cardiac affections evolution	20
5	Systematic classification of short term and long term cardiac assist devices	22
6	Some material used.	35
7	Some electronics components used.	37
8	Some basic operations on signals.	37
9	Some electronic devices used.	38
10	Basic cardiac assist device.	42
11	Simplification of basic cardiac assist device.	44
12	Amplitude-response curve of the mechanical oscillator versus frequency in sinusoidal regime	47
13	Some phase diagrams of the electrical signal and mechanical displacement in sinusoidal regime	48
14	Amplitude-response curve of the mechanical oscillator versus voltage amplitude in sinusoidal regime	49
15	Variation of the amplitude of vibration obtained from the analytical derivation and the numerical simulation for small displacement	50
16	Nonlinear capacitor made of diodes, operational amplifier, resistor and capacitors.	51
17	Amplitude-response curve of the mechanical oscillator versus frequency in the bursting regime	53
18	Some time evolutions of the electrical signal and mechanical displacement with sinusoidal modulation of burstings	55

19	Some time evolutions of the electrical signal and mechanical displacement as the damping increases in the bursting regime	56
20	Setup of the fluid flow servo-control.	57
21	Time histories of the current and mechanical displacement under frequency servo-control at $f/f_p = 1.65 \times 10^{-2}$	59
22	Time histories of the mechanical displacement under frequency servo-control at $f/f_p = 5.00 \times 10^{-1}$	59
23	Time histories of the mechanical displacement under frequency servo-control at $f/f_p = 9.99 \times 10^{-1}$	60
24	Time histories of the current and mechanical displacement with random frequency change	61
25	Spectrums of sinusoidal input, derived rectangular signal, and mechanical displacement	61
26	Setup of the fluid flow and pull-in servo-control.	62
27	Amplitude response of the electrical and mechanical oscillator versus the applied voltage without and with control	64
28	Synoptic diagram of the electromechanical system made of a ferromagnetic mass fixed on a spring and subjected to an electromagnet powered by a VDP electronic oscillator.	64
29	Time histories of the mechanical part for different values of the VDP non-linearity coefficient	66
30	Time histories of the mechanical part for different values of the VDP oscillator pulsation	67
31	Time histories of the input signal, the response of the VDP oscillator and that of the mechanical part as the applied voltage frequency increases . . .	68
32	Time histories of the input signal, the response of the VDP oscillator and that of the mechanical part as the applied voltage amplitude increases . . .	69
33	Time histories of the input signal, the response of the VDP oscillator and that of the mechanical part as the applied voltage duty cycle increases . . .	70
34	Synoptic diagram of the electromechanical system made of a ferromagnetic mass fixed on a spring and subjected to an electromagnet under HR voltage excitation.	72
35	Time histories for different values of the applied DC current showing transition from bursting oscillations to spikes in both electrical oscillator and electromechanical system	74

36	Time histories for different amplitudes of the square wave excitation showing the remaining spiking form in both the HR oscillator and the electromechanical system	75
37	Time histories for different frequency values of square wave excitation showing the transition from driven distorted spikes to sinusoidal dynamics in the electromechanical system	76
38	Analogical Van der Pol oscillator.	77
39	Breadboard implementation of the analogical Van der Pol oscillator.	77
40	Low frequency signals of VDP oscillator and parameters sets.	79
41	Numerical signals of VDP oscillator and parameters sets.	80
42	Closest numerical signals of VDP oscillator and parameters sets.	80
43	VDP oscillator under various square wave excitation.	81
44	Isometric view of biventricular assist device (total artificial heart) model.	83
45	Simplification of BIVAD-TAH.	84
46	Variation of the amplitude of vibration in term of the frequency obtained from the analytical derivation and the numerical simulation for small displacement	90
47	Variation of the amplitude of vibration of the second mass in term of the stiffness coefficients ratio obtained from the analytical derivation and the numerical simulation for small displacement	90
48	Variation of the amplitude of vibration of the second mass in term of the masses ratio obtained from the analytical derivation and the numerical simulation for small displacement	91
49	Variation of the amplitude of vibration in term of the voltage amplitude obtained from the analytical derivation and the numerical simulation for small displacement	91
50	Amplitude-response curves of the mechanical oscillators versus the frequency under sinusoidal voltage	94
51	Amplitude-response curves of the mechanical oscillators versus voltage amplitude under sinusoidal voltage for different values of stiffness coefficients ratio	95
52	Amplitude-response curves of the mechanical oscillators versus voltage amplitude under sinusoidal voltage for different values of the masses ratio	96
53	Amplitude-response curves of the mechanical oscillators versus the stiffness coefficient ratio under sinusoidal voltage	97

54	Amplitude-response curves of the mechanical oscillators versus the stiffness coefficient ratio under sinusoidal voltage	97
55	Amplitude-response curves of the mechanical oscillators versus the frequency under a square wave voltage	98
56	Time histories and phase diagrams of the first mass for different values of frequency in the case of excitation by a square wave	99
57	Amplitude-response curves of the mechanical oscillators versus voltage amplitude under a square wave voltage	100

List of Tables

I	Sources of ethical conflict	13
II	NYHA classification of cardiac heart insufficiency	19
III	AHA classification of cardiac heart insufficiency	19
IV	Some characteristics and images of pneumatic pumps	23
V	Some characteristics and images of electrical pumps	24
VI	Some characteristics and images of centrifugal pumps	25
VII	Some characteristics and images of axial pump	26
VIII	Some characteristics and images of hydraulic pump	27

Abstract

In this work a preliminary study is performed in order to propose a new approach to tackle the increasing demand of heart transplant by the use of artificial heart. One solution is developed taking as basis a ferromagnetic blade fixed on a spring and subjected to an electromagnet under variable current. Two derivations of the device are done to obtain left ventricular assist device and biventricular assist device, known respectively in the literature as partial artificial heart and total artificial heart since the pumping function is performed mainly by the ventricles. As results, both devices exhibit subharmonic oscillations that can be used to pump blood and present an intrinsic instability; an efficient approach to control the instability is presented. Furthermore, the interest of the device is based on translation movement allowing the pumping function in all directions; blood flow frequency servo-control to adapt pumping function of the left ventricular assist device to body needs; unstationary flow induced by blood flow frequency servo-control and the possibility to obtain heartbeat like pumping function with induced bursting in the pump.

Keywords: Ferromagnetic mass; Electromagnet; Bursting oscillations; Pull-in; frequency servo-control; Artificial heart; Biventricular assist device; Left ventricular assist device.

Résumé

Dans ce travail, une nouvelle approche pour juguler la demande croissante de transplantation cardiaque par l'utilisation de cœur artificiel est proposée. Une solution est développée en prenant comme base une lame ferromagnétique fixée à un ressort et soumise à un électroaimant sous courant variable. Deux déclinaisons du dispositif sont faites pour obtenir une assistance du ventricule gauche et une double assistance des ventricules respectivement connus dans la littérature comme cœur artificiel partiel et cœur artificiel total, eu égard de la fonction de pompage principalement jouée par les ventricules. Comme résultats, les dispositifs montrent des oscillations sous-harmoniques qui peuvent être utilisées pour pomper du sang et présentent une instabilité intrinsèque; une approche efficace de contrôle de l'instabilité est présentée. De plus, l'intérêt du dispositif est basé sur le mouvement de translation permettant la fonction de pompage dans toutes les directions; l'asservissement à la fréquence cardiaque de l'assistance ventriculaire gauche pour adapter la fonction de pompage aux besoins de l'organisme; l'écoulement instationnaire induit par l'asservissement à la fréquence cardiaque et la possibilité d'obtenir un pompage semblable au battement du cœur.

Mots clés: Masse ferromagnétique; Électroaimant; oscillations de bouffées; Pull-in; asservissement de fréquence; cœur artificiel; Dispositif d'assistance biventriculaire; Dispositif d'assistance ventriculaire gauche.

General Introduction

Organs are parts of living organisms specialized in a particular biological function within the organism and made of different tissues. They are well described by their physiological and anatomical study. During their life, interactions with neighbouring organs, environment effects or genetic disorders can lead to failures in such a way that they should be replaced when they could not be treated. In this case the patient needs a new organ, therefore biological organ or artificial organ can be used.

Biological organs transplants are studied as the natural solution when facing a severe organ failure. Transplants are performed taking into account factors like age, diseases so that some patient can be excluded from the transplantation waiting list getting longer with only few relieved [1]. As they are also living structures, transplants are very sensitive and subjected to rejection in their new environment according to their origins. To face the increasing need for transplant, cross species transplant can be performed, sometimes with genetic modifications leading to transgenic bodies [1, 2].

Due to the high and increasing demand of same species transplants, researches on transgenic manipulation, coupled with technical, ethic, moral and religious issues, genetic incompatibilities between donor and receiver, side effects of complementary medication, organized crime associated with human organs traffic are taking more importance so that one consensus solution could be artificial organs [2-4].

As the research in artificial organs cover a wide range of organs, in this thesis we focus on artificial heart and cardiac assist device, following the fact that cardiovascular diseases are the main causes of death in the world [5, 6]. This choice is also done because it is another step of the global work on the cardiovascular system already started by the study of arterial endoprosthesis carried out in the team [7-9]. Indeed, as an artificial heart can be view as a mechanical pump, a lot has to be done to increase the beneficence of what has been done in artificial heart research [2, 3].

An artificial heart is a device that can pump blood throughout the body as biological heart can do. In the literature, due to the pumping action of the ventricles, the study of the dynamical behaviour of artificial heart is dominated by that of artificial ventricles so that artificial ventricle is called artificial heart, despite the fact that other parameters such as artificial valves need to be included. Therefore artificial heart in this thesis is equivalent to artificial ventricle. Research on artificial heart has been carried out since 1927 with Charles Lindbergh and Alexis Carel as precursors who developed the Heart-Lung machine [10] with many advances and some misfortunes. Studies on artificial heart have been done in the literature, following well defined and non exhaustive specifications [11]. Some of their major issues based on their types are infections, the size reducing patient mobility in case of external device such as pneumatic pump; the effects of blood

stagnation, thrombus, axis problems, gyroscopic effects in case of centrifugal rotative pumps; high speed, hemolysis, poor flow, increased wear, axis problems in case of axial rotative pumps [3]. Both pumps types have to be optimized to increase duty life, survival and life comfort especially adaptation to body needs.

We are interested by a preliminary study of a new artificial heart and related cardiac assist devices especially, to develop a model of artificial heart according to recognized specifications and optimization needs, taking into account the effects of natural or external pacing, nerves stimulation, followed by a theoretical study of the model, some experimental works and some prospects for a more beneficent artificial heart.

Considering the specifications of the NHLBI [10,11] and the limitation of the devices available by now [3], the major issues are to:

- Reduce thrombosis which are stationary clots in blood vessels, more observable with stationary or regular flow which are favourable to platelets deposits [12]
- Reduce hemolysis observable with high speed blood flow due to increased shear
- Allow the functioning in all orientations
- Allow the adaptation to body needs
- Reduce wear that reduce the lifetime and increase generated heat
- Increase device lifetime and beneficence
- Imitate at the best the natural heart.

In this sense, even much has been done in the research on artificial heart with recent breakthrough; we attempt to solve the following problems:

- **Find a new approach of artificial heart which allows to have a closer pumping function as the native heart, especially obtain a device characterized by a pulsatile flow, the ability to work in all directions, a reduced energy consumption, a reduced wear, the possibility to adapt the flow to body needs and possessing an extended duty life**
- **Use mathematical and numerical tools to access the behaviour of the device and analyse the influence of external factors on it**
- **Realize an example of device needed to achieve pumping adaptation to native pacemaker in case of CAD or artificial pacing and nerve control in case of TAH.**

So, the thesis is structured as follows:

- The first chapter of this research work focuses on the generalities on biological organs, general points on artificial organs, generalities on artificial heart and cardiac assist devices with the drawbacks observed in the available types
- Secondly, the tools and methods used for proposed devices analysis are presented in the second chapter
- Thirdly, our results are presented in chapter three. They are of three types: the proposition of monoventricular CAD and biventricular CAD with their modelling; the results from mathematical and numerical studies and then experimental realization. These results are presented in two main parts. In the first part, a CAD without and with servo-control to the body needs is proposed, followed by a mathematical modelling of its dynamics. The mathematical and numerical results are presented and discussed. Then a realization of an artificial electronic self-sustained power generator is done and the experimental results are shown. The second part of the results chapter is the proposition of a biventricular CAD, which is also modelled and the analytical and numerical results are presented.
- We end this thesis with a summary of the principal results after which perspectives for future investigations are given.

Chapter I

Literature Review

I-1- Introduction

Organs are recognizable by their functions and can be arranged in functional groups. As examples the lung is an organ of the respiratory system, the stomach an organ of the digestive system and both are parts of a functional group within the human body [12]. In order to contribute to the study of artificial organ, especially to the study of an artificial organ such as an artificial heart, we should pay attention on the different biological organs which can be replaced by an artificial device, on how artificial organ are built and on how artificial heart are implemented in the literature while noticing the challenge faced.

I-2- Generalities on biological organs

I-2-1- Functional groups, systems and organs in the human body

Biological bodies such as the human body can be subdivided in four functional groups to have a general view on how the human body functions. They are: the group of support, movement and protection systems; the group of integration and coordination systems; the group of the maintenance of the body; the group of reproduction and development [12].

I-2-1-1- The group of support, movement and protection systems

The group of support, movement and protection systems is a group of organs involved in the:

- Integumentary system with the skin and accessory structures of the skin such as the hair, nails, sweat, sebaceous, mammary glands; involved in underlying tissue protection, preventing infection, water loss, temperature shocks; communication through sense and chemical with the environment
- Skeletal system consisting of bones, joints along with the ligaments and cartilages observed at joints. This system is engaged in standing up position support, protecting soft body parts, producing blood cells, storing minerals and fat
- Muscular system consisting of the smooth muscles, cardiac muscles and skeletal muscles. This system is important for gesture, facial communication also to maintain posture and produce heat.

I-2-1-2- The group of integration and coordination systems

The group of integration and coordination systems is formed with organs involved in the command of the body, information about neighbouring environment and communication among organs. Within this group ones have:

- The nervous system made of the central nervous system including the brain, the spinal cord and the peripheral nervous system divided into the afferent system (sensory) and efferent system (motor)
- The sensory system where we have sensory receptors made of proprioceptors, cutaneous receptors, pain receptors, with the sense of taste, smell, vision, hearing and equilibrium
- The endocrine system with endocrine glands such as the hypothalamus and pituitary gland; thyroid and parathyroid glands; testes and ovaries; pineal gland and hormones of other tissues such as the heart that produces atrial natriuretic hormone; adrenal glands, pancreas, thymus gland, the kidney producing the erythropoietin hormone, adipose tissue producing leptin, growth factors, prostaglandins and pheromones.

I-2-1-3- The group of systems of the maintenance of the body

The maintenance of the body is all about keeping the body in a good state, thus it contains:

- The blood composed of the plasma, red blood cells, white blood cells, platelets; acting as a mean of communication between tissues, transportation of nutrient and oxygen to the cells, carrying waste molecules to be excreted from the body, defence against external agents, regulation of heat and body pH
- The cardiovascular system with the heart pumping blood, blood vessels such as arteries, arterioles, capillaries, veins and venules carrying blood throughout the body
- The lymphatic system and body defences with lymphatic vessels, lymphatic organs such as the red bone marrow, thymus gland, spleen, lymph nodes, lymphatic nodules protecting the body from diseases
- The respiratory system possessing organs like the lungs oxygenating the blood and eliminating Carbon dioxide from the blood, the nose, pharynx, larynx, trachea, bronchial tree taking air to and from the lungs
- The digestive system made of the mouth, pharynx, oesophagus, stomach, small intestine, large intestine, pancreas, liver and gallbladder. This system receives and digests foods into nutrients which will be used by cells
- The urinary system and excretion with organs like the kidney, ureters, urinary bladder and urethra that rid the body from waste and help to control fluid and chemical content level in the blood

I-2-1-4- The group of reproduction and development with the reproductive system

This group is formed with organs involved in the perpetuation of the species through sex cells production and subdivided in two according to the gender:

- Male possesses testes, male internal accessory organs such as epididymides, vas deferens, seminal vesicles, prostate, Cowper glands and male external genital, the penis involved in sperm production, transport and delivery
- Female possesses ovaries, female internal accessory organs such as uterine tubes, uterus, cervix, vagina and female external genital, the vulva involved in eggs production, sperm reception, transport of menstrual fluid to the exterior, development of fertilized eggs and delivery. Moreover female breast is involved in lactation.

The complexity of biological bodies and their interaction with the environment can lead to injury, failure of an organ, genetic disorders at different level of seriousness and different effects on the whole body.

I-2-2- Effects of organs failures and remedies

Organ failure, injury or disorder leads to a single disease or to multiple and simultaneous diseases. According to the level of seriousness, imminent death, chronic disease, acute disease can be observed.

I-2-2-1- Different levels of diseases and consequences

An acute disease is a disease with either or both rapid onset and short course that is often less than one month clinical course. Examples of acute diseases are appendicitis and pneumonia [13].

Chronic disease is the opposite of acute disease. Its characteristic is that the course of the disease lasts for more than three months with slow progression. Some chronic diseases observed are heart disease, cancer, stroke, chronic respiratory diseases and diabetes. According to the World Health Organization chronic diseases are the leading cause of mortality in the world [13]. Due to the long term characteristic of chronic diseases, their treatment is very expensive; their complications can lead to the upset of multiple chronic diseases. Premature deaths observed during chronic disease appear mostly in low-and middle-income countries.

I-2-2-2- Organs failure remedies

During the life of a biological system, organs failures can be observed. To treat or relieve the inconvenience coming with both acute and chronic diseases, medication, physical and supportive therapies, surgery can be proposed to the patient.

Medication is concerned by the use of drugs to cure and / or ameliorate the symptoms of a disease.

The aim of physical and supportive therapies is to improve the quality of life and independence of the patient.

When classic remedies such as medication, physical and supportive therapies failed to give the needed quality of life, invasive treatment such as surgery is used and transplant often used in case of end-stage organ failure (when the organ reconstruction is impossible) to replace the affected or destroyed organ.

I-2-2-3- Types of transplant

In case of end-stage organ failure, the transplant is the effective therapy. A transplant is an organ or tissue moved from one body to another. Typically there are three types of transplant or organ replacement according to the origin of the substitution organ [2]:

- Autotransplantation which is the replacement of a tissue of the patient with his own surplus and/or regenerated tissue. It is often considered as the " gold standard in surgery ", but it is limited in availability and can deteriorate with time due to the difference in their physiological load and/ or biological environment in the transplant site
- Allotransplantation which is organ replacement from a donor to a recipient from the same species. This type is limited by the supply, the cost and the lifetime immunosuppression drugs having side effects such as cancer, renal insufficiency. A subset of allographic transplant is the isographic transplant; it is when the recipient and donor are identical twins. In this subset the observed rejection by the immune system due to genetic difference is reduced, but the occurrence of identical twins is rare
- Xenotransplantation that can be defined as an organ replacement from a donor to a recipient of different species. In this type of transplant, genetic difference is greater and there is an increased genetic concerns such as transgenic species

The replacement of an organ by a device, machine or material which is not biological is more referred as an implant or prosthesis. An implant is a device inserted surgically in the body while prosthesis is a device used inside the body to replace, repair or augment a diseased, damaged or missing part. Hence the terminology prosthesis insists on the therapeutic use. Implant and prosthesis are often used as synonyms [2].

I-3- Generalities on artificial organs

An artificial organ is a device designed to imitate the biological functions of a natural organ. Artificial organs are developed in order to give a solution to surgery organ needs with reduced technical, moral, ethical, religious objections.

I-3-1- Motivation of artificial organs

Artificial organs are investigated for many purposes such as to:

- Give a response to the fast growing need for a transplant with reduced donors
- Give the opportunity to patient not meeting transplant criteria to receive a substitute despite their age or diseases
- Prevent imminent death while waiting for a biological transplant
- Help native organ recovery
- Offer aesthetic restoration after accident
- Improve patient ability to interact socially and to self care
- Tackle the immune response of the body as artificial transplant do not elicit immune response from the host as they do not contain foreign proteins
- Avoid transgenic species
- Give an end to human organ trafficking associated to transnational organized crime rising in third world countries.

I-3-2- Artificial organs

Some researches have been carried out or are going on artificial organs. There are some common points on different types of artificial organs

I-3-2-1- Common points of artificial organs

A common characteristic of artificial organs is that they cannot self-repair after an injury or replace all the biological functions of the natural organ. Artificial organs as they are intended to be implanted within the body should be [2]:

- Biocompatible, the artificial organ in contact with body tissues should not induced rejection
- Stable in the biological environment (no corrosion, reduce wear, reduce fatigue)
- Of high beneficence (achieve $> 85 - 95\%$ success at use over 10 – 20 years).

I-3-2-2- Examples of artificial organs and assist devices

Throughout years many artificial organs have been developed by researchers, engineers and physicians as their developments need multidisciplinary competences. By now the more studied artificial organs [1, 2] in the literature are:

- The dialysis machine which is the intended artificial substitute of a kidney, invented by Kolff in the 1940s. Recent development by David Humes leads to a clinical trial on a bio-artificial kidney, which combine haemo-filtration and a chamber with billion of renal proximal tubule cells
- The artificial heart. The first truly artificial heart was the Abioco^r implanted in 2001. Previous generation were intended not to last more than 5 years with wires or tubes passing through the skin
- Lung assist device, which is a gas exchange machine imitating only part of the various and too intricate functions of lungs cells, used as a short term support while waiting lungs recovery
- In the liver machine the only function implemented among thousand is the blood detoxification through plasmapheresis which is similar to dialysis and cryofiltration. By now, the only way to replace the liver is to use tissue-engineered constructs; alternatively stem cells can be used as they are injected in the damaged liver for regeneration
- Some prototypes of artificial pancreas are under development: a first approach of device containing as basic function glucose sensing, information treatment and insulin delivery by a pump through the skin, by now they are not fully implantable; the second approach is an artificial hybrid pancreas device using live pancreas cells protected from body's natural immune response to secrete insulin in response to changing glucose level

- Artificial skin bandages such as clear oxygen-permeable polyurethane film, silicon rubber-nylon compound coated with collagen extract. Sheets of skin can be grown by tissue engineering to supply to artificial skin bandages or to extend the limits of the two-part artificial skin made from polysaccharide glycosaminoglycan and collagen technique
- Artificial ear is designed according to the affected region of the natural ear. Conductive and sensorineural deafnesses can be cured respectively by Bioglass® or HAPEX® prosthesis and cochlear implant
- The eventuality of an artificial eye is under consideration based on two silicon microchips, one providing solar power the other processing the image taken by a camera to send electric pulse to the retina's receptor cells that forward the signal to the brain
- Bionic noses, which by now are intended just for machines for quality assurance. They are based on odor absorbing materials such as fatty material, protein and carbohydrates (found in the olfactory epithelium) coating pairs of thermistors. After a vacuum pump pulls in air at the sniffing end, the coated thermistor sends a signal in response to the condensation on the odour-adsorbing material and to the following temperature increase an electronic signal is delivered to the computer for processing
- Electronic larynxes such as the Servox Inton are used. They contain a vibrating electronic sound source activated by a push-button in contact with the neck. In perspective devices may have electrodes implanted on the throat to record signals preceding speech production that will be sent to a minicomputer for analysis and voice production
- Artificial Sphincter to relieve faecal and urinary incontinence.

I-3-3- Some technical, ethical, moral and religious issues related to artificial organs

I-3-3-1- Technical issues

Technical challenges in artificial organs research are to reduce implant rejection by the body, provide stable implant while being surrounded by a living and dynamics environment, be of high beneficence, emulate all the functions of the natural organ, respond to body needs with adequate adaption to events, reduce human errors in implant fabrication [2].

I-3-3-2- Ethical issues

Ethical problems come from the conflict of uncertainties, making the relative value of alternative medical treatments more and more difficult to choose. The big ethical questions are: which problem? Which solution? As many treatment alternatives are available with different risks, costs, benefits, false expectations of "miracle cure", different histories of patient access to treatment, lobbies of firms, all of them add more uncertainties, ethical and moral dilemmas for appropriate solution choice for each patient's problem [2].

I-3-3-3- Moral issues

In the case of artificial organs, as our technology-based society created infinite desires with only finite resources, the big questions are who should benefit in priority of the available treatment? How to achieve the balance between the quantity of life and the quality of life? [2] Proposed treatment should be capitalist profit based or socialist profit based?

I-3-3-4- Religious issues

Religious are more concern about: the sacred character or not of the life under all its forms; irresponsibility coming from excessive trust in science and technology to provide all the solution to daily life problems; being enslaved by technology; false expectations sustained by greed; also by deceit, internal pain.

I-3-4- Common moral principle in artificial device

Philosophers agree on three general principles that should help in transplant or implant process, they are the principle of autonomy, beneficence and justice [2].

The principle of autonomy assumes that individual possess an intrinsic value and have the right to choose their own destiny. It is considered as the highest principle during transplant or implant.

The principle of beneficence says that it is morally right to aid, or to prevent harm to another. This principle implicates in the case of transplant or implant high standards with 85 to 95 % of success over 10-20 years.

The principle of justice: it requires that like cases should be treated alike. However it does not state how to determine equality. As individual are different, results can be different even if the treatment is the same and the difference in results can be perceived

as unjust. This wrong perception is exalted by the facts that human by nature wants the same thing as others, that technologies amplifies the problems with escalation in healthcare cost and that inherent greed promotes novelty and images rather than high beneficence, keeping thus unsolved both long term beneficence and reliability problems.

There are some sources of ethical conflict that can be summarized in Table 1 [2].

Table I: Sources of ethical conflict [2].

Sources of ethical conflict
Perception that the principle of justice has been violated.
Unjustified expectations of equal consequences of an act instead of equal performance of an act.
Emphasis that technology provides certainty.
Failure to understand that all technological solutions have some risks. A risk-free life is impossible.
Greed feeds on technology and conflict.
Legal system that fails to recognize that all individuals are different.

One should note that the all technology society in which we are living, can give birth to devices that could be remote controlled, so the eventuality to switch off intentionally an organ need to be prohibited and firmly controlled to avoid remote murders, this can be resumed as the principle of security.

I-4- Artificial heart

I-4-1- Motivation of choice of the study of an artificial heart

As one of the major conclusions of the report of Ref [14] in 2010, chronic diseases contribute mostly on the global burden of diseases worldwide, with the largest contribution coming from cardiovascular diseases. In this sense in 2008, 17.3 million died due to CVDs, representing 30% of global deaths and it is projected that by 2030 there will be 23.6 million of deaths due to CVDs [5]. Hence CVDs stand as the first cause of death in the world and a major public health concern, and will remain thus if no adequate action is taken. As low and middle income countries pay the highest tribute to CVDs, with over 80% of the death attribute to CVDs in the world in 2008; As there is an equal prevalence among men and women [5] and that the trends observed show that CVDs death rate is increasing

in most low and middle income countries while they are declining in most high income countries, adequate actions should be taken in low and middle countries and in such area as Africa, especially in Cameroon.

Some actions taken to tackle most of CVDs are a healthier diet, physical activity, avoidance of tobacco [14]. In case of complications, medication, surgery and organ replacement can be performed, but when the affection is severe the only remaining alternative is surgery.

In Africa, the main CVD is hypertension with 25% prevalence among the population of more than 18 years. The complications are renal failure with 20-69% prevalence, cerebral stroke 24-50% and heart problems 16-34% according to medical series [6, 15].

In Cameroon, hypertension prevalence is about 25.6% for men and 23.1% for women [16]. As a result of a retrospective study in 1995 in Cameroon based on 312 adult patients with CVDs, average age 44 years, revealed high blood pressure (38.5%), rheumatic valvular heart diseases (25.6%), cardiomyopathies (22.5%), and other cardiovascular diseases (13.5%). Rheumatic valvulopathies were predominant among the age group 20 to 39 years, hypertension was predominant from the age of 40 years, and cardiomyopathies were observed in the age range 20 to 60 years [17, 18].

A Cameroonian study between 1992 and 1997 ranked coronary artery disease eighth among the CVDs registered with a prevalence of 1.53% (2.42% in males and 0.45% in females). Myocardial infarction was the most frequent clinical form of CAD observed (43%), followed by angina pectoris (23%), unstable angina (20%), and other forms of ischemic heart disease (13%). The cardiovascular risk factors were obesity (80%), hypertension (60 %), dyslipidemia (43%), smoking (36%), diabetes/hyperglycemia (26%), and hyperuricemia (20%). 76 % of the patients had at least three cardiovascular risk factors [17–19].

According to the Cameroonian Society of Cardiology in 2010 there were only 31 specialists in cardiovascular medicine for 18 million patients in charge with invasive cardiology still limited to cardiac stimulation in Yaoundé and infantile cardiac surgery at the Shisong Sisters hospital. Although there exist similar projects of cardiac surgery at the General Hospital of Yaoundé and at the General Hospital of Douala, the one of Douala is the most advanced. Furthermore in Yaoundé, there is two cardiology centres dealing with medical treatment of cardiac pathologies: the Centre Médical de l'Hippodrome and the Centre Cardiologique de Tam-Tam. Adults who need cardiac surgery are whether transferred in European hospitals or operated in the framework of humanitarian missions of cardiac surgery supported by the government [16].

As some work have been already done in the sense of reflectionless arterial endoprosthesis [7–9], this thesis focuses on an artificial heart to continue the team work carried on the cardiovascular system and to give some solution elements to the still open problem of cardiovascular disease in the world especially in Cameroon.

I-4-2- Anatomy and physiology of native heart

The heart is located at the upper left side of the body in the thoracic cavity, between the lungs. It is cone-shaped, hollow, and muscular, approximately at the size of a fist clasped with the other hand, 105 mm of width, 98 mm of height and 300 to 350 g of weight [12].

This muscle is made of two ventricles ejecting blood and two atria holding and filling the ventricles. The left heart is formed by the left ventricle and the left atrium: it pumps blood in the systemic circulation. The right heart on the other side is made of the right ventricle and the right atrium: it pumps blood in the pulmonary circulation.

The blood enters the left heart by the superior vena cava and the inferior vena cava and leaves it by the pulmonary artery. As the blood enters the lungs, it is purified with the removal of CO₂ and intake of O₂. After leaving the lung the blood enters the left heart by the pulmonary vein and leaves it by the aorta. Coronary arteries are the first branches of the aorta, they nourish the heart itself with purify blood. After usage of the purify blood by cardiac cells, cardiac capillaries collect the blood and join to form the cardiac veins. Cardiac veins through coronary sinus enter the right atrium.

The heart works during 1/3 of its cycle (systole) and rest during 2/3 of its cycle (diastole). It is also an endocrine gland that produces the atrial natriuretic peptide and pumps under the regulation of sympathetic and parasympathetic nerves and hormones.

Internally, the four hollow chambers of the heart are separated. The left heart is separated from the right heart by the septum. The atria are isolated by the interatrial septum while the ventricles are separated by the interventricular septum. Heart valves prevent blood circulation from backflow. Between the left atrium and the left ventricle there is the mitral or bicuspid valve while at the other side between the right atrium and the right ventricle there is the tricuspid valve. Through the pulmonary semilunar valve blood enters the pulmonary trunk while through the aortic semilunar valve blood enters into the aorta.

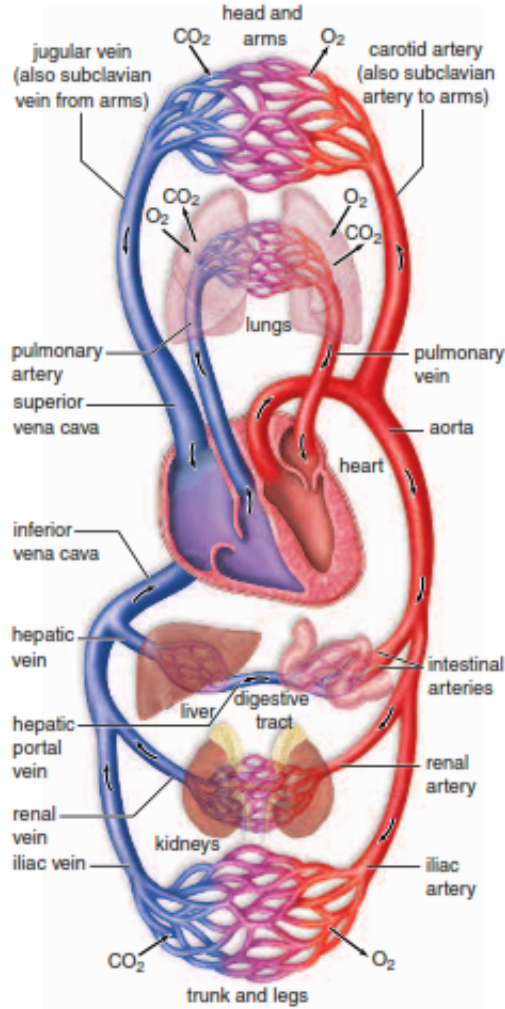
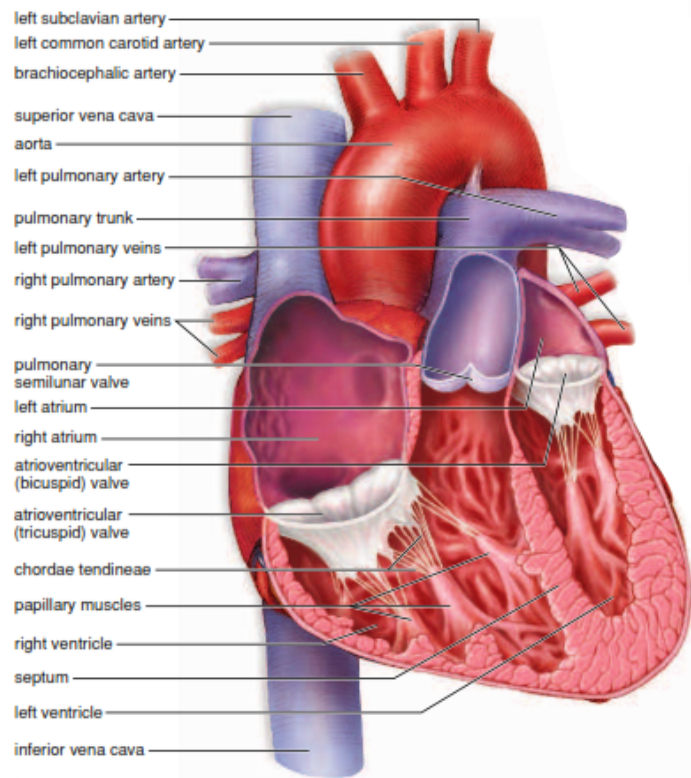


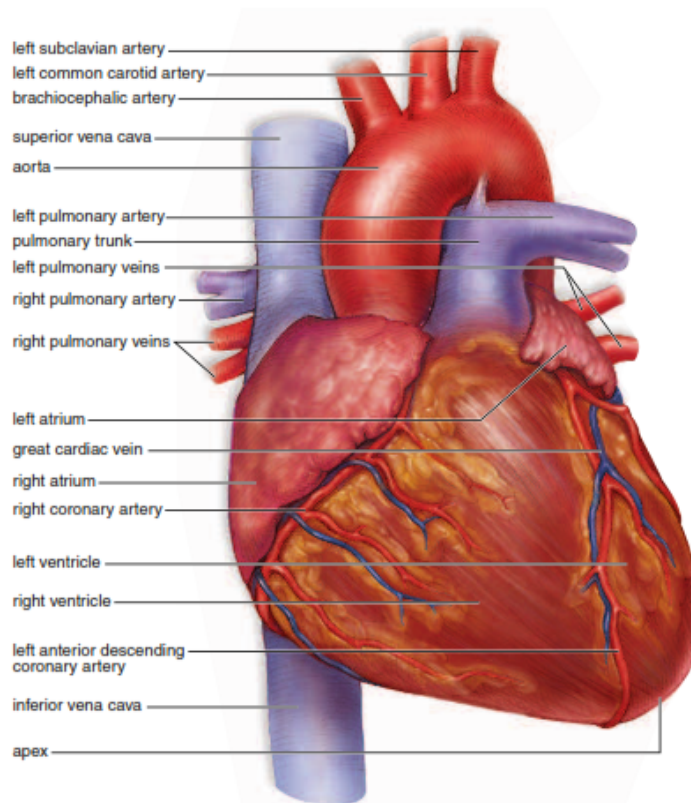
Figure 1: Cardiovascular system [12].

The cardiac muscle, like any other muscle during its contraction is subjected to electrolyte changes. Moreover the myocardium is endowed of self-sustained electrical activity. The graph that records this activity is called the electrocardiogram (ECG). An ECG is made of several waves: the P wave reproducing the atria depolarization when an impulse coming from the sino-atria node propagate throughout the atria; the QRS complex showing the ventricles depolarization after the excitation of Purkinje fibers; the T wave corresponding to ventricles repolarization. ECG is used to detect among others, irregular heartbeat. Heartbeats rate fewer than 60 beats per minute are referred as bradycardia while those greater than 100 beats per minute referred as tachycardia [12].

Although in the rhythm of the electrical activity of native heart there is variability, with is chaos observed [20,21], we focus on periodic behaviour of the native heart.

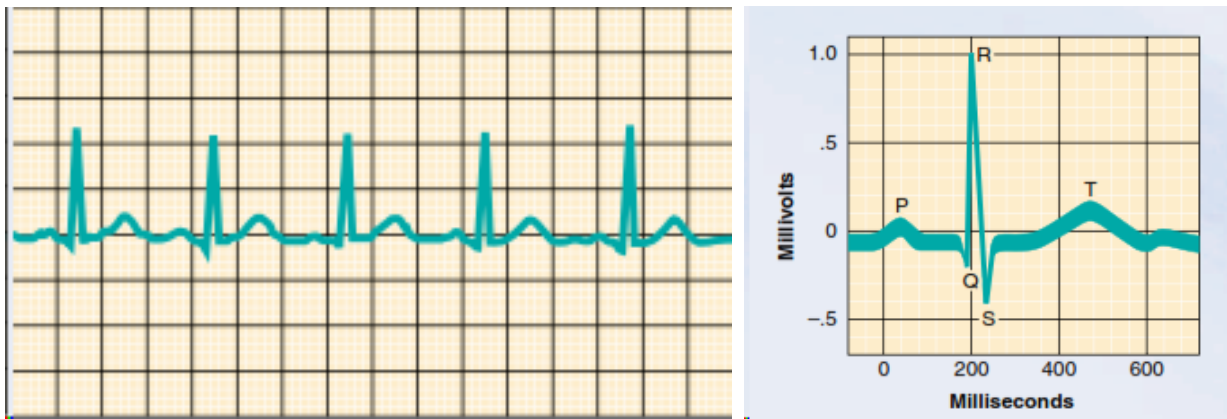


(a) Internal heart anatomy



(b) Anterior view of exterior heart anatomy

Figure 2: Internal heart and anterior view of exterior heart anatomy [12]



(a) A portion of an electrocardiogram

(b) An enlarged ECG normal cycle

Figure 3: Electrocardiogram [12]

I-4-3- Historical view of research on artificial heart

To reproduce the physiology and anatomy of a natural heart intensive researches have been conducted. On the 18 July 1963 the first step was made with the Heart-Lung machine that worked 4 days before being disconnected from the patient.

During the same year Mickael Debakey implanted for the first time a pneumatic intra-corporal device mimicking the heart pumping function, unfortunately the patient died due to neurological complications. In 1966 Mickael Debakey achieved with a similar system, the first implantation of a cardiac assist device that stays 10 days in the body before removal following a recovery of a normal pumping function of the ventricle.

The next year, Christian Barnard achieved the first heart transplant in Capetown. In 1969, D Colley implanted the first artificial heart developed in collaboration with D Liotta, the patient died few days later due to sepsis.

In 1978 for the first time a cardiac assist device was used as a bridge to transplantation, also since the 70s started the development of most of the devices we know now, among them are the Novacor, HeartMate, Thoratec and the Jarvick-7 which are used to serve as a bridge to transplantation. During 1984 for the first time an artificial heart replaced a native heart. Since 1994 cardiac assist devices have been commercialized [3, 10, 22].

I-4-4- Typical Profile of Patient in need of an total artificial heart and cardiac assist device

Patients in needs of an artificial organ or an assist device are those with an end stage heart failure. Cardiac Heart insufficiency is classified mostly by the American Heart

Association classification (Table II) or by the New York Heart Association classification (Table III). With these classifications, end stage heart failure is identified as the D stage of the AHA classification or III-IV stage of the NYHA classification.

Table II: NYHA classification of cardiac heart insufficiency translated from [22].

Class	Patient Symptoms
I	No limitation of physical activity. Ordinary physical activity does not cause undue fatigue, palpitation, or dyspnea (shortness of breath).
II	Slight limitation of physical activity. Comfortable at rest, but ordinary physical activity results in fatigue, palpitation, or dyspnea.
III	Marked limitation of physical activity. Comfortable at rest, but less than ordinary activity causes fatigue, palpitation, or dyspnea.
IV	Unable to carry out any physical activity without discomfort. Symptoms of cardiac insufficiency at rest. If any physical activity is undertaken, discomfort is increased.

Table III: AHA classification of cardiac heart insufficiency translated from [22].

Stade	Patient Symptoms
A	Patients at high risk for developing HF in the future but no functional or structural heart disorder
B	Structural heart disorder but no symptoms at any stage
C	Previous or current symptoms of heart failure in the context of an underlying structural heart problem, but managed with medical treatment
D	Advanced disease requiring hospital-based support, a heart transplant or palliative care

A detailed description of heart affections with medical treatment available can be given as in [10]. Mainly the causes of an artificial implant can be a myocardium irreversible affection, impossible surgical correction or cardiac postsurgery complications in case of unavailability of heart for a transplant. Hence the more patients in need for a transplant with a reduced number of donors, the more artificial heart could be used.

Considering the severity of the failure a patient could be implanted for a Bridge To Recovery (BTR), Bridge To Transplantation (BTT) or for a Destination Therapy (DT) / Permanent Support (PS) [22].

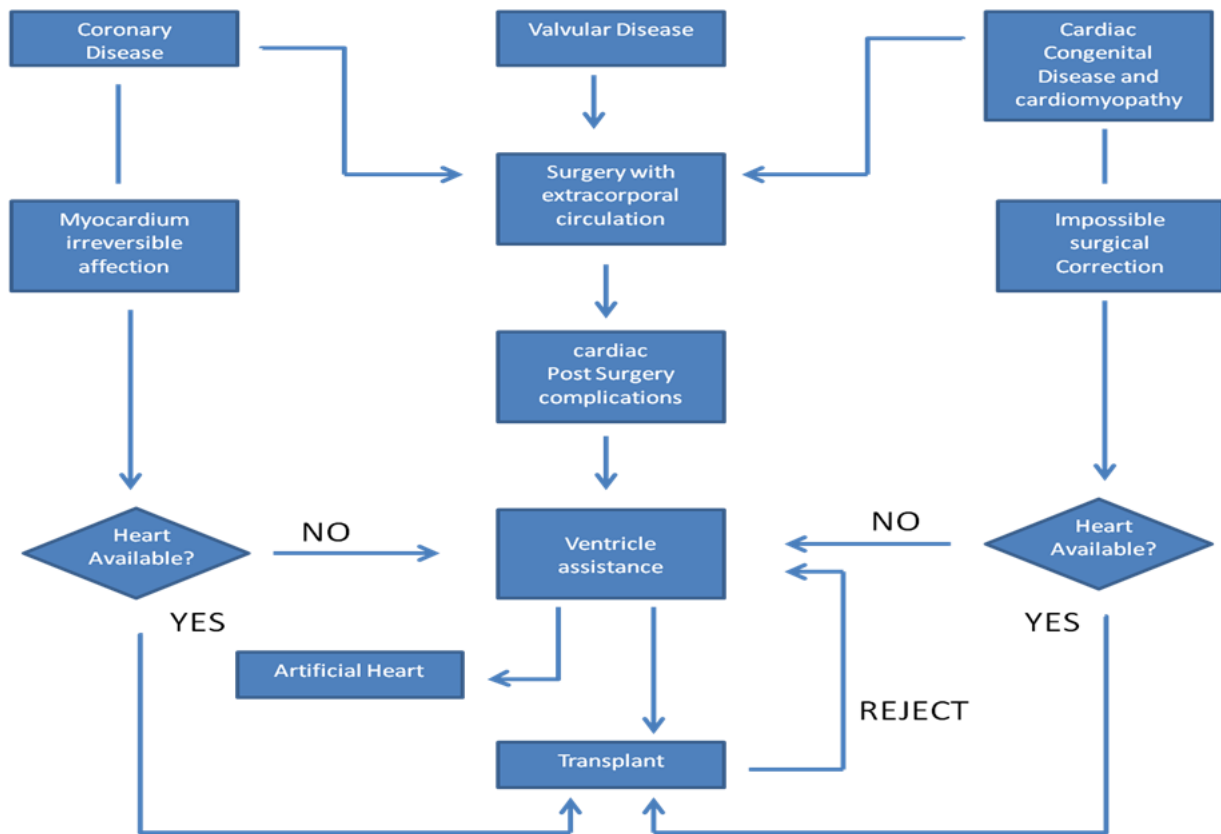


Figure 4: Decision Flow chart for different cardiac affections evolution translated from [10].

BTR is used when the implantation of the artificial device, is intended to help the recovery of the diseased heart, this is the case when there is acute myocarditis and acute myocarditis with decompensation.

BTT is used when the patient is in need for an immediate transplant while there is no available donor by the time. BTT is used in 80% of implants cases.

DT is the last alternative to keep in life a patient suffering from severe heart failure, or who is contraindicated for a heart transplant; this counts for about 10% of implants cases.

For a BTR or BTT cardiac assist devices are used and for DT artificial heart is used.

I-4-5- Specifications of cardiac assist device and artificial heart

The National Heart, Lung and Blood Institute in 1980 [10,11] issued specifications on a typical cardiac assist device, summarize as follow:

- Able to assist the left ventricle with a constant flow of 10 l/mn without exceeding the frequency of 120 bpm, with a mean aortic pressure of 120 mmHg and a maximum of 150 mmHg

- Lifetime of 2 years without a new operation
- Possess a simple control responding to the cardiovascular system needs
- Reduce hemolysis, thrombus
- Ventricle should be biocompatible and stable in the biological environment (non toxic, non corrosive)
- Not produce excessive heat that can affect neighbouring tissues
- Possess a 10 h autonomy with an external electrochemical energy accumulator
- Possess a 30 mn or more with an internal energy accumulator. Within this conditions the ventricle should deliver a 7 l/mn flow rate and a mean aortic pressure of 100 mmHg
- Function in all possible orientations, in presence of vibrations, shocks, muscles movement: Gyroscopic effects should be minimized
- The shape, weight, volume of the ventricle should be compatible with the human anatomy
- The noise and the induced vibrations should be acceptable physiologically and psychologically
- Patient life quality should be sufficient for him to have a decent life.

These specifications for a left ventricle assist device can be extended to the specifications of an artificial heart. To the previous specifications could be added the fifth generation artificial heart (still under research and development) specifications [2]:

- Have a high beneficence that is possessing high standards with 85 to 95 % of success over 10-20 years
- Adapt to body needs.

I-4-6- Some approach carried out in artificial heart and cardiac assist device research

To meet the requirement of cardiac assist device, some solutions have been provided. Figure 5 gives a classification primarily based on lifetime and body location [22].

For a general view of devices available or still under development, we have the following tables summarizing the group, the device characteristics and some images [3].

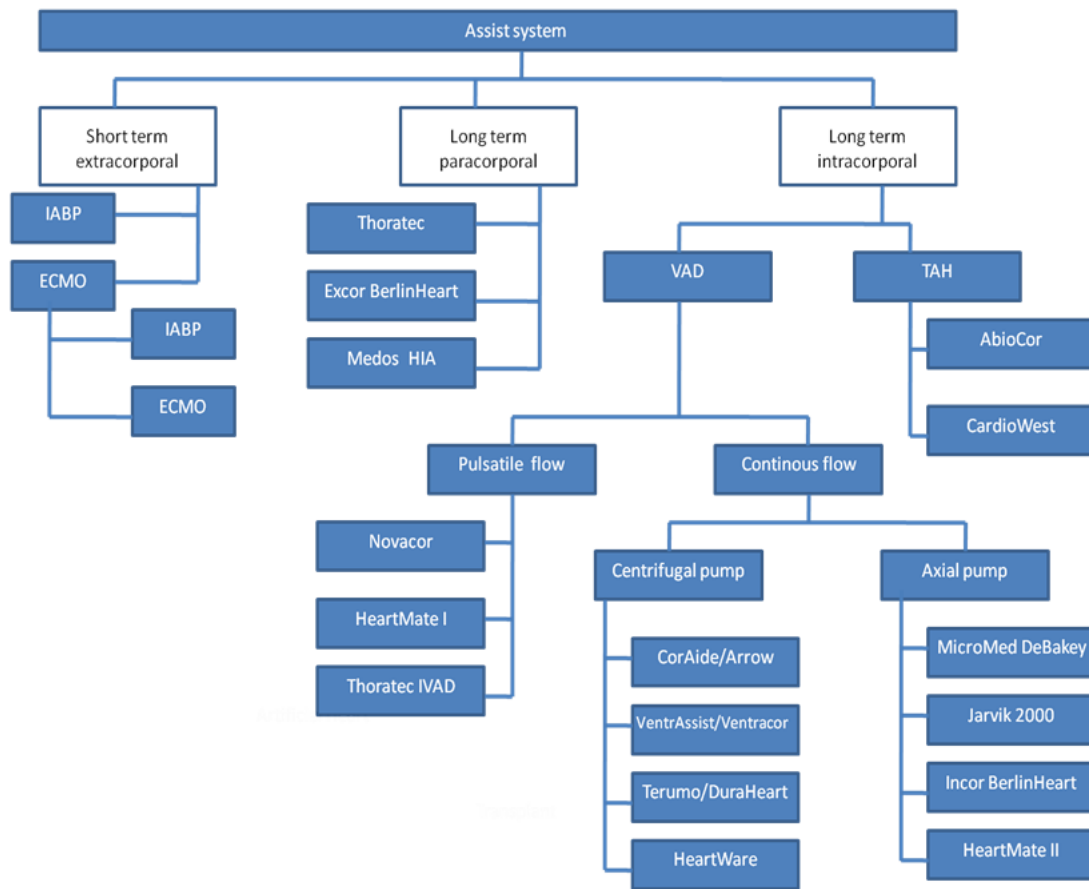






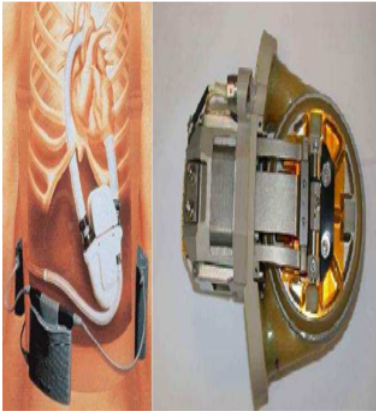

Figure 5: Systematic classification of short term and long term cardiac assist devices translated from [22].

Table IV: Some characteristics and images of pneumatic pumps [3].

Pneumatic pump		
use pneumatic energy and are part of the first generation of artificial heart		
Name	Characteristics	View
Cardiowest/Jarvik-7	Total Artificial Heart. 70 ml each ventricle and 750 ml when united. Console dimensions 80 x 50 x 110 cm, weight 200 Kg.	
Thoratec	Cardiac assist device. Two versions (paracorporeal and implantable). 65 ml stroke volume pumping 5-6 l/mn. Console dimensions of 60 x 50 x 150 cm, weight 100 Kg.	
Berlin Heart	Cardiac assist device. Paracorporeal air-driven blood pump. Available in 12, 15, 25, 30, 50, 60 and 80 ml. Continuous heparin infusion.	

Advantages: technology mature, can serve as left or right ventricular assist device as biventricular assist device. Can be used as BTR or BTT.
Inconveniences: mostly external, limited mobility due to external pneumatic console, higher risk of infection.

Table V: Some characteristics and images of electrical pumps [3].

Electrical pump		
part of the second generation of artificial heart		
Name	Characteristics	View
Abiocor	Total Artificial Heart. Internal battery. Wireless energy transmission. Unidirectional valves. Centrifugal pump. High bulk.	
Novacor	LVAD. Electromagnetic pump with two electromagnet in attraction. Blood pocket crushed by two plates fixed on pivots and spring, commanded during electromagnet attraction. Flow rate of 5 to 7 l/mn. Brief 240 V impulses with 15 A, commanding the electromagnet attraction. Dimensions 16 x 13 x 6 cm ; weight 800 g. The most robust of assist devices. Source of thromboembolic accidents. Pivots are sources of defects after 3 to 4 years.	
HeartMate/TCI	LVAD. 83 ml of blood pocket crushed by plates. Plate commanded by a commutation motor. Weight 900 g. Bulk of 460 ml. Maximum flow of 10 l/mn. Also use pneumatic energy for pumping.	

Advantages: better autonomy.

Inconveniences: internal infections and haemorrhages, Novacor and TCI need a right ventricle in good state, cannot serve as RVAD and need another type assist device to serve as BIVAD.

Table VI: Some characteristics and images of centrifugal pumps [3].

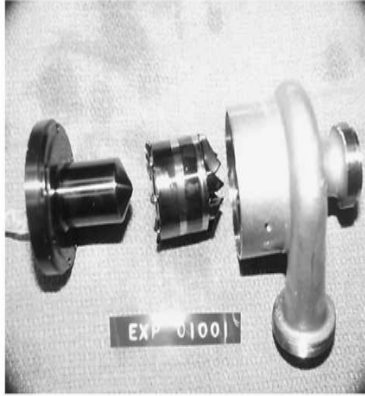

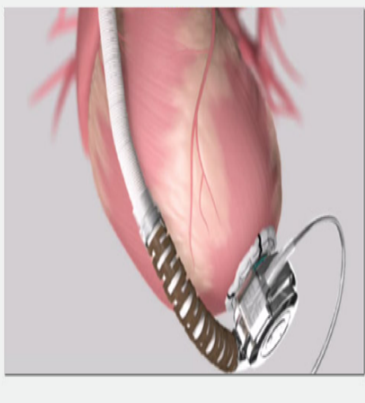
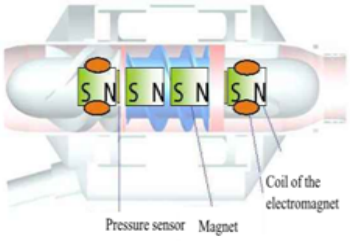
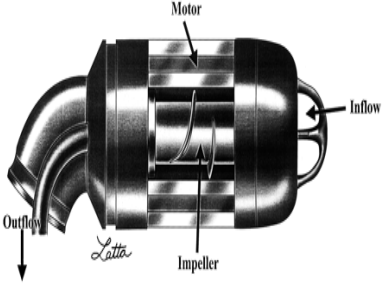
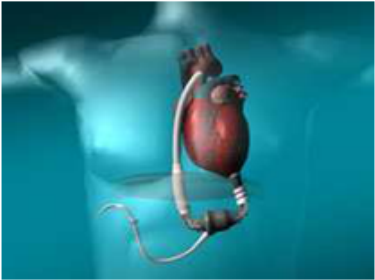
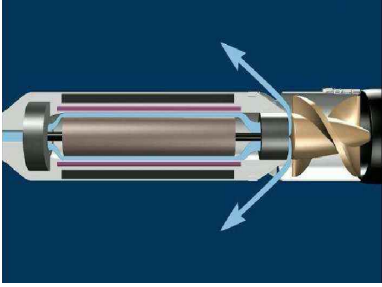
Centrifugal		
blood accelerated in a centrifugal way by the impeller rotation, third generation of artificial heart		
Name	Characteristics	View
Coraide/Arrow	Build up with a stator, a rotor and a spiral. Weight 207 g. 62 ml of bulk. Filling volume of 12 ml. 6.5 W of consumption.	
Duraheart	Magnetically levitated centrifugal pump. Weight 540 g, diameter of 7.3 cm and 4.6 cm thick. Flow rate from 2 to 8 l/mn. Motor speed from 1200 to 2400 rpm.	
HeartWare/TCI	10 l/mn, displacement volume of 50 ml. 2,400 and 3,200 rpm. Passive magnets and hydrodynamic thrust bearings. Dual motor stators with independent drive circuitry.	
<p>Advantages: more important flow rate for less important rotation speed, no vibration, direct coupling between the pump and the motor, no valve need.</p> <p>Inconveniences: high bulk, axis problems complicated by control mechanism like magnetic sustentation, short term usage, continuous flow rate and difficulty to adapt to body needs, need a protective pocket for implantation, appearance of destructive resonance.</p>		

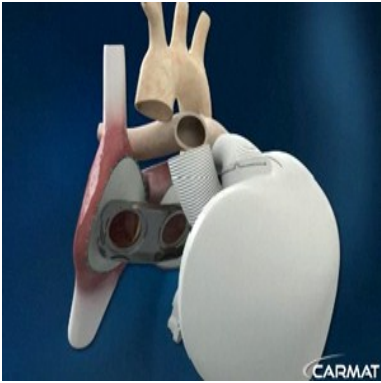
Table VII: Some characteristics and images of axial pump [3].

Axial pump		
blood accelerated in a centrifugal way by the impeller rotation, third generation of artificial heart		
Name	Characteristics	View
Incor	<p>By now the only one available for clinical trials. Made of Titanium. 114 mm length, internal diameter of 16 mm and external diameter of 30 mm. Weight of 200 g. Consumption of 8.5 W, with 5 W due to the control. Mean speed of 8500 rpm with 5 l/mn, 100 mmHg. Minimal speed of 5000 rpm and maximal speed of 10000 rpm.</p>	
Jarvik 2000	<p>Continuous flow, axial rotor supported by ceramic bearings. Length of 5 cm length and diameter of 1.8 cm. Mean speed of 16000 rpm to 18000 rpm. Powered by a redundant dual-coil motor.</p>	
HeartMate II	<p>Designed to run for 5 to 8 years. Rotor driven continuous axial flow, ball and cup bearings.</p>	
Impella	<p>Implantable by endovascular way. 4 to 7 mm of diameter Produce. 4.2 l/mn and a 32500 rpm</p>	

Advantages: small size, reduce weight, better life quality compared to recent pulsatile pump.

Inconveniences: high speed and increased hemolysis, cause platelets activation, poor flow, increased wear, axis problems complicated by control mechanism like magnetic sustentation, short term usage, continuous flow rate, difficulty to adapt to body needs; all used as LVAD.

Table VIII: Some characteristics and images of hydraulic pump.

Hydraulic pump		
Hydraulic fluid moving the membrane containing blood		
Name	Characteristics	View
Carmat	Two artificial ventricles. Two pumps alternatively sucking and injecting silicon oil, moving the membrane containing blood. Bovine valve treated chemically. Internal part in contact with blood covered with hemocompatible bio-membrane (animal pericardium chemically treated). embedded system controlled by microprocessor, 7 sensors to adapt to body needs. Estimate life duty of 5 years, weight of 900 g. External monitoring, fixed on the belt and subcutaneous energy transfer by wires. Two rechargeable batteries. By now, three clinical trials have been performed.	
<p>Advantages: Adaptation to effort and to rest. Two ventricles. No need of associated medication against rejection</p> <p>Inconveniences: Need a charging device, limited autonomy. Subcutaneous energy transfer by wires potentially source of infection, risk of hydraulic fluid leakage. Weight limiting the transplant to female. Expensive. Still under development</p>		

The major limitations of available devices are classified according to the pumping mechanism [3]:

- Pneumatic pumps limit patient mobility and show a higher risk of infection since they are mostly external with a higher bulk and tubes going through the skin and require an external console for control
- Electrical pumps with their action on neighbouring tissues elicit infections and haemorrhages
- Centrifugal pumps have axis problems coupled with gyroscopic effects, friction, wear limiting device lifetime and patient mobility with posture inconvenience. As they are continuous flow pumps, they are difficult to adapt to body needs
- Axial pumps easily cause hemolysis with thrombosis triggered by platelet activation. Moreover axis, friction, wear problems are also limiting factors which increase occupied volume when it is wanted to control friction

- With hydraulic fluid leakage problems, hydraulic pump have a shorter expected duty life, so that the long term beneficence is compromised.

The devices acting by now as TAH are the Carmat, Abiocor and the Cardiowest. In the Abiocor, rotative parts and continuous flow are reducing factors on life quality for the patient. For the Cardiowest its pneumatic mechanism nature and external control console also limit patient mobility and life quality. At intensive preliminary test there is the Carmat, with few results available.

In the group of biventricular models of cardiac assist devices, leaders are the Thoratec and the Berlin Heart, both are pneumatically driven and require tubes passing through the skin which are sources of infection. They are also limited by the external control console associated to the pneumatic pumping function and they need extended stays in hospitals.

The most commonly use left ventricular assist device (LVAD) is the HeartMate which is the reference standard. Among this category are the Jarvik 2000, HeartMate II, Novacor. By now only the implantable version of the Thoratec can serve as LVAD and / or RVAD.

With recent devices, clinical trials results are not better and sometime are worse than those obtained with older systems. Current research efforts are to improve already existing devices with the ambition to reduce the device size, weight and energy consumption. Major limitations of available devices are:

- Reduced life quality due to external invasive components
- Reduced device lifetime due to rotative components and increased wear
- Pumping function not in accordance to body needs
- Thrombosis and/or hemolysis on long term use.

The challenge of this work is to conceive reliable systems, with reduced size, weight, low energy consumption, good efficiency and high beneficence [2, 3]. The specifications we want for our model is to be declined under LVAD, RVAD, BIVAD, TAH with minor changes; offer to patients a better life quality with a pulsatile flow pump as the natural heart, a normal mobility, the lowest possible thrombosis and hemolysis; increase device lifetime using translation movement; pump according to body needs.

Indeed, pumping according to body needs shall be based on biological electrical signal such as the native pacemaker ones, and the one coming from a nerve. For these biological signals can be recorded by microelectrodes [23–29] called chronic electrode implants that can be used in the long term scale. The obtained signals can be amplified through instrumentation preamplifier and amplifier [30–32]. After insertion, since their recording capability deteriorate over time [33–35], their use in the long term can be optimized by reducing the interaction between electrode and tissue [23, 36–41], while increasing biocompatibility and alleviating chronic effects such as glial scar, inflammatory reactions [23, 42–49].

I-5- Approach of the cardiac assist device and total artificial heart

Considering the specifications of the NHLBI [10, 11] and the limitation of the devices available by now [3], the major issues are to:

- Reduce thrombosis which are stationary clots in blood vessels, more observable with stationary or regular flow which are favourable to platelets deposits [12]
- Reduce hemolysis observable with high speed blood flow due to increased shear
- Allow the functioning in all orientations
- Allow the adaptation to body needs
- Reduce wear that reduce the lifetime and increase generated heat
- Increase device lifetime and beneficence
- Imitate at the best the natural heart.

Pragmatically, the specifications of our device are as follows :

- Avoid rotative parts (axial or centrifugal pump approach) giving birth to gyroscopic effects [3] and pivots source of defects, by using translation movements
- Use a field force easily, to command the pumping function with a sufficient force, and the possibility to couple easily devices from LVAD to TAH
- Use low power for an extended autonomy
- Use fluid flow frequency servo-control to adapt the device to body needs, reducing at the same time stationary flow and thrombosis without using special coating as heparin, metacryloyl-phosphorylcholine lauryl-methacrylate polymer [3, 50, 51].

I-6- Conclusion

In this chapter, we have presented the generalities on organs, artificial organs and attention was paid on the artificial heart which is the topic of this thesis, as the devices available in the literature need to be more beneficent. We also presented some essential works carried out in the literature with their drawbacks, that we intend to solve some. The next Chapter will be devoted to theoretical, numerical and experimental methods used to analyse the dynamical states of the devices proposed in this work.

Chapter II

Methodology

II-1- Introduction

In this chapter, we present the approach used to propose the devices conceived taking into account international standards specifications, with the intention to obtain a device behaving as closest as possible to heart. Analytical, numerical and experimental methods used to access the behaviour of the devices in this preliminary study are given.

II-2- Analytical Methods

Generally, physics problems modelling only time dependent phenomenon are described by NODE. Therefore system of NODE could be obtained and there are some specific methods to analyse them.

II-2-1- Principle of harmonic balance

To determine an approximate periodic solution of an NODE under sinusoidal excitations, the harmonic balance method can be used [52–55]. Let us consider the following differential equation:

$$\ddot{x} + x = f(\dot{x}, x, t) \quad (1)$$

where the dot over x refers to the differentiation with respect to time. The function f is such that $f(\dot{x}, x, t + T) = f(\dot{x}, x, t)$.

The harmonic solution of equation is expressed under the form

$$x = A \sin(\omega t + \phi) \quad (2)$$

where A is the amplitude of oscillations, ω the pulsation of the sinusoidal excitation and ϕ the phase at the origin. Replacing equation (2) into equation (1) and equating separately the coefficient of sine and cosine terms which have the same harmonics, one obtains after neglecting harmonics order greater than one, a system of algebraic equations which are the amplitude equations. This method is the principle of harmonic balance, used to obtain small amplitudes solutions.

II-2-2- Principle of Cardano's Method

The Cardano's method is used to solve third-order polynomial equations [56]. Let us consider the following equation:

$$ax^3 + bx^2 + cx + d = 0. \quad (3)$$

Letting $x = z - b/3a$ we obtain the canonical equation

$$z^3 + pz + q = 0 \quad (4)$$

where $p = \frac{-b^2}{3a^2} + \frac{c}{a}$ and $q = \frac{b}{27a}(\frac{2b^2}{a^2} - \frac{9c}{a}) + \frac{d}{a}$.

According to the sign of the discriminant $\Delta = q^2 + \frac{4}{27}p^3$ the solutions of equation (4) are obtained:

- If $\Delta > 0$ the equation possess one real z_0 and two complexes z_1, z_2 solutions

$$\begin{cases} z_0 &= u + v \\ z_1 &= ju + \bar{j}v \\ z_2 &= j^2u + j\bar{v} \end{cases} \quad (5)$$

where $j = -\frac{1}{2} + i\frac{\sqrt{3}}{2} = \exp^{i(\frac{2\pi}{3})}$; $u = \sqrt[3]{\frac{-q+\sqrt{\Delta}}{2}}$; $v = \sqrt[3]{\frac{-q-\sqrt{\Delta}}{2}}$

- If $\Delta = 0$ the equation possess two real solutions, one simple z_0 and one double z_1

$$\begin{cases} z_0 &= 2\sqrt[3]{\frac{-q}{2}} = -2\sqrt{\frac{-p}{3}} = \frac{3q}{p} \\ z_1 &= z_2 = -\sqrt[3]{\frac{-q}{2}} = \sqrt{\frac{-p}{3}} = -\frac{3q}{2p} \end{cases} \quad (6)$$

- If $\Delta < 0$ the equation possess three real solutions z_0, z_1, z_2

$$z_k = 2\sqrt{\frac{-p}{3}} \cos\left(\frac{1}{3} \arccos\left(\frac{-q}{2} \sqrt{\frac{27}{-p^3}} + \frac{2k\pi}{3}\right)\right) \quad k \in \{1, 2, 3\}. \quad (7)$$

This method is used to solve the third order polynomial equation, for equilibrium and instability studies.

II-3- Numerical methods

II-3-1- Fourth-order Runge-Kutta method for first-order differential equation

To access more accurate solution of NODE numerical simulation are often used. One of the most used numerical simulation algorithm for NODE problems is the Fourth-order Runge-Kutta (RK4), it is the algorithm used in this thesis [57]. Its implementation used Fortran 90. Let us consider the first order differential equation

$$\frac{dy}{dt} = f(t, y) \quad (8)$$

with $y(t_0) = y_0$; this equation can also be under a vectorial form (y and f being vectors). The aim of the RK4 method is to find solutions after each time step h , the next solution as a function of the previous one. This method stipulates that:

$$y(t+h) = y(t) + \frac{1}{6}(L_1 + 2L_2 + 2L_3 + L_4) \quad (9)$$

where

$$\begin{aligned} L_1 &= hf(t, y(t)); L_2 = hf\left(t + \frac{h}{2}, y(t) + \frac{L_1}{2}\right); \\ L_3 &= hf\left(t + \frac{h}{2}, y(t) + \frac{L_2}{2}\right); L_4 = hf(t+h, y(t) + L_3). \end{aligned}$$

This procedure needs in its iteration only the initial value $y(t_0) = y_0$, to calculate all the other values taken by the function y at other times separated by the time step h .

II-3-2- Fourth-order Runge-Kutta method for m-order differential equation

In the case m-order differential equation

$$\begin{cases} \frac{d^m y}{dt^m} &= f_m(t, y, \frac{dy}{dt}, \frac{d^2 y}{dt^2}, \dots, \frac{d^{m-1} y}{dt^{m-1}}) \\ \frac{d^k y}{dt^k}(t_0) &= y_0^{(k)} \end{cases} \quad (10)$$

with successive variables change, the equation (10) can be written under the form

$$\left\{ \begin{aligned} \frac{d^0 y}{dt^0} &= U_0 = y = f_0(t, U_0, U_1, U_2, \dots, U_{m-1}) \\ \frac{dy}{dt} &= \frac{dU_0}{dt} = U_1 = f_1(t, U_0, U_1, U_2, \dots, U_{m-1}) \\ \frac{d^2 y}{dt^2} &= \frac{dU_1}{dt} = U_2 = f_2(t, U_0, U_1, U_2, \dots, U_{m-1}) \\ &\vdots \\ \frac{d^{m-1} y}{dt^{m-1}} &= \frac{dU_{m-2}}{dt} = U_{m-1} = f_{m-1}(t, U_0, U_1, U_2, \dots, U_{m-1}) \\ \frac{d^m y}{dt^m} &= \frac{dU_{m-1}}{dt} = f_m(t, U_0, U_1, U_2, \dots, U_{m-1}) \\ \frac{d^k y}{dt^k}(t_0) &= U_k(t_0) = y_0^{(k)} \quad k \in \{1, 2, 3, \dots, m-1\}. \end{aligned} \right. \quad (11)$$

With this general vectorial and form, iterations can be performed to determine all the values of y and its derivative at different time separated by the time step h using :

$$U_k(t+h) = U_k(t) + \frac{1}{6}(L_1^k + 2L_2^k + 2L_3^k + L_4^k) \quad (12)$$

where

$$\begin{aligned}
L_1^k &= hf_k(t, U_0(t), U_1(t), \dots, U_{m-1}(t)); \\
L_2^k &= hf_k(t + \frac{h}{2}, U_0(t) + \frac{L_1^0}{2}, U_1(t) + \frac{L_1^1}{2}, \dots, U_{m-1}(t) + \frac{L_1^{m-1}}{2}); \\
L_3^k &= hf_k(t + \frac{h}{2}, U_0(t) + \frac{L_2^0}{2}, U_1(t) + \frac{L_2^1}{2}, \dots, U_{m-1}(t) + \frac{L_2^{m-1}}{2}); \\
L_4^k &= hf_k(t + h, U_0(t) + L_3^0, U_1(t) + L_3^1, \dots, U_{m-1}(t) + L_3^{m-1}).
\end{aligned}$$

This generalized form can also serve to solve numerically first-order coupled ODEs.

II-4- Experimental procedure and devices

II-4-1- Materials

The devices proposed, as they are based on magnetic lifting force, use electromagnet acting on a movable ferromagnetic plate crushing a biocompatible pocket containing blood. For experiments, the electromagnet is built using recycled components taken mostly from used transformers.

The iron core of the transformer is used for the movable ferromagnetic mass and to build the iron core of our device; its wiring is used for our electromagnet wiring. As the iron core of the transformer possess E and I shapes, these shapes can be cut and processed under the movable mass electromagnet and iron core desired geometry and dimensions (see Figure 6).

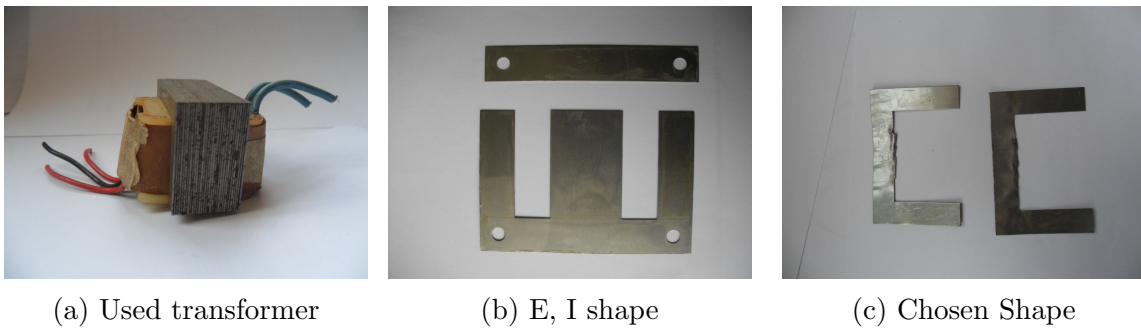


Figure 6: Some material used.

II-4-2- Declinations

Under variable excitation, the electromagnet can lift the ferromagnetic mass according to the signal at input. To produce a TAH, as the native heart is removed and replaced by an artificial organ, the native pacemaker included in the native heart is hence removed,

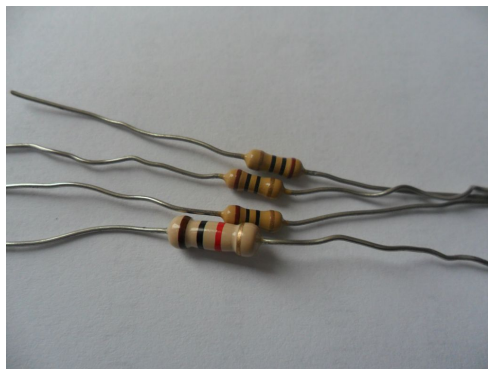
therefore the artificial heart need to be paced artificially and servo-controlled to body needs.

In the literature native pacemaker is modelled by a Van der Pol oscillator [58,59]. In the case of artificial heart, this Van der Pol oscillator can represent the effect of natural pacing on assist device or represent an artificial pacing acting on an artificial heart.

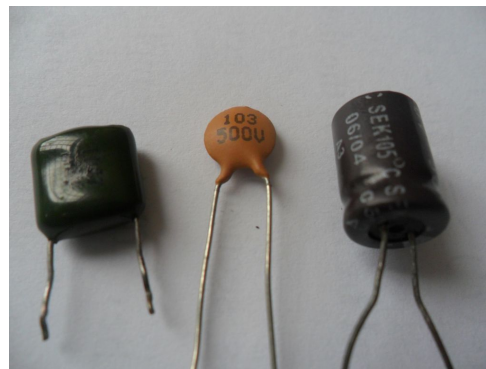
In case of servo-control to body needs, a simple approach is to use the sensed electrical signals coming from sympathetic and parasympathetic nerves to adapt pumping to temperature, pressure, emotions effects. In the literature nerves are modelled by various oscillators such as Hindmarsh-Rose oscillator [60,78].

So if experimentally one reproduces the signal of a Van der Pol oscillator and the one of Hindmarsh-Rose oscillator acting on a pumping device, it could reproduce the behaviour of a cardiac assist device under the pacing of the natural pacemaker, the behaviour of an artificial heart under artificial pacing and nerves control. Hence if conclusive, it could be possible to achieve a better life quality for the patient with adaptation to body needs based on nerves action.

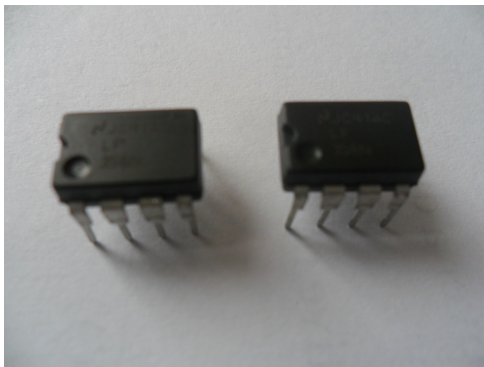
Therefore using analogical simulation approach, based on computing differential equations with operational amplifiers, one can build computing systems based on Van der Pol equation or on Hindmarsh-Rose oscillator. The bases of analogical computing is the use of electronic components such as resistors, capacitors and operational amplifier, voltage multiplier (Figure 7). Indeed, combinations of resistors, capacitors, operational amplifier, and voltage multiplier lead to obtaining signal inversion, summation, difference, integration, etc...(See Figure 8).



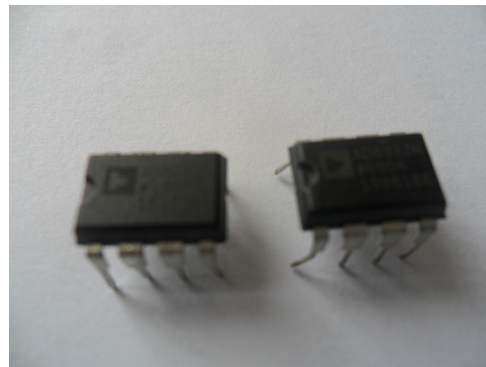
(a) Resistors



(b) Capacitor

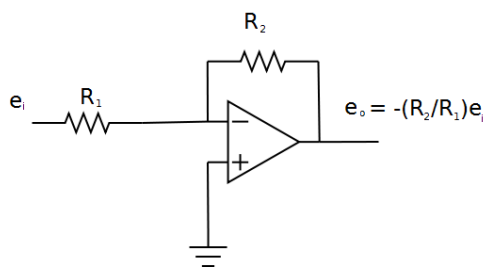


(c) Operational amplifier LF356N

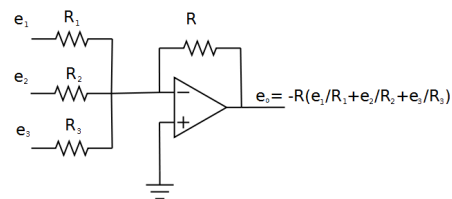


(d) Voltage multiplier AD633JN

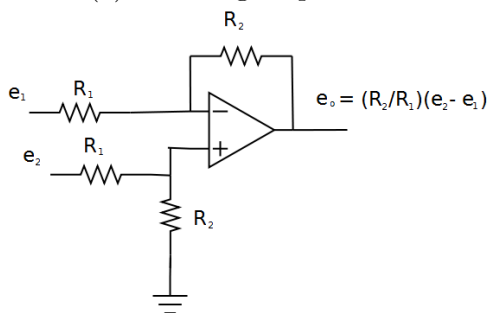
Figure 7: Some electronics components used.



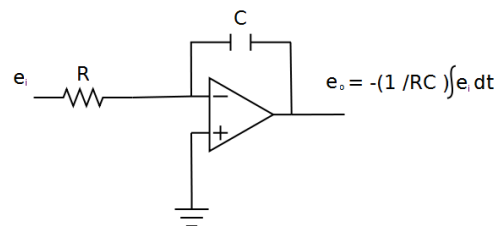
(a) Inverting amplifier



(b) Adder



(c) Differential input amplifier



(d) Integrator

Figure 8: Some basic operations on signals.

To polarize electronic components or apply a DC external voltage; apply a sinusoidal, square or triangle external voltage and visualise the electronic signals, we use respectively the DC generator, low frequency generator, numerical oscilloscope as presented on Figure 9.



(a) PS2303, Tri output 5 V fixed, 0 – 30 V/0 – 3 A × 2 ways



(b) FX1641A, Function generator counter, 2 MHz



(c) HM507, Digital oscilloscope, bandwidth 0 – 50 MHz, rise time < 7 ns

Figure 9: Some electronic devices used.

With these components, combinations of components, electronic devices we can build and visualize a signal based on an NODE, to control our different devices and mimic the effects of pacing or nerves action on our devices.

II-5- Conclusion

In this chapter, we have presented the systematic approach of the devices studied in this thesis, analytical, numerical and experimental methods are also presented as they are used to study the dynamical behaviours of the physical systems proposed in this thesis.

These methods will be used in chapter 3 to:

- Describe the basic system that can act as a LVAD or RVAD along with the prescribed servo-control
- Obtain the analytical solutions of the NODE describing the mathematical models of our devices
- Analyse the pull-in instability in these systems

- Find the behaviour of small amplitudes vibrations
- Obtain time histories, phase diagram and amplitudes diagrams
- Perform preliminary experimental tests.

Chapter III

Results and discussions

III-1- Introduction

In the second section of this chapter, the basic model of our devices proposed is described, modelled and its dynamical study performed, as it is subjected to optimization. It starts by dealing with the description and dynamical behaviour of our basic cardiac assist device, then presents the optimized cardiac assist device as we want to reproduce heartbeat like dynamics, adapt our device pumping rhythm to native heart rhythm, reduce observed instability, pace it artificially, command it by nerves and confirm some numerical results by experimental results.

The fourth section presents the description, model and analysis of our biventricular artificial heart. In this sense it focuses first on the description, dynamical model of our biventricular device and device dynamical behaviour under sinusoidal excitation. Secondly presents its dynamical behaviour under square wave excitation and finally gives some other applications of the device.

III-2- Basic cardiac assist device with ferromagnetic mass actuated by an electromagnet with its servo-control

In most cases only the left ventricle needs to be assisted as it works the most to pump blood in the whole body. Also in some case assist devices help native ventricle recovery or allow to wait for an upcoming transplant. The device studied here can serve as a LVAD commanded by an independent signal to help in such situations.

III-2-1- Description of the device and mathematical model

III-2-1-1- Description of the ventricular assist device

Let us consider Figure 10 giving an isometric, left and top views of our device with global dimensions 8 cm length, 4 cm width and 4 cm height. These dimensions are compatible with natural heart physiology given in subsection I-4-2-. It is made of a biocompatible elastic internal blood pocket B containing the blood we want to pump and possesses an inlet E and an outlet D. Attached to one of its sides is a ferromagnetic blade C under the attraction effect of an electromagnet A attached to the other side of the internal blood pocket B. The biocompatible elastic external pocket contains all the device elements and preserves it from external assault and shocks. As a current flows in the electromagnet, a magnetic field is created. This magnetic field passes through the blood contained in the biocompatible elastic internal pocket B and attracts the movable ferromagnetic mass

through the magnetic lifting force. During its movement the ferromagnetic blade compresses the blood pocket and pumps the blood it contains. According to the form of the current, the pumping process is repeated. Therefore, using sensors, the device could be servo-controlled to the natural heart frequency to pass the rhythm of the natural heart to the pumping device.

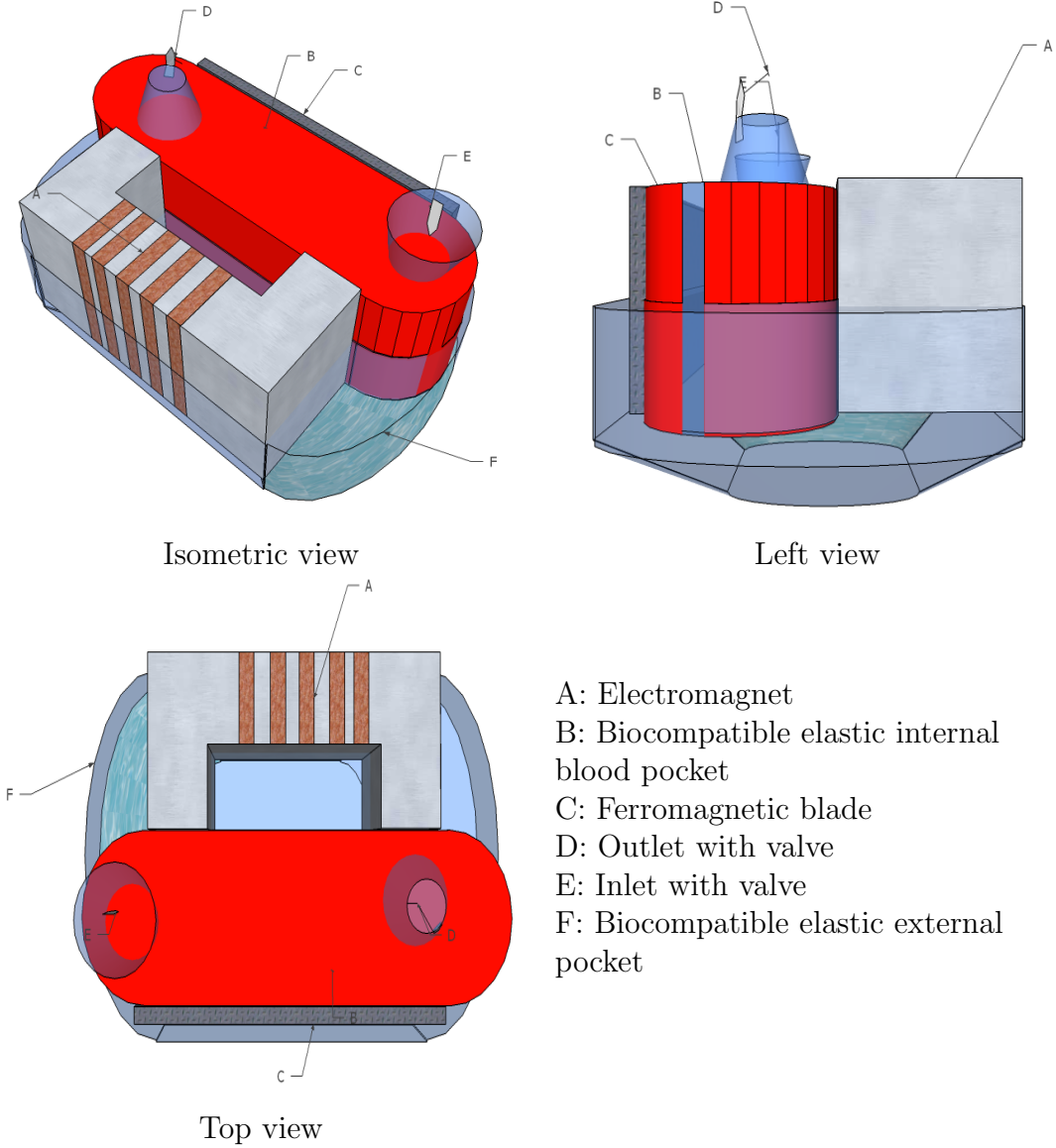


Figure 10: Basic cardiac assist device.

As effects a recent study show that, strong magnetic field aligns red cells disk plane with the field and can reduce blood viscosity within a selected range, with the function of red blood cells appearing not affected. This behaviour is considered to prevent heart attacks [62]. Furthermore a comprehensive review show that there is no health hazard associated with strong magnetic field exposure or cumulative exposure of tissue especially

with strong static fields, the only risk being embedded foreign ferromagnetic bodies reaction to external magnetic fields applied [63]. On the aspect of genotoxicity, exposure to extremely low frequency magnetic fields ($< 300Hz$) do not lead to significant difference between exposed and unexposed samples [64].

So as preliminary positive results of short term study of strong magnetic fields on blood and tissue, we can use strong magnetic field acting on blood without other known risk than the one of an external magnetic field applied on our device. As awaited long term consequence, blood when subjected to magnetic field, takes some time to return to its original state, so that it could be permanently more fluid [62]. Typically, as blood thinner are used to prevent strokes, a more fluid blood could prevent strokes; but increased fluidity could lead to risks when facing hemorrhages, with possible cartilage degeneration, resorption of underlying bones, nerve damage, muscular atrophy [12]. So to avoid an impaired clotting or an excessive clotting, there should be a maximum value of magnetic field not to be exceeded.

III-2-1-2- Model of the ventricular assist device

Knowing that from the mechanical point of view, the movement of one of the natural ventricles during its pumping function can be considered as the movement of a mass, the biocompatible elastic internal pocket representing one ventricle is also considered as a mass. Moreover due to its restoring force, the elastic internal blood pocket is also considered as a spring coupled to the mass. The ferromagnetic nature of the mass allows the action of the magnetic force generated by the electromagnet on the mass to be possible. The electromagnet is powered by variable current, that at best case should have an ECG shape, to reproduce the biological heart pumping function at best.

Taking into account these considerations, the device of Figure 10 can be simplified for analysis under the form of Figure 11. The device shown is a ferromagnetic blade of mass m fixed to a spring and subjected to the action of an electromagnet under variable current. The electrical part is made of a circuit that has an inductor L (electromagnet inductance), a resistor (wiring resistance) supplied by a voltage source $u(t) = U \sin(2\pi ft)$, U and f being respectively the amplitude and frequency, and t the time. The mechanical part consists of a ferromagnetic mass, fixed to a spring and subjected to viscous damping. The spring represents here, the elasticity of the biocompatible internal elastic pocket while the viscous damping represents the effects of blood on the moving mass. The coupling between both parts is realized by the magnetic circuit. When a current flows through the coil of the electromagnet, it induces a magnetic flux in the core of the electromagnet. Hence a lifting force attracts the ferromagnetic mass toward the electromagnet according to the signal at input.

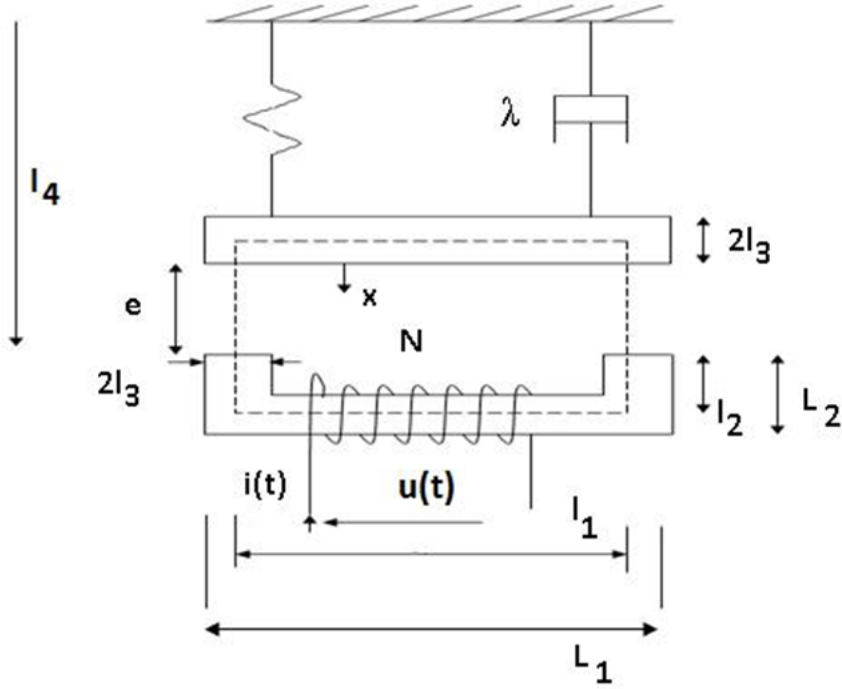


Figure 11: Simplification of basic cardiac assist device.

One should note that, this simplified device presenting one dimensional displacement used for dynamics study can describe the vibrations of a more general three-dimensional membrane with three-dimensional displacement. In this sense this simple approach just considers the first vibration mode of the membrane under radial movement after modal projection.

To derive the dynamics of the mass under the magnetic lifting force, we use Hopkinson's law which is the magnetic analogue of Ohm's law for magnetic circuits. In this law the reluctance plays the role of the resistance in an electrical circuit although it does not dissipate magnetic energy, the magnetic flux plays the role of current intensity, and the magnetomotive force plays the role of the voltage.

Using Hopkinson's law in the mean magnetic circuit represented with dash-line, assuming that magnetic circuit saturation is neglected, and ignoring leakage and fringing fluxes, we have:

$$Ni = R(x)\phi \quad (13)$$

where Ni is the magnetomotive force of the coil, N is the number of turns of the coil, i is the current flowing in the coil, $R(x)$ the reluctance of the magnetic circuit, x the displacement of the mass and ϕ the magnetic flux. The reluctance is given by

$$R(x) = \frac{2l_1 + 2l_2 + 2l_3}{\mu_0\mu_r a} + \frac{2e}{\mu_0 a} \quad (14)$$

where a is the cross section of the iron core, $\mu_0\mu_r$ is the magnetic permeability of the electromagnet iron core and e the gap between the moving ferromagnetic mass and the free edge of the electromagnet. The mean circuit delineated by dash lines has the following dimensions:

$$l_1 = L_1 - 2l_3 \quad (15)$$

$$l_2 = L_2 - l_3 \quad (16)$$

$$e = l_4 - l_0 - 2l_3 - x \quad (17)$$

L_1 is the external length of the electromagnet, L_2 is the external width of the electromagnet, $2l_3$ is the ferromagnetic blade and electromagnet thickness, l_0 the unload spring length, l_4 the distance between the fixed part of the spring and the free edge of the electromagnet that can be in contact with the moving blade.

The total flux flowing in the whole coil is:

$$\Phi = N\phi = Li = \frac{a\mu_0\mu_r N^2 i}{2(l_1 + l_2 + l_3 + \mu_r e)}. \quad (18)$$

Using Ohm's law in the electrical circuit, one obtains

$$\frac{d\Phi}{dt} + \frac{\rho N P_m}{s} i = u(t) \quad (19)$$

where ρ is the wire resistivity, P_m the mean perimeter, s the wire cross section, $u(t)$ the applied voltage. Hence, the equation describing the electric phenomena in the electrical part is

$$\begin{aligned} \frac{a\mu_0\mu_r N^2}{2(l_1 + l_2 + l_3 + \mu_r(l_4 - l_0 - 2l_3 - x))} \frac{di}{dt} + \frac{a\mu_0\mu_r^2 N^2 i}{2(l_1 + l_2 + l_3 + \mu_r(l_4 - l_0 - 2l_3 - x))^2} \frac{dx}{dt} \\ + \frac{\rho N P_m}{s} i = u(t). \end{aligned} \quad (20)$$

Taking the mechanical part, its dynamics is described by the following equation

$$m \frac{d^2 x}{dt^2} + \lambda \frac{dx}{dt} + kx = \frac{\partial W_{mag}}{\partial x} \quad (21)$$

where x is the displacement of the mechanical part, λ the damping coefficient, k the spring stiffness and $W_{mag} = L(x)i^2/2$ is the magnetic energy of the coil. Replacing $L(x)$ by its

expression derived from equation (18), one obtains

$$m \frac{d^2x}{dt^2} + \lambda \frac{dx}{dt} + kx = \frac{a\mu_0\mu_r^2 N^2 i^2}{4(l_1 + l_2 + l_3 + \mu_r(l_4 - l_0 - 2l_3 - x))}. \quad (22)$$

Therefore the electromechanical system is described by the set of equations (20) and (22). Introducing the normalization and change of variables, the equations of motion (20) and (22) are reduced to the following form:

$$\dot{I} + \frac{p\dot{X}I}{(1+p(1-X))} + A_1 I(1+p(1-X)) = E_1 U_0(1+p(1-X)) \sin(2\pi f T_1 \tau) \quad (23a)$$

$$\ddot{X} + F_1 \dot{X} + \Omega_1^2 X = G_1 \frac{pI^2}{(1+p(1-X))^2} \quad (23b)$$

with $X = \frac{x}{l_p}$; $I = \frac{i}{i_p}$; $\tau = \frac{t}{T_1}$; $U_0 = \frac{U}{u_{p1}}$; $L_0 = \frac{a\mu_0\mu_r N^2}{2l_a}$; $i_p = \frac{2l_p T_1 u_{p1}}{a\mu_0}$; $p = \frac{\mu_r l_p}{l_a}$;
 $A_1 = \frac{\rho N P_m}{s L_0} T_1$; $E_1 = \frac{1}{N^2 p}$; $F_1 = \frac{\lambda T_1}{m}$; $\omega_0^2 = \frac{k}{m}$; $T_1 = \sqrt{\frac{m}{k}}$; $\Omega_1^2 = 1$; $G_1 = \frac{2L_0 m u_{p1}^2}{a^2 k^2 \mu_0^2}$.

The dot over a dynamical variable stands for the time derivative. In case of additive noise [65–69], equation (23a) is modified and one have

$$\dot{I} + \frac{p\dot{X}I}{(1+p(1-X))} + A_1 I(1+p(1-X)) = E_1 U_0(1+p(1-X)) \sin(2\pi f T_1 \tau + \varepsilon(\tau)) \quad (24a)$$

$$\ddot{X} + F_1 \dot{X} + \Omega_1^2 X = G_1 \frac{pI^2}{(1+p(1-X))^2} \quad (24b)$$

with $\langle \varepsilon(\tau) \cdot \varepsilon(\tau') \rangle = d\delta(\tau - \tau')$ and $\langle \varepsilon_1(\tau) \cdot \varepsilon_2(\tau') \rangle = 0$.

III-2-2- Dynamical behaviour of the device

In this section the effects of the amplitude and frequency of the AC voltage are analysed as they affect the amplitude of vibration and give rise to subharmonic oscillations. The results of the numerical simulation will be complemented with a mathematical analysis in the case of small displacement. The values of the parameters are given as $f_1 = \frac{1}{T_1} = 70.71 \text{ Hz}$, $u_{p1} = 1.00 \text{ Volt}$, $l_p = 3.00 \times 10^{-2} \text{ m}$, $i_p = 6.75 \times 10^6 \text{ A}$, $p = 600 \text{ m/A}$ the natural frequency of the mechanical part is given as $f_0 = 0.16 f_1$.

III-2-2-1- Effects of the frequency

Figure 12 shows the variation of the amplitude of vibration of the mechanical part as the frequency f varies. Two resonances are found at $f_{r1} = 7.56 \times 10^{-2} f_1$ and $f_{r2} =$

$3.95 \times 10^{-2}f_1$. These two states correspond to two subharmonic resonances of the type $f_0/2$ and $f_0/4$ (see Figure 12). One can also observe a sort of jump of amplitude around the frequency $0.075f_1$. Figure 13 shows some representatives of phase portraits of the electrical and mechanical parts for two values of the frequency. At the subharmonic resonance $f_0/4$, there is a distortion on the sinusoidal movement of the mechanical part, with an inflexion point and an asymmetry on the displacement. Around this frequency, the inflexion point is shifted down for frequency values less than $f_0/4$ and shifted up for frequency values greater than $f_0/4$. At the subharmonic resonance $f_0/2$, an important distortion of the current is observed. This is due to the current induced by the high value of the mechanical displacement. Here there is symmetry on the behaviour of both current and displacement.

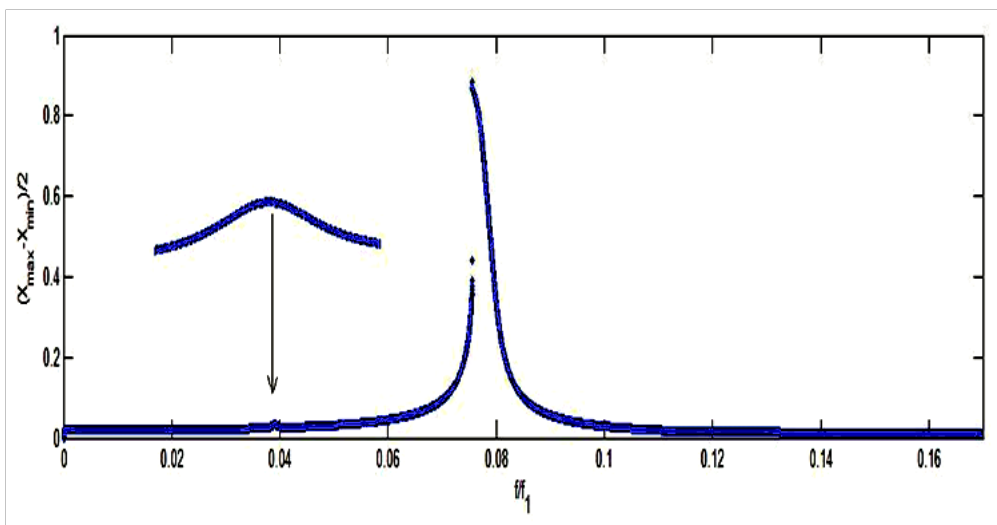


Figure 12: Amplitude-response curve of the mechanical oscillator versus f/f_1 in the sinusoidal regime with enlargement shown around $f/f_1 = 0.04$: $N = 80, U_0 = 1.40, A_1 = 1.14 \times 10^{-1}, F_1 = 2.12 \times 10^{-2}, G_1 = 2.04 \times 10^{12}$.

III-2-2-2- Effects of the voltage amplitude and white noise

For this analysis, the frequency is taken equal to that of the subharmonic frequency $f_0/2$. We have found that the current oscillations amplitude increases linearly as U_0 increases. On Figure 14, the amplitude of vibration of the mechanical also increases monotonously till $U_0 = 1.39$ where it exhibits a jump. The mechanical part oscillates with almost constant amplitude for $1.39 \leq U_0 \leq 1.48$. Above $U_0 = 1.48$, the mechanical part is bounded to the electromagnet. In presence of an additive white noise on the applied voltage (equations (24)), with maximal amplitude of a tenth the applied voltage, one observes on Figure 14 that qualitatively the system under white noise is similar to the one without noise.

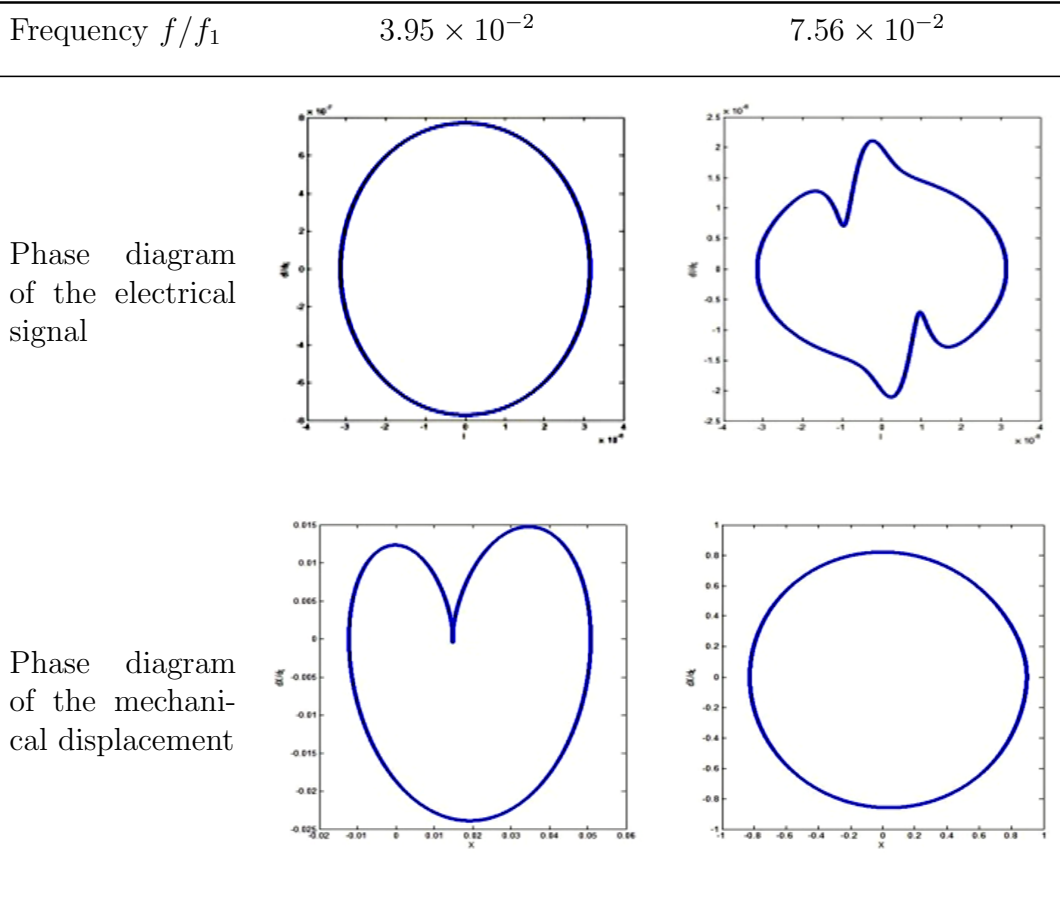


Figure 13: Some phase diagrams of the electrical signal (a) and mechanical displacement (b), with parameters of Figure 12 in the sinusoidal regime.

To end this part devoted to the presentation of some results from the numerical simulation of equations (23), we note that by increasing the number N of turns of the coil, a decrease of the oscillations amplitude of both current and displacement is found.

III-2-2-3- Analytical approach of the amplitude curves

Assuming small current and displacement, the set of equations (23) can be reduced to

$$\dot{I} + A_1 I(1 + p) = E_1 U_0(1 + p) \sin(2\pi f T_1 \tau) \quad (25a)$$

$$\ddot{X} + F_1 \dot{X} + \Omega_1^2 X = G_1 \frac{p I^2}{(1 + p)^2}. \quad (25b)$$

The solution of equation (25a) can be written as

$$I = I_1 \cos(w_{p1} \tau) + I_2 \sin(w_{p1} \tau) \quad (26)$$

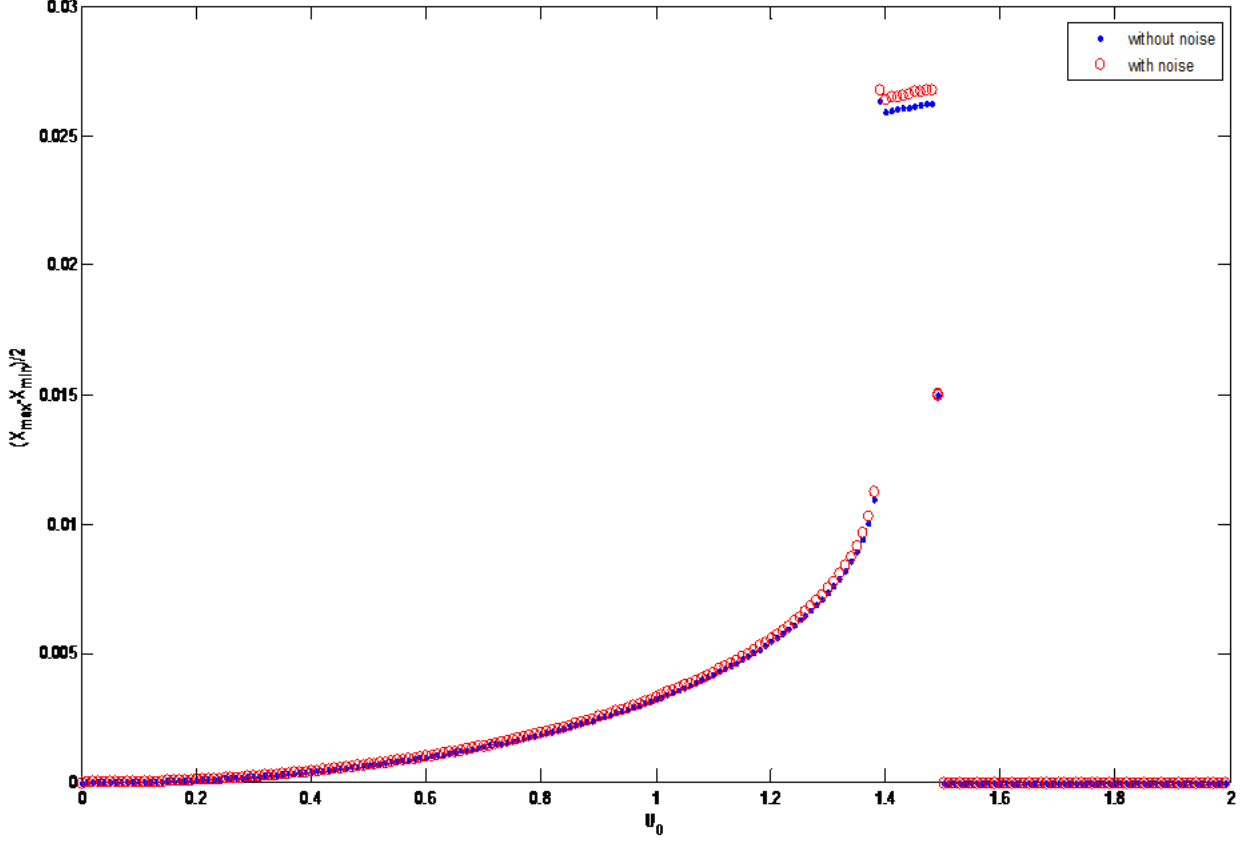


Figure 14: Amplitude-response curve of the mechanical oscillator versus U_0 in the sinusoidal regime, without and with white noise of maximal amplitude of a tenth the applied voltage: $N = 80$, $f/f_1 = 7.56 \times 10^{-2}$, $A_1 = 1.14 \times 10^{-1}$, $F_1 = 2.12 \times 10^{-2}$, $G_1 = 2.04 \times 10^{12}$.

with $I_1 = -\frac{w_{p1}U_0(b_0+1)}{w_{p1}^2N^2+A_1^2(b_0+1)^2}$ and $I_2 = \frac{A_1U_0(b_0+1)^2}{N(w_{p1}^2N^2+A_1^2(b_0+1)^2)}$. Equation (26) can also be written as

$$I = I_m \sin(w_{p1}\tau + \phi_I) \quad (27a)$$

$$I_m = \frac{U_0(b_0 + 1)}{N\sqrt{w_{p1}^2N^2 + A_1^2(b_0 + 1)^2}} \quad (27b)$$

$$\tan(\phi_I) = -\frac{Nw_{p1}}{A_1(b_0 + 1)} \quad (27c)$$

with $w_{p1} = 2\pi fT_1$ and $b_0 = 1/p$. Substitution of (27a), (27b) and (27c) in (25b) leads to:

$$X = X_0 + X_m \sin(2w_{p1}\tau + \pi + \phi_X) \quad (28a)$$

$$X_0 = \frac{G_1 N^2 I_m^2}{2(b_0 + 1)^2 \sqrt{16w_{p1}^4 + 4F_1^2 w_{p1}^2 - 8w_{p1}^2 + 1}} \quad (28b)$$

$$X_m = \frac{G_1 N^2 I_m^2}{2(b_0 + 1)^2 \sqrt{16w_{p1}^4 + 4F_1^2 w_{p1}^2 - 8w_{p1}^2 + 1}} \quad (28c)$$

$$\tan(\phi_X) = \frac{I_2^2 - I_1^2 - 4w_{p1}^2(I_2^2 - I_1^2) + 4I_1 I_2 F_1 w_{p1}}{2(F_1 w_{p1}(I_2^2 - I_1^2) + I_1 I_2(4w_{p1}^2 - 1))} \quad (28d)$$

I_1 and I_2 are given by equation (26). Figure 15 shows the variation of X_m in terms of the frequency. A good agreement is found between the analytical and the numerical results.

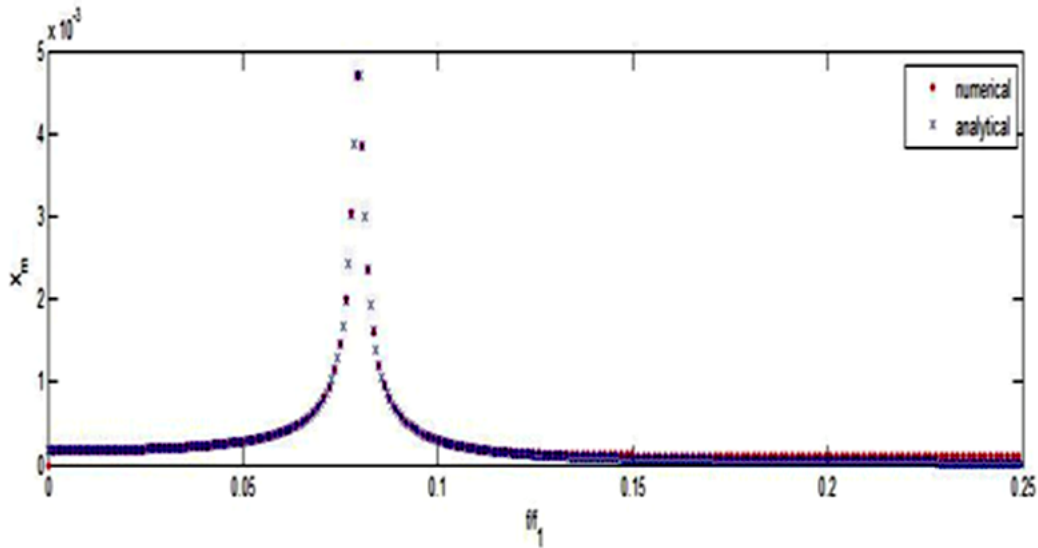


Figure 15: Variation of the amplitude of vibration obtained from the analytical derivation and the numerical simulation for small displacement, in the sinusoidal regime with other parameters of Figure 12 and $U_0 = 0.14$.

III-3- Optimized cardiac assist device

III-3-1- Heartbeat like induced dynamics: bursting dynamics

Bursting is the alternation of active oscillations phase and quiescence phase.

III-3-1-1- Description of the device

Let us consider the system of Figure 11 with a nonlinear capacitor in the electrical circuit. The capacitor is constructed from the electronic components as it appears in Figure 16 (see Figure 16). This capacitor is introduced to reproduce a fast and slow dynamics necessary for bursts, with periodic jump between two equilibrium points induced by a slow varying external force. [70–72]

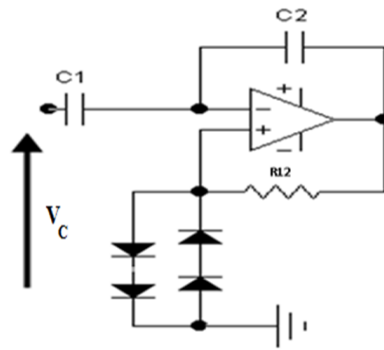


Figure 16: Nonlinear capacitor made of diodes, operational amplifier, resistor and capacitors.

The approach is to induced bursting in the vibration of the mechanical part by the bursting dynamics of the electrical system.

III-3-1-2- Model of bursting dynamics

Considering the virtual loop with the capacitor C_2 and the resistor R_{12} Kirchoff's law gives

$$\frac{q}{C_2} + R_{12} \frac{dq}{dt} = 0. \quad (29)$$

With this equation, we obtain the current flowing in the diodes and using the characteristic equation of diodes:

- for the positive voltage alternation we have:

$$\frac{dq}{dt} = -\frac{q}{R_{12}2C_2} = i_0(e^{\frac{V_+}{n_0V_0}} - 1) \quad (30)$$

with V_+ the voltage at the non-inverting pin of the operational amplifier, n_0 the number of diodes per branch, i_0 the reverse saturation current of the diode, V_0 the thermal voltage.

- for the negative voltage alternation we have:

$$-\frac{dq}{dt} = \frac{q}{R_{12}2C_2} = i_0(e^{-\frac{V_+}{n_0V_0}} - 1) \quad (31)$$

for an ideal operational amplifier considered, the voltage across the device is:

$$V_c = \frac{q}{C_1} + V_- = \frac{q}{C_1} + V_+. \quad (32)$$

Hence for the two alternations, summing equation (30) and (31) we obtain the charge q during both alternations and thus the device charge-voltage characteristics can be easily derived to give

$$V_c = \frac{q}{C_1} + n_0V_0 \sinh^{-1}\left(\frac{-q}{R_{12}i_0C_2}\right) \quad (33)$$

In the case of small apply voltage, we can expand V_c till the third order to give

$$V_c = a_1q + a_3q^3 \quad (34)$$

with $a_1 = V_0n_0\left(\frac{1}{n_0C_1V_0} - \frac{1}{C_2R_{12}i_0}\right)$ and $a_3 = \frac{V_0n_0}{6C_2^3R_{12}^3i_0^3}$.

It is assumed in this work that $\frac{1}{C_1} - \frac{n_0V_0}{C_2R_{12}i_0} < 0$, consequently $a_1 < 0$ and $a_3 > 0$, to obtain a Duffing electrical nonlinearity with a double well potential system. With this capacitor in the circuit, the electromechanical system is now described by the following dimensionless equations

$$\begin{aligned} \ddot{Q} + \frac{p\dot{X}\dot{Q}}{(1+p(1-X))} + A_2\dot{Q}(1+p(1-X)) + B_2(1+p(1-X))Q + C_2(1+p(1-X))Q^3 \\ = E_2U_0(1+p(1-X))\sin(2\pi fT_2\tau') \end{aligned} \quad (35a)$$

$$\ddot{X} + F_2\dot{X} + \Omega_2^2X = G_2\frac{p\dot{Q}^2}{(1+p(1-X))^2} \quad (35b)$$

with $Q = \frac{q}{Q_p}$; $U_0 = \frac{U}{u_{p2}}$; $\tau' = \frac{t}{T_2}$; $A_2 = \frac{\rho NP_m T_2}{sL_0}$; $B_2 = \frac{a_1 T_2^2}{L_0}$; $C_2 = \frac{a_2 Q_p^2 T_2^2}{L_0}$; $E_2 = \frac{u_{p2} T_2^2}{L_0 Q_p}$; $F_2 = \frac{\lambda T_2}{m}$; $\Omega_2^2 = \omega_0^2 T_2^2$; $G_2 = \frac{L_0 Q_p^2}{2ml^2}$; the other parameters as in (23).

III-3-1-3- Dynamical behaviour

An appropriate choice of the coefficients of equations (35) is done as $T_2 = 10^{-3}$ s, $u_{p2} = 10^2$ V, $Q_p = 10^{-6}$ C. The control parameters are the frequency and amplitude of the AC voltage, the number of turns of the coil and the viscous damping.

Figure 17 shows the maximal amplitude-response curve of the mechanical part in the bursting regime in terms of the frequency. It appears the following subharmonic resonances $f_0/2$, $f_0/4$, $f_0/6$, $f_0/8$ and subharmonic antiresonances at $f_0/3$, $f_0/5$, $f_0/7$, $f_0/9$ (see Figure 17).

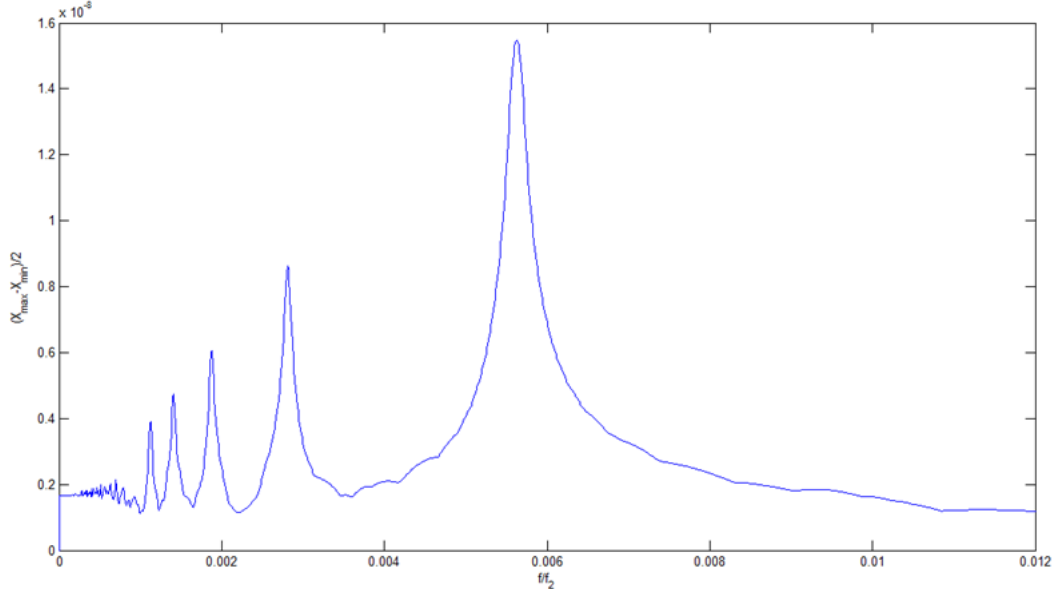


Figure 17: Amplitude-response curve of the mechanical oscillator versus f/f_2 in the bursting regime: $N = 3 \times 10^2$, $U_0 = 8.00 \times 10^{-6}$, $A_2 = 2.16 \times 10^{-3}$, $B_2 = 4.78 \times 10^{-3}$, $C_2 = 2.84 \times 10^{-4}$, $E_2 = 8.84 \times 10^2$, $F_2 = 1.50 \times 10^{-3}$, $\Omega_2^2 = 5.00 \times 10^{-3}$, $G_2 = 1.88 \times 10^{-6}$.

Plotting some time histories of the electrical signal and mechanical displacement for some selected values of the frequency, as the frequency increases, the period of the bursting oscillations in the electrical signal is obviously affected while the amplitude remains almost constant. For the mechanical response, it is found that its amplitude increases with the frequency and the bursting phenomenon manifests by a sort of pulse packages presenting decreasing amplitude vibration patterns. The number of vibration per pattern decreases as the frequency increases.

As concerns the effects of U_0 on the phenomenon, it can be seen in Figure 18 that the increase of U_0 leads to a sort of sinusoidal modulation, and the appearance of one more bursts within the same time frame. This modulation is clearly visible on the mechanical part where instead of having a pattern of vibration with decreasing amplitude, the amplitude first increases, and then decreases.

The effects of the number of turns in the coil show the appearance of the decreasing behaviour of the bursting amplitude in the electrical part. The pulse package behaviour of the mechanical part is characterized by an increase of amplitude.

The effects of the last control parameter considered in this work are represented in Figure 19. This Figure shows that the value of the viscous coefficient has an interesting impact on the shape of burstings. Indeed, the mechanical oscillations in the pattern decrease quickly as the viscous coefficient increases, when the behaviour in the electrical part is almost identical. This is obviously the consequence of the well-known exponential decrease of mechanical vibration due to viscous damping. Hence, sharp bursting oscillations of the mechanical part are made more visible when the viscous damping increases. A quantitative comparison between the real ECG (Fig.3) is of interest. However, this has not been possible here since we have not recorded the ECG ourselves to have data. All the same, there is good qualitative agreement between (Fig.3) and (Fig.19) for the dimensionless damping coefficient equal to 2.40×10^{-2} .

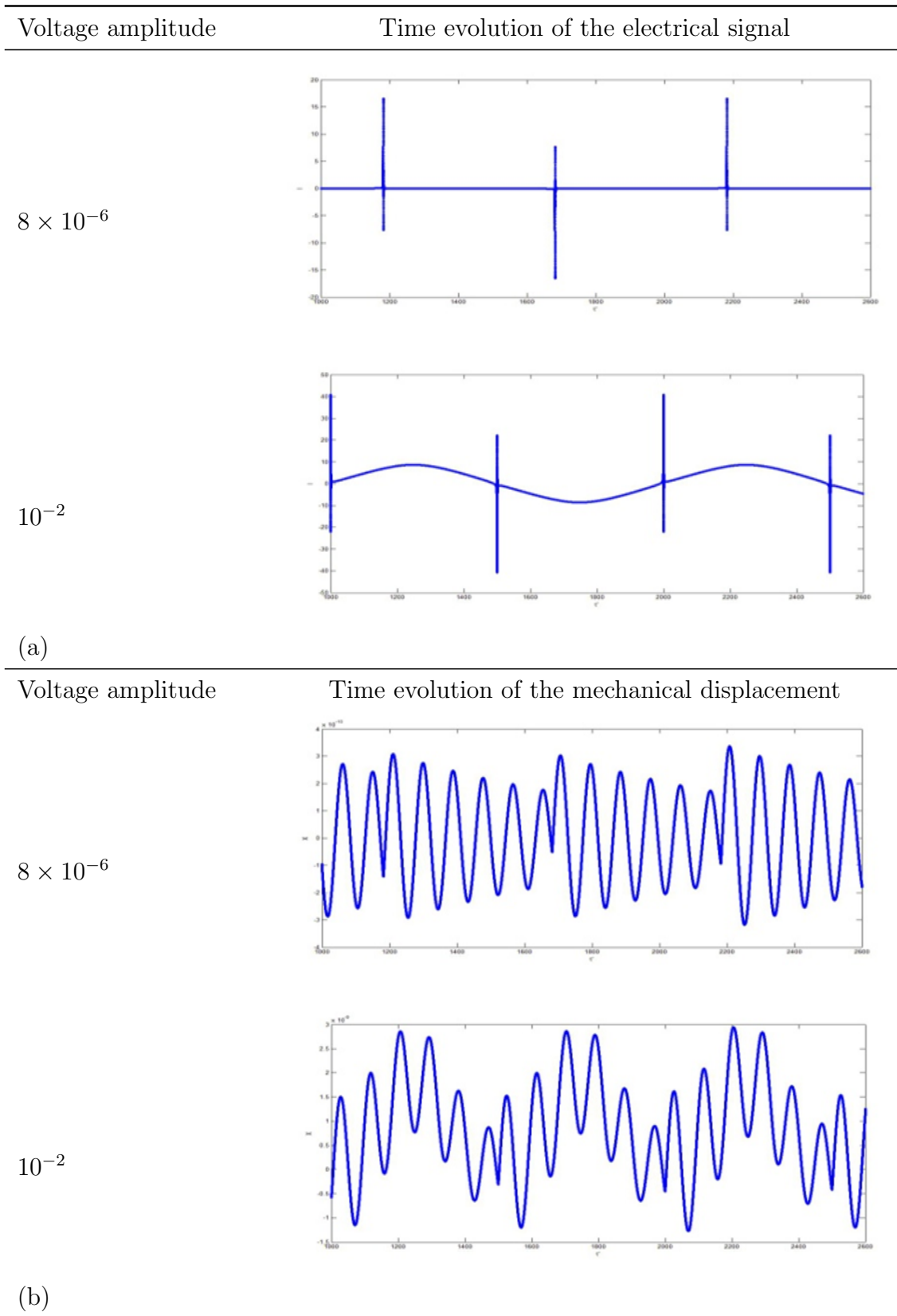


Figure 18: Some time evolutions of the electrical signal (a) and mechanical displacement (b), showing the sinusoidal modulation of burstings as U_0 increases: $N = 80$, $f/f_2 = 1.00 \times 10^{-3}$, $A_2 = 8.10 \times 10^{-3}$, $B_2 = 6.72 \times 10^{-2}$, $C_2 = 3.99 \times 10^{-3}$, $E_2 = 12433.98$, $G_2 = 1.34 \times 10^{-7}$.

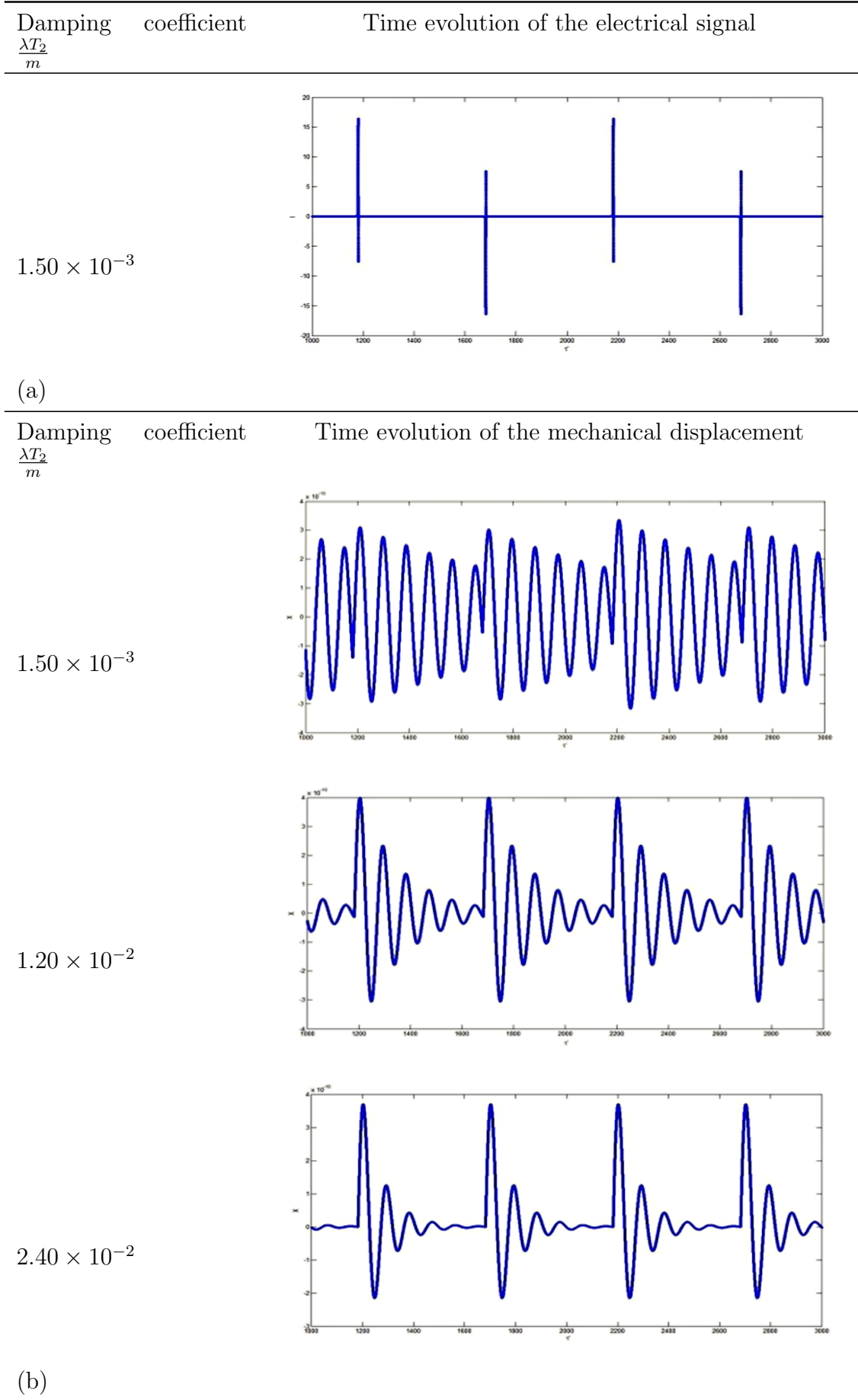


Figure 19: Some time evolutions of the electrical signal (a) and mechanical displacement (b) as the damping increases in the bursting regime: $U_0 = 8.00 \times 10^{-6}$, $f/f_2 = 1.00 \times 10^{-3}$, $N = 80$, $A_2 = 8.10 \times 10^{-3}$, $B_2 = 6.72 \times 10^{-2}$, $C_2 = 3.99 \times 10^{-3}$, $E_2 = 12433.98$, $G_2 = 1.34 \times 10^{-7}$.

III-3-2- Description of fluid flow frequency servo control, mathematical model and dynamical behaviour

III-3-2-1- Description of fluid flow frequency servo control

To adapt the frequency of the device to the frequency of the natural heart in case of LVAD (BIVAD) a servo-control is used as presented on Figure 20

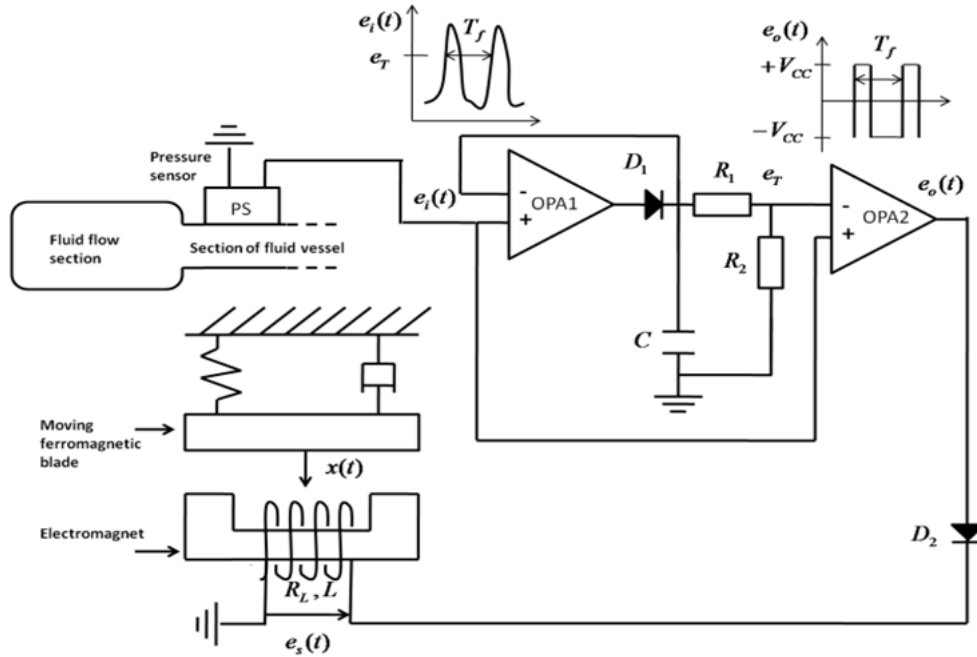


Figure 20: Setup of the fluid flow servo-control.

On this setup of fluid flow frequency servo-control, we have a fluid flow section from which a pulsatile flow comes out with a flow rate $q(t)$, this flow enters a section of deformable tube. At a fixed point of the tube, where the section is $s(t)$, the flow velocity $v(t)$ and the pressure $p(t)$, is inserted a silicon piezoresistive pressure sensor that convert the pressure $p(t)$ into a voltage $e_i(t)$ through a polarization voltage. The analogical pressure image $e_i(t)$, is put in a digital form more convenient $e_0(t)$. To do this an operational amplifier OPA1 detects peaks, and the operational amplifier OPA2 compares the input signal $e_i(t)$ with the threshold e_T . When $e_i(t) > e_T$, the output of OPA2 saturates at $+V_{CC}$ (V_{CC} the polarization voltage). And if $e_i(t) < e_T$, the output of OPA2 saturates at $-V_{CC}$. The threshold is set by the peak detector, which store the previous maximum level of $e_i(t)$ established by the signal, and the two resistors R_1 and R_2 [73]. Finally the last diode selects the positive alternation of the signal $e_0(t)$ to give $e_s(t)$, that feeds the electromechanical system.

III-3-2-2- Model of fluid flow frequency servo control

Using the previous modelling approach, the dynamics of this electromechanical system is obtained; hence introducing the normalization and change of variables under e_S the system is described by the canonical form:

$$\dot{I} + \frac{\dot{X}I}{(1-X)} + AI(1-X) = EE_S(1-X) \quad (36a)$$

$$\ddot{X} + F\dot{X} + \Omega^2 X = G \frac{I^2}{(1-X)^2} \quad (36b)$$

$$E_S = \begin{cases} +U_{AA} & \text{if } (n_1 - 1)\frac{T_f}{T_p} \leq t' \leq (n_1 - 1 + \alpha)\frac{T_f}{T_p} \\ 0 & \text{if } (n_1 - 1 + \alpha)\frac{T_f}{T_p} \leq t' \leq n_1\frac{T_f}{T_p} \end{cases}$$

with $X = \frac{px}{(1+p)l_p}$; $I = \frac{i}{i_p}$; $t' = \frac{t}{T_p}$; $E_S = \frac{e_s}{u_p}$; $L_0 = \frac{a\mu_0\mu_r N^2}{2l_a}$; $i_p = \frac{2l_p T_p u_p}{a\mu_0}$; $p = \frac{\mu_r l_p}{l_a}$;
 $A = (1+p)\frac{\rho N P_m}{s L_0} T_p$; $E = \frac{1+p}{pN}$; $F = \frac{\lambda T_p}{m}$; $\omega_0^2 = \frac{k}{m}$; $T_p = \sqrt{\frac{m}{k}}$; $\Omega^2 = 1$; $G = \frac{L_0 T_p^2 i_p^2 p^2}{2ml_p^2(1+p)^3}$;
 $U_{AA} = \frac{\beta V_{CC}}{u_p}$ and n_1 an integer.

III-3-2-3- Dynamical behaviour of the fluid flow frequency servo control

The values of the physical and the dimensionless parameters are given by: $f_p = 1/T_p = 70.71 \text{ Hz}$, $u_p = 1.00 \text{ Volt}$, $l_p = 3.00 \times 10^{-2} \text{ m}$, $i_p = 6.75 \times 10^6 \text{ A}$, $p = 600 \text{ m/A}$, $A = 6.89 \times 10^1$, $E = 1.25 \times 10^{-2}$, $F = 3.53 \times 10^{-1}$, $G = 3.38 \times 10^9$, and the natural frequency of the mechanical part given by $f_0 = 0.16f_p$. For the input signal e_i sensed by the piezoresistive pressure sensor, taken on a sinusoidal form, with amplitude V_{cc} , and the threshold at $(3/4)V_{cc}$, we observe on Figure 21, that under frequency servo-control (Eqs (36)) the mechanical system adapts its frequency to the one of the sensed signal (current), with a two-level modulated bursting behaviour for low frequencies.

We observe on Figures 22 and 23 that for some other values of the sensed signal frequency (not plot for the electric signal as it keeps the same form), the frequency of vibration of the mechanical system remains equal to the frequency of the sensed signal. Moreover For $f/f_p = 5.00 \times 10^{-1}$ the frequency change brings distorted relaxation oscillations in the mechanical system, while at $f/f_p = 9.99 \times 10^{-1}$ the mechanical system shows almost sinusoidal behaviour.

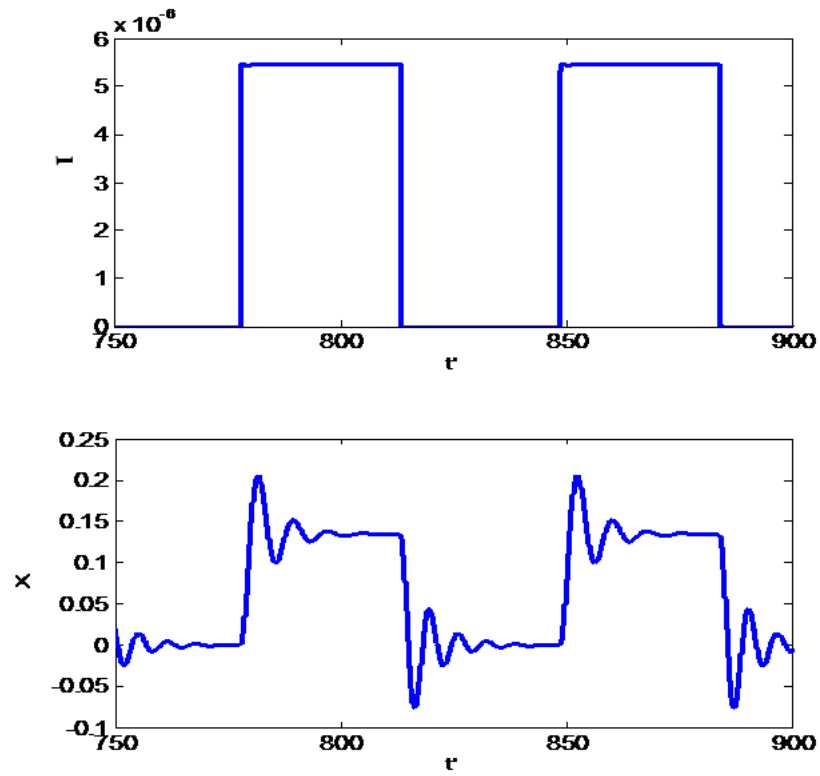


Figure 21: Time histories of the current and mechanical displacement under frequency servo-control: $U_{AA} = 3.0 \times 10^{-2}$, $f/f_p = 1.65 \times 10^{-2}$.

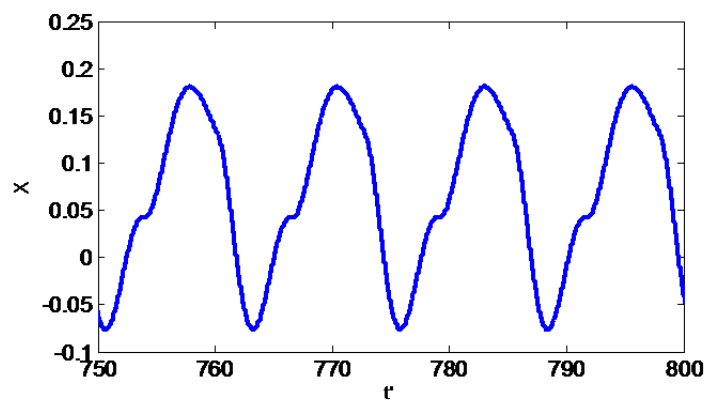


Figure 22: Time histories of the mechanical displacement under frequency servo-control: $U_{AA} = 3.0 \times 10^{-2}$, $f/f_p = 5.00 \times 10^{-1}$.

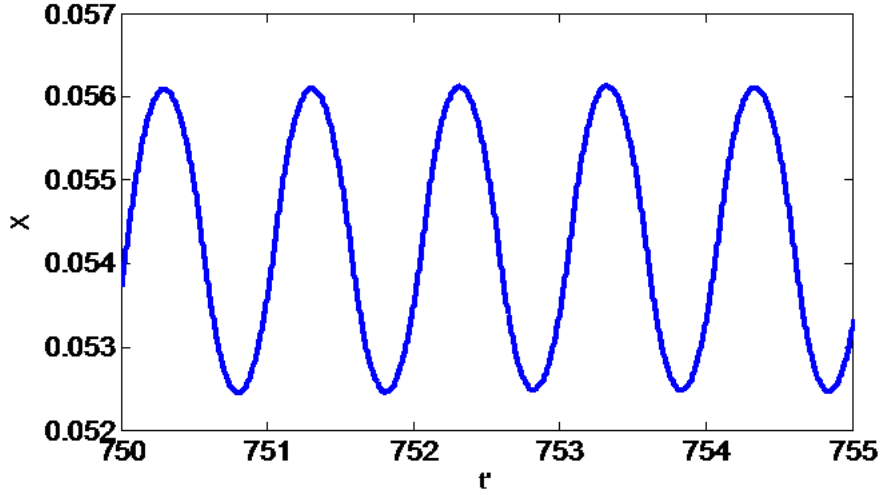


Figure 23: Time histories of the mechanical displacement under frequency servo-control: $U_{AA} = 3.0 \times 10^{-2}$, $f/f_p = 9.99 \times 10^{-1}$.

Looking at the dynamic adaptation of the mechanical system under constant change of the frequency, we introduce a random fluid flow frequency, specifically when the frequency can change only after a period the sinusoidal input signal is taken on the form:

$$e_i = U_0 \sin(2\pi f(t)) \quad (37)$$

$$f(t) = \begin{cases} f_r & \text{for } t = t_0 \\ f_r + \chi \times \text{random} & \text{for } t = t_{peak} \\ f(t_{peak}) & \text{for } t_{peak} < t < t'_{peak} \end{cases}$$

f_r the reference frequency, χ the deviation, t_{peak} , t'_{peak} the moments of appearance of two consecutive peaks of the same nature.

The rectangular signal derived is also random with the same frequency, and with the obtained signal we plot the time histories of the electrical and mechanical parts on Figure 24.

As the frequency undergoes random fluctuation, on Figure 25 we see that mechanical dynamics follows with the same frequency as the sensed signal, giving thus more evidences of the mechanical vibration frequency adaptation to the fluid flow frequency even at random frequency variation.

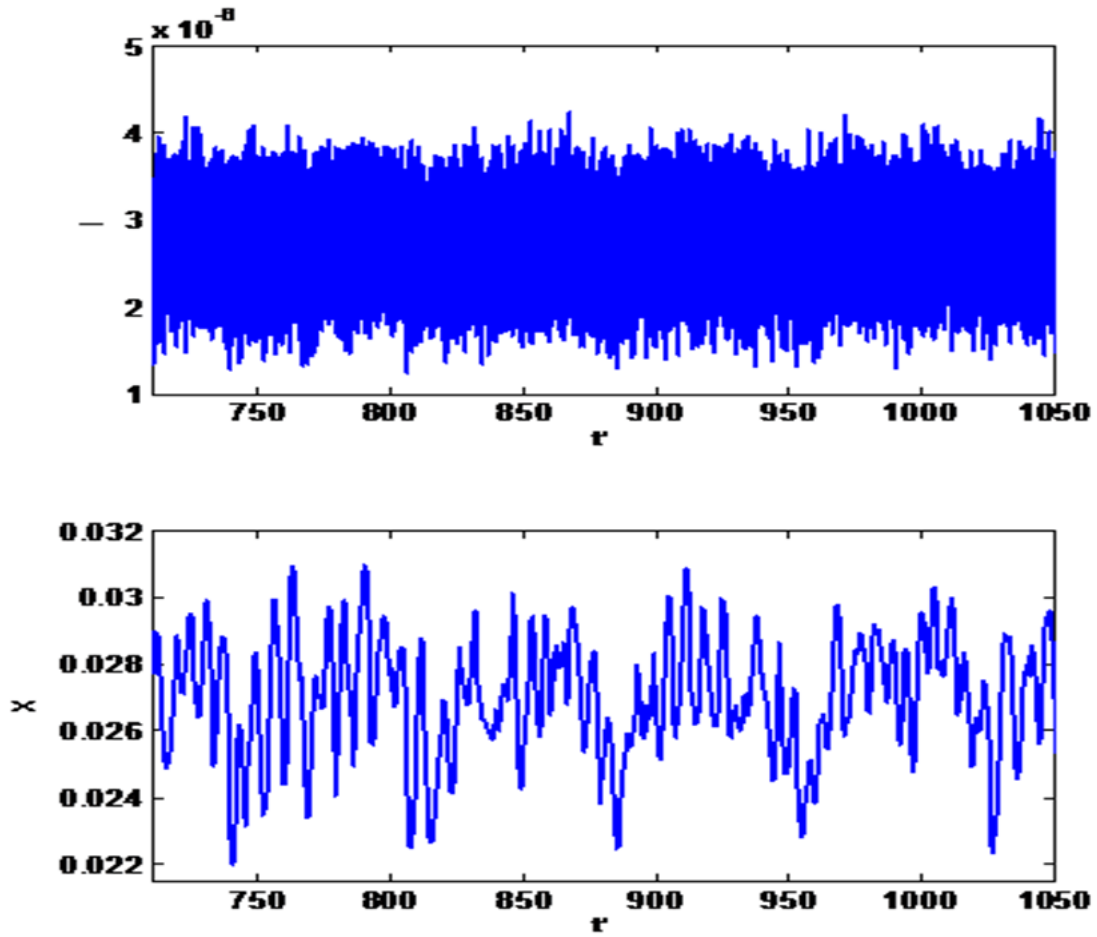


Figure 24: Time histories of the current and mechanical displacement with random frequency change: $\chi = 1$, $U_{AA} = 3.0 \times 10^{-2}$, $f_r/f_p = 1.65 \times 10^{-2}$.

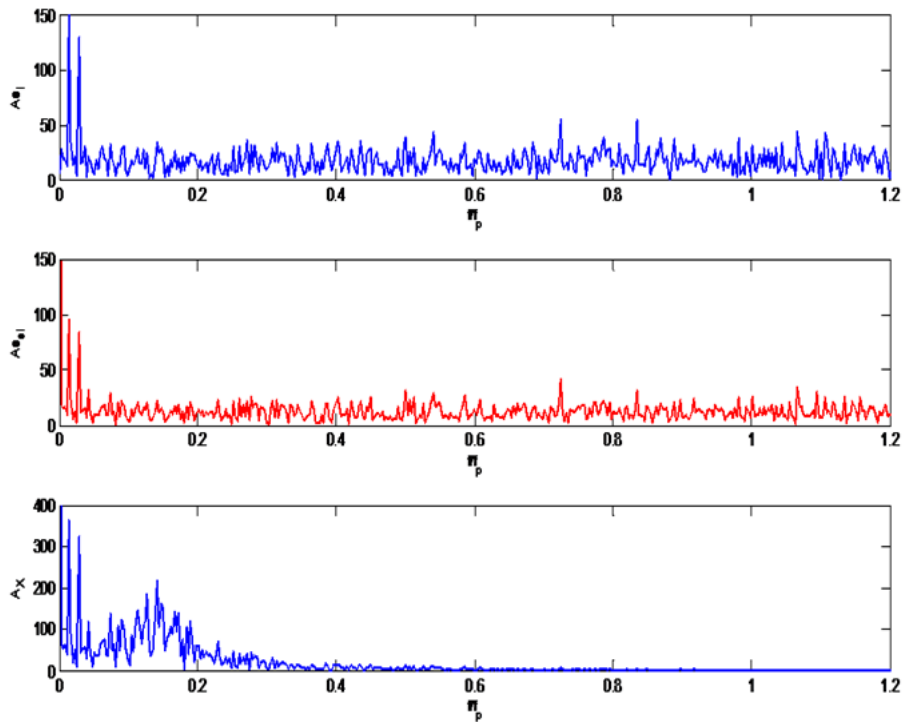


Figure 25: From top to bottom, spectrums of sinusoidal input, derived rectangular signal, and mechanical displacement with parameters of Figure 24.

variables i and x at the moment $t - \tau$, hence:

$$e_f(t) = k_B \frac{\mu_0 \mu_r N^2 i(t - \tau)}{(2(l_a + \mu_r(l_p - x(t - \tau))))}. \quad (39)$$

The injected voltage across the electromechanical system is give by:

$$e_c(t) = \frac{R_3(R_2 + R_4)}{R_2(R_1 + R_3)} e_s - \frac{R_4}{R_2} e_f. \quad (40)$$

Likewise the dynamics of the electromechanical system is given by the dimensionless equations:

$$\dot{I} + \frac{\dot{X}I}{(1 - X)} + AI(1 - X) = EE_C(1 - X) \quad (41a)$$

$$\ddot{X} + F\dot{X} + \Omega^2 X = G \frac{I^2}{(1 - X)^2} \quad (41b)$$

$$E_C = \begin{cases} +U_{BB} - K_f \frac{I(t' - \tau')}{(1 - x(t' - \tau))} & \text{if } (n_2 - 1) \frac{T_f}{T_p} \leq t' \leq (n_2 - 1 + \alpha) \frac{T_f}{T_p} \\ -K_f \frac{I(t' - \tau')}{(1 - x(t' - \tau))} & \text{if } (n_2 - 1 + \alpha) \frac{T_f}{T_p} \leq t' \leq n_2 \frac{T_f}{T_p} \end{cases}$$

with $U_{BB} = \beta \frac{R_3(R_2 + R_4)}{R_2(R_1 + R_3)} \frac{V_{CC}}{u_p}$; $K_f = \frac{k_B L_0 i_p R_4}{a(1+p)R_2 u_p}$ and n_2 an integer.

III-3-3-3- Dynamical behaviour of fluid flow frequency and pull-in servo-control

Under pull-in control we investigated numerically Eqs. (41) and we plot on Figure 27 the amplitudes of the electrical and mechanical parts without control and under control. As the feedback control is applied one observes that the amplitudes of both current and mass displacement are reduced when the applied voltage amplitude increases. Under the control the mechanical system can oscillate with larger amplitude and with larger value of the applied voltage compare to the situation without control, until reaching a limit where the pull-in comes back.

III-3-4- Excitation by the Van der Pol oscillator

III-3-4-1- Synotic diagram and model

We consider in this part the previous pump made of a ferromagnetic mass fixed on a spring subjected to an electromagnet powered by a pacemaker modelled by a VDP oscillator [58] (see Figure 28). This system acts like a cardiac assist device under the excitation of the native pacemaker, or under the excitation of an artificial pacemaker. As the VDP oscillator is described by the dimensionless equation giving the time evolution of the

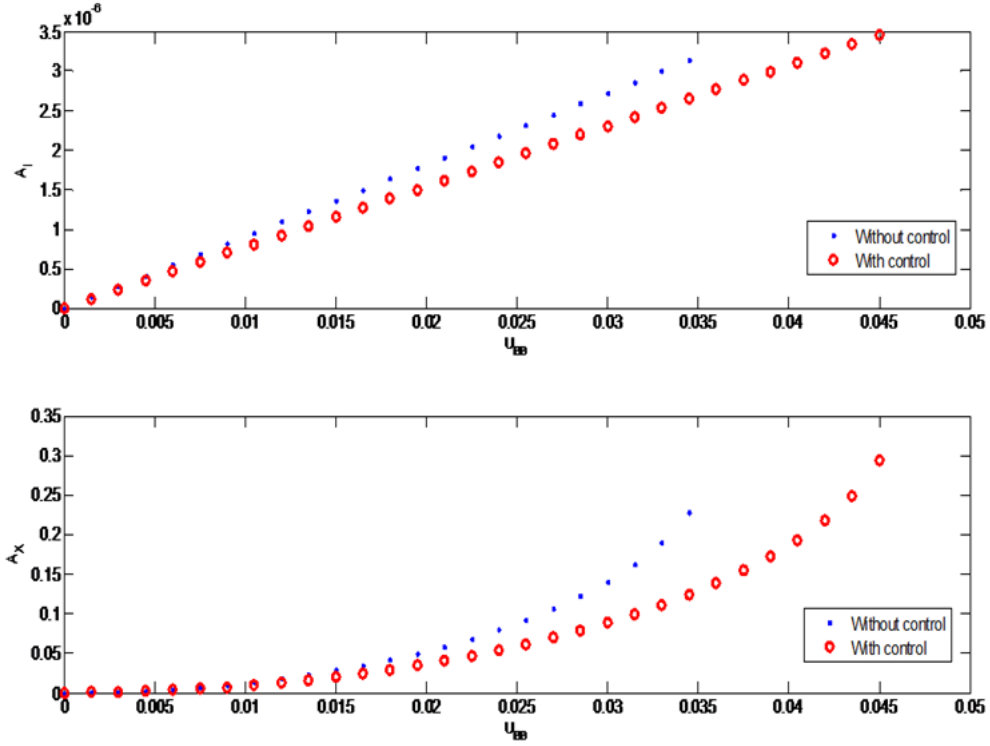


Figure 27: Amplitude response of the electrical and mechanical oscillator versus the applied voltage without and with control: $f/f_p = 1.65 \times 10^{-2}$; $\tau' = 1.0 \times 10^{-2}$; without control $K_f = 0$; with control $K_f = 10^{-3}$.

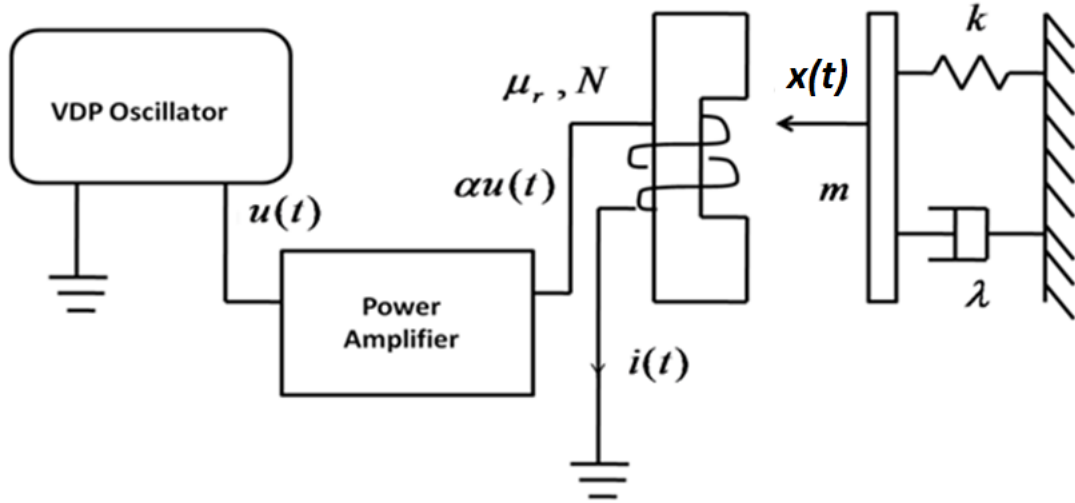


Figure 28: Synoptic diagram of the electromechanical system made of a ferromagnetic mass fixed on a spring and subjected to an electromagnet powered by a VDP electronic oscillator.

potential U

$$\ddot{U} - \varepsilon \omega_r T_p (1 - U^2) \dot{U} + \omega_r^2 T_p^2 U = \omega_r^2 T_p^2 V(t') \quad (42)$$

with ω_r its pulsation, ε the VDP nonlinear coefficient, T_p the normalization time scale, $V(t')$ the external applied voltage and t' the dimensionless time. Using the amplified

voltage αU powering our device, we have the following dimensionless equations governing our system under VDP oscillator excitation.

$$\ddot{U} - \varepsilon\omega_r T_p(1 - U^2)\dot{U} + \omega_r^2 T_p^2 U = \omega_r^2 T_p^2 V(t') \quad (43a)$$

$$\dot{I} + \frac{\dot{X}I}{(1 - X)} + AI(1 - X) = E\alpha U(1 - X) \quad (43b)$$

$$\ddot{X} + F\dot{X} + \Omega^2 X = G \frac{I^2}{(1 - X)^2} \quad (43c)$$

where the dimensionless coefficients and parameters are defined as in equation (36) with $U = u/u_p$.

III-3-4-2- Dynamical behaviour of the free electromechanical system

The external voltage applied to the VDP oscillator is set to zero, and we study the effects of the nonlinearity coefficient and that of the frequency of the VDP oscillator on the evolution of the electromechanical system, in order to analyse the effects of phenomena such as normal sinus arrhythmias in the electromechanical system.

An increase of the nonlinearity coefficient results in a progressive transformation of the behaviour of the mechanical actuator behaviour from harmonic oscillation into biperiodic and bursting oscillations with an increase of the amplitude and a decrease of the frequency (Figure 29). One also observes that as the nonlinear coefficient increases, the frequency of oscillation decreases, the maximal value of current amplification to obtain oscillation without pull-in decreases and the frequency of the bursting oscillation is equal to the double of the frequency of the VDP oscillator (not plotted). The bursting oscillations observed here are similar to those found in III-3-1-3- and can also allow high stroke pulsatile pumping in heartbeat like sequence.

Decreasing the pulsation ω_r , it is found a reduction of the amplitude of vibration of the mechanical actuator, a refinement of the bursting shape leading to a simple pulse with disappearance of negative displacement in low frequencies (Figure 30).

III-3-4-3- Effects of the parameters of the external excitation

External excitation on the native pacemaker can be done by the action of sympathetic and parasympathetic nerves, sensed here through microelectrodes, preamplified and amplified at needs. The external influence is taken into account by a DC plus square wave external voltage applied on the VDP oscillator. This voltage is taken on a continuous square wave form. The DC plus square wave signal is consistent with the analogical to digital conversion of the electrical sensed signal acting on the native pacemaker. The conversion

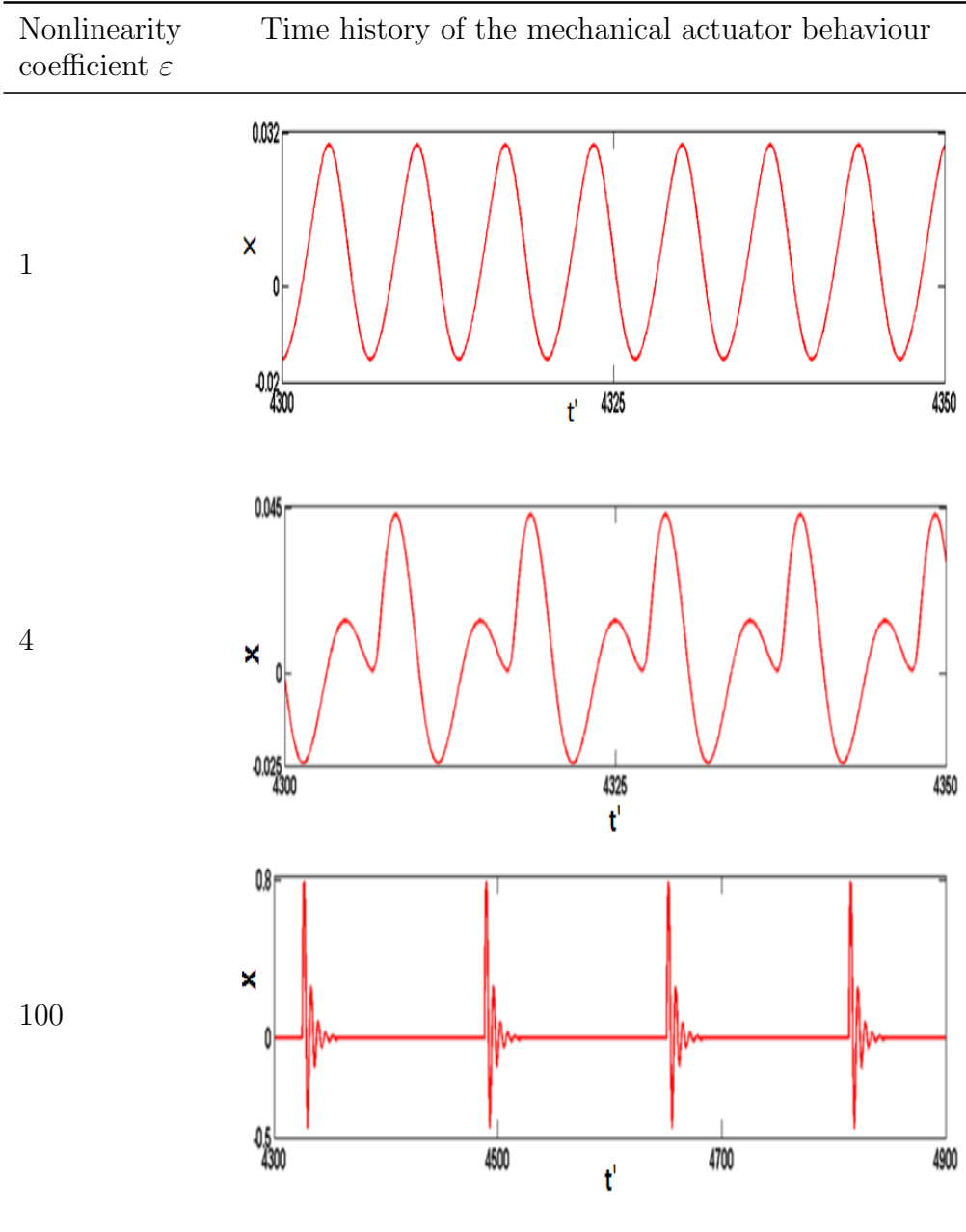


Figure 29: Time histories of the mechanical part for different values of the VDP nonlinearity coefficient ε with $\alpha = 10^{-2}, \omega_r = \omega_0/2$.

is to reduce the noises on the original sensed signal as in section dedicated to servo-control. Some results of the behaviour of the VDP oscillator under square wave can be found in Ref. [77].

As the frequency of the external applied voltage changes, the periodicities of the electrical and mechanical part are equal. Moreover as the applied signal V is at zero, the dynamics of the electrical and mechanical parts are those of the free dynamics, and when the applied voltage passes to a non zero value, the dynamics of the electrical and mechanical parts are modulated by the applied voltage (see the time histories in Figure 31). So there is a coexistence of the free dynamics and a excited dynamics in both electrical

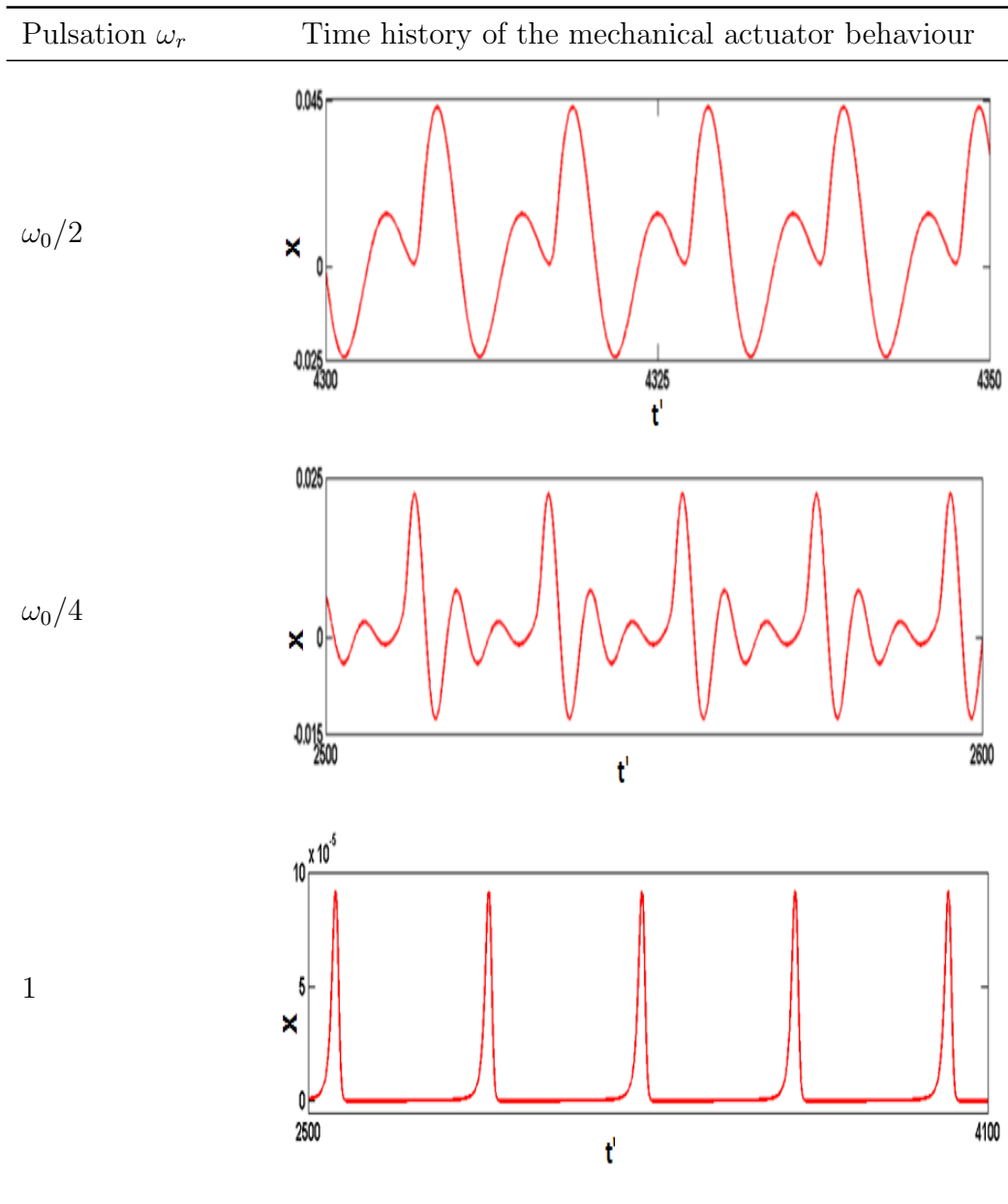


Figure 30: Time histories of the mechanical part for different values of the VDP oscillator pulsation ω_r with $\alpha = 10^{-2}$, $\varepsilon = 4$.

and mechanical parts under the form of frequency modulation. As the applied voltage frequency increases, the free dynamics vanishes.

As the amplitude of the applied voltage increases, the displacement of the mechanical part decreases because of the dispersion of the energy at higher harmonics. Moreover the free dynamics of the electrical and mechanical parts are quenched progressively (Figure 32).

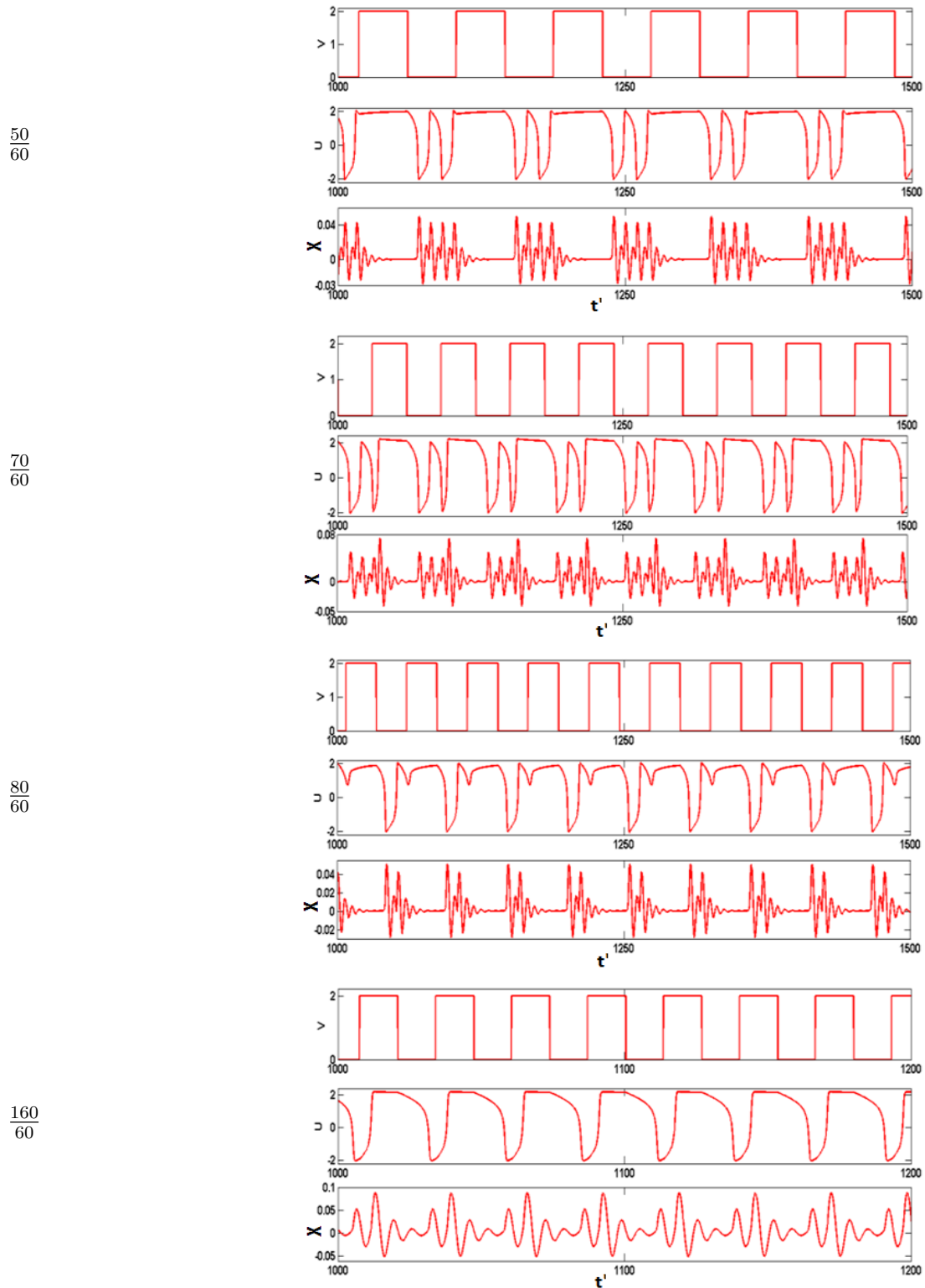
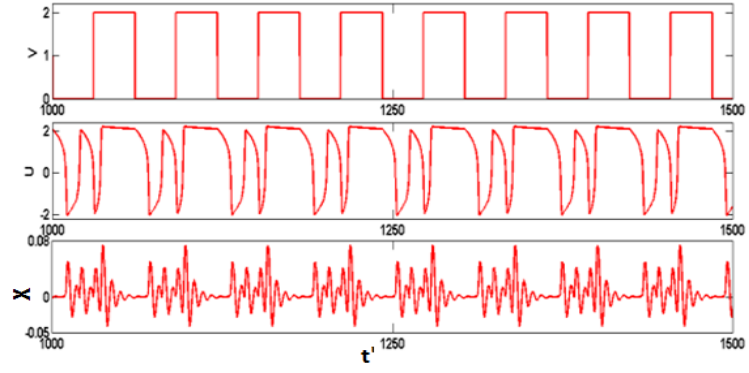
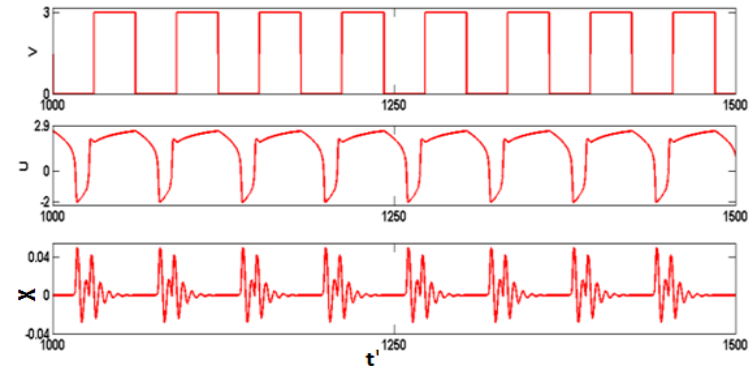


Figure 31: Time histories of the input signal, the response of the VDP oscillator and that of the mechanical part as the applied voltage frequency increases for $\alpha = 10^{-2}$, $\varepsilon = 4$, $\omega_r = \omega_0/2, V_{max} = 2, d = 50$.

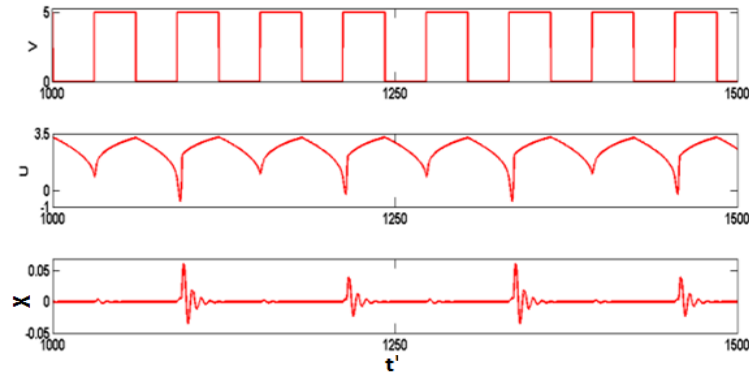
2



3



5



7

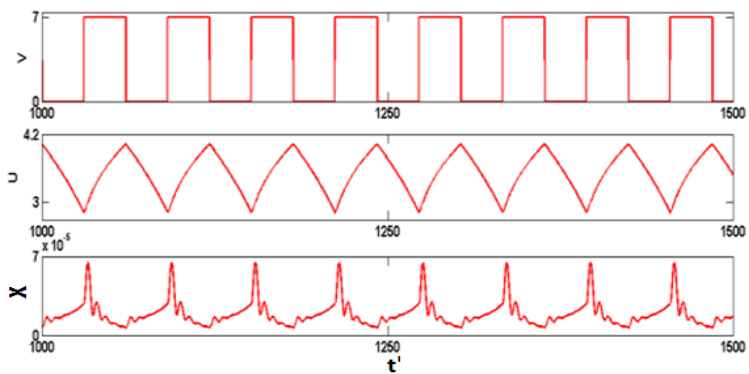


Figure 32: Time histories of the input signal, the response of the VDP oscillator and that of the mechanical part as the applied voltage amplitude increases for $\alpha = 10^{-2}$, $\varepsilon = 4$, $\omega_r = \omega_0/2$, $f = 70/60$, $d = 50$.

The duty cycle of the applied voltage can change due to the threshold used during the conversion from analogical to digital form of the electrical sensed signal. As the duty cycle

increases, the free dynamics of the electrical and mechanical displacement are quenched progressively (see Figure 33). One also observes a modulated dynamics.

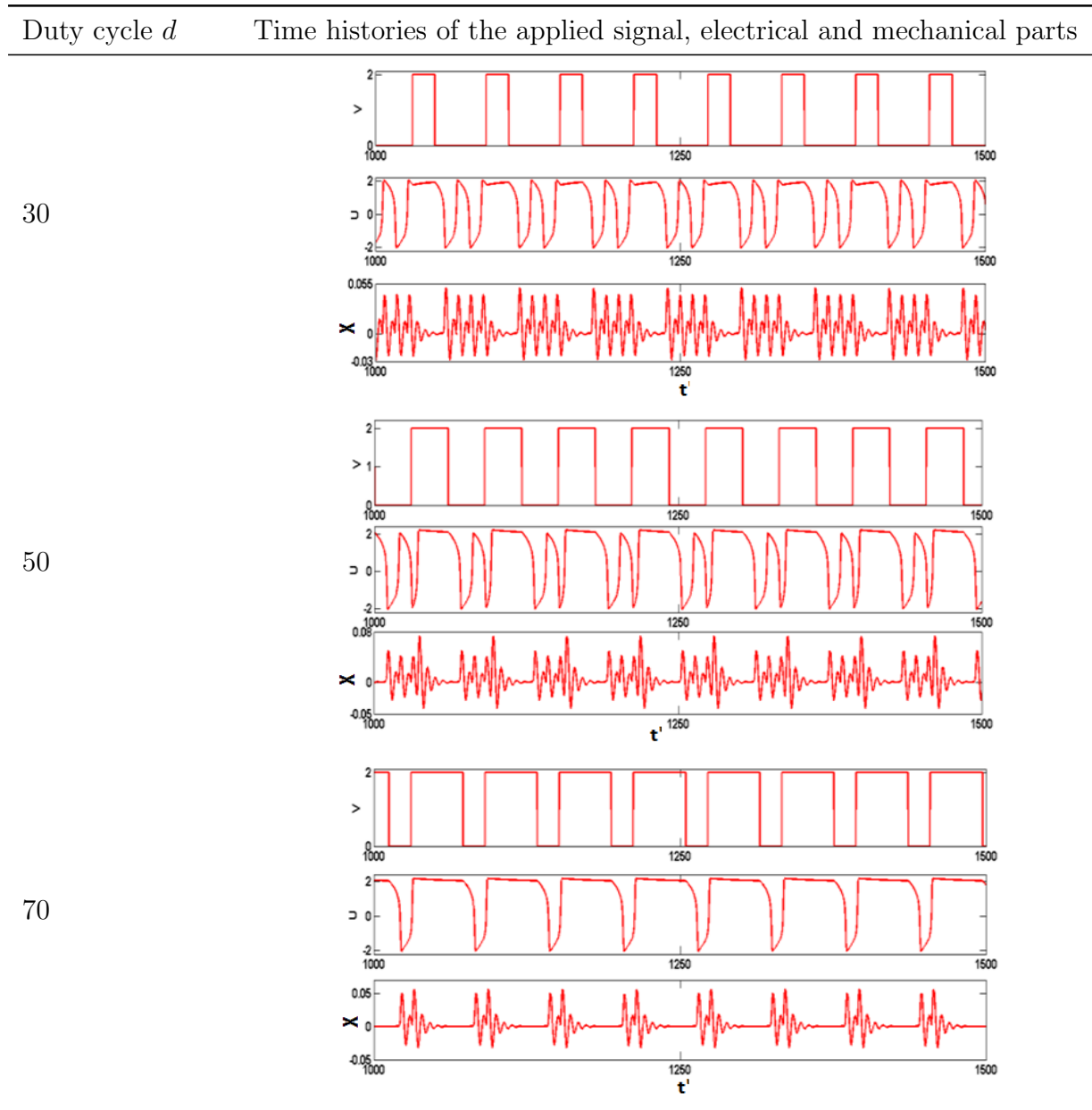


Figure 33: Time histories of the input signal, the response of the VDP oscillator and that of the mechanical part as the applied voltage duty cycle increases for $\alpha = 10^{-2}$, $\varepsilon = 4$, $\omega_r = \omega_0/2$, $f = 70/60$, $V_{max} = 2$.

The mechanical system under the free VDP oscillator excitation mode shows a transition from harmonic, periodic, biperiodic up to bursting oscillations. When the VDP oscillator is submitted to an external continuous square wave excitation, there is a coexistence of a free dynamics and a modulated dynamics. As the external applied voltage modulates the dynamics of the mechanical part, the periodicities of the applied voltage, that of the electrical oscillator and mechanical part are equal with some distortions occurring in the electromechanical system. The pulsatile shape of the mechanical system under the

VDP oscillator is like the dynamics of the myocardial muscle subjected to the natural pacemaker. An important result is that the mechanical system can show high stroke displacement (8/10 of the initial gap) in a heart like sequence without pull-in instability, under a $2V$ excitation by a VDP oscillator. A good prospect could be how to obtain a free dynamics frequency of the mechanical part equal to the one of the VDP oscillator. Also an interesting prospect could be to study the behaviour of the pump under a VDP oscillator submitted to a variable frequency excitation just like in a native heartbeat with its variable interbeat intervals.

III-3-5- Excitation by the Hindmarsh-Rose oscillator

The center of environment sensing and command of most biological systems is located in the brain. This center activity is due to neurons which, by their dynamics allow the communication among neurons and the appropriate reaction to incoming information from the environment, for an appropriate response to the need raised. As a nerve is formed of a group of neurons, in our study we focus on the effect of a single neuron on an electromechanical system acting as a cardiac assist device. This approach is to mimic the effects of sympathetic and parasympathetic innervations of the heart, through electrical signals that they deliver, signals sensed by microelectrodes, preamplified and amplified at needs. These signals are used to power an electromechanical system acting as a cardiac assist device or total artificial heart.

Neurons behaviour can be described by some models such as the Hodgkin-Huxley (HH) model, the FitzHugh–Nagumo (FN) model, and the Hindmarsh–Rose (HR) model. The FN model serves as a paradigm for type II spiking, while the HR model can exhibit spikes, bursting oscillations and chaos under the effects of an injected bias current acting as the principal bifurcation parameter [78, 79]. The choice to describe the dynamics of a neuron is set on the HR oscillator which is a simplification of the HH model. Moreover the HR oscillator is based on biological observations and possesses a rich dynamics, for a relative simplicity in case of building an equivalent analogical device for experiments.

III-3-5-1- Synoptic diagram and model

Let us consider the system on Figure 34 It is made of a HR oscillator which delivers a voltage that is amplified or attenuated to feed an electromagnet. This electromagnet attracts a ferromagnetic mass that is subjected to damping and to the elastic restoring force of a spring.

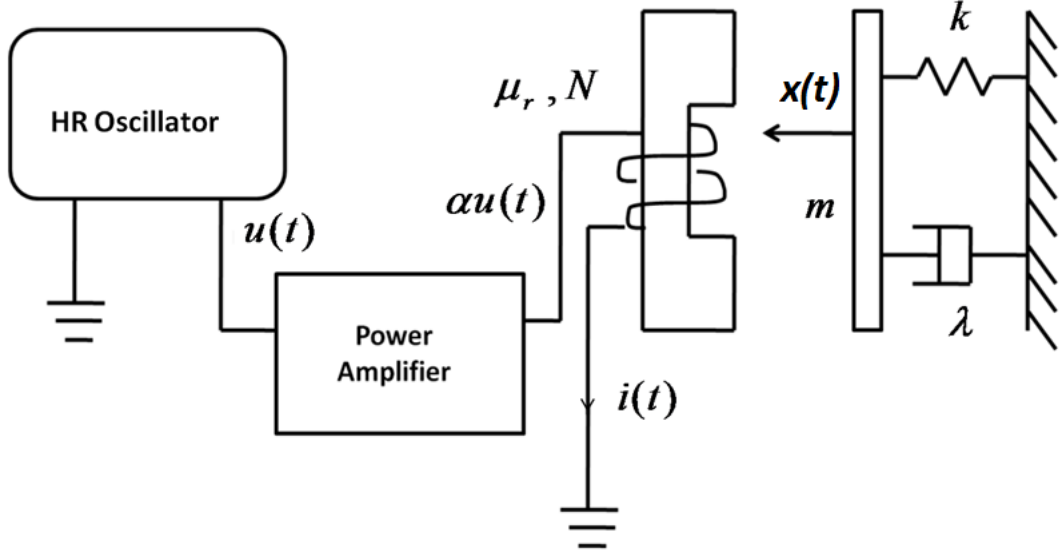


Figure 34: Synoptic diagram of the electromechanical system made of a ferromagnetic mass fixed on a spring and subjected to an electromagnet under HR voltage excitation.

The dynamical evolution of the membrane potential of the three dimensional HR oscillator is given by Hindmarsh and Rose [60] and written under the form

$$\frac{dx_m}{dt} = -x_m^3 + 3x_m^2 + y_m + I_i - z_m \quad (44a)$$

$$\frac{dy_m}{dt} = 1 - 5x_m^2 - y_m \quad (44b)$$

$$\frac{dz_m}{dt} = r_r(s_s(x_m - x_0) - z_m) \quad (44c)$$

where x_m stands for the membrane potential of the neuron, x_0 the stable subthreshold equilibrium point of the membrane potential, y_m the rapid current through the membrane and z_m the slow current through the membrane, I_i the external applied current.

Its dimensionless form is given by

$$\dot{X}_M = T_p(-X_M^3 + 3X_M^2 + X_M + I_I - Z_M) \quad (45a)$$

$$\dot{Y}_M = T_p(1 - 5X_M^2 - Y_M) \quad (45b)$$

$$\dot{Z}_M = T_p r_r(s_s(X_M - X_0) - Z_M) \quad (45c)$$

with T_p the normalization time scale, X_M stands for the dimensionless membrane potential of the neuron, Y_M the dimensionless rapid current through the membrane and Z_M the dimensionless slow current through the membrane, I_I the dimensionless external applied current and t' the dimensionless time. Using the amplified membrane voltage αX_M powering our device, we have the following dimensionless equations governing our system

under HR oscillator excitation

$$\dot{X}_M = T_p(-X_M^3 + 3X_M^2 + X_M + I_I - Z_M) \quad (46a)$$

$$\dot{Y}_M = T_p(1 - 5X_M^2 - Y_M) \quad (46b)$$

$$\dot{Z}_M = T_p T_r (s_s(X_M - X_0) - Z_M) \quad (46c)$$

$$\dot{I} + \frac{\dot{X}I}{(1-X)} + AI(1-X) = E\alpha X_M(1-X) \quad (46d)$$

$$\ddot{X} + F\dot{X} + \Omega^2 X = G \frac{I^2}{(1-X)^2} \quad (46e)$$

where the dimensionless coefficients and parameters are defined as in equation (36) with $X_M = \frac{x_m}{x_r}$; $X_0 = \frac{x_0}{x_r}$; $Y_M = \frac{y_m}{y_r}$; $Z_M = \frac{z_m}{z_r}$; $I_I = \frac{I_i}{I_r}$ and $x_r = 1$; $y_r = 1$; $z_r = 1$; $I_r = 1$.

With the parameters of Ref [78], the dynamics of the HR oscillator is well studied in Ref [79].

III-3-5-2- Dynamical behaviour of the device under DC current

To look on the effects of the value of a direct current, the applied DC current is taken outside of the parameter set giving a chaotic dynamics [3.135, 3.150] and [3.222, 3.319] where chaos to chaos transition occurs, with a continuous interior crisis [79].

As the continuous injected current increases, the HR oscillator exhibits square-wave bursting oscillations which are progressively transformed into spikes. These tonic bursting oscillations and tonic spikes are reproduced in the mechanical part (see Figure 35). The number of bursts of the HR oscillator and that of the electromechanical device increase with an increase of displacement amplitude as the value of the DC current increases.

With the choice of external current applied taken inside of the parameter set giving a chaotic dynamics [3.135, 3.150], [3.222, 3.319] where chaos to chaos transition with a continuous interior crisis occur, the chaotic bursting sequence and crisis of the HR oscillator is also reproduced in the mechanical system.

III-3-5-3- Dynamical behaviour of the device under square wave current

In order to control the frequency of the oscillator and thus the one of the electromechanical system, the injected current is taken on a square wave signal form, as it can easily allow the analysis of the effects of amplitude, periodicity and duty cycle. Moreover this square wave is consistent to the analogical to numeric signal form conversion which is more resilient to noises. Hereafter the duty cycle of the square wave current is taken at 10%.

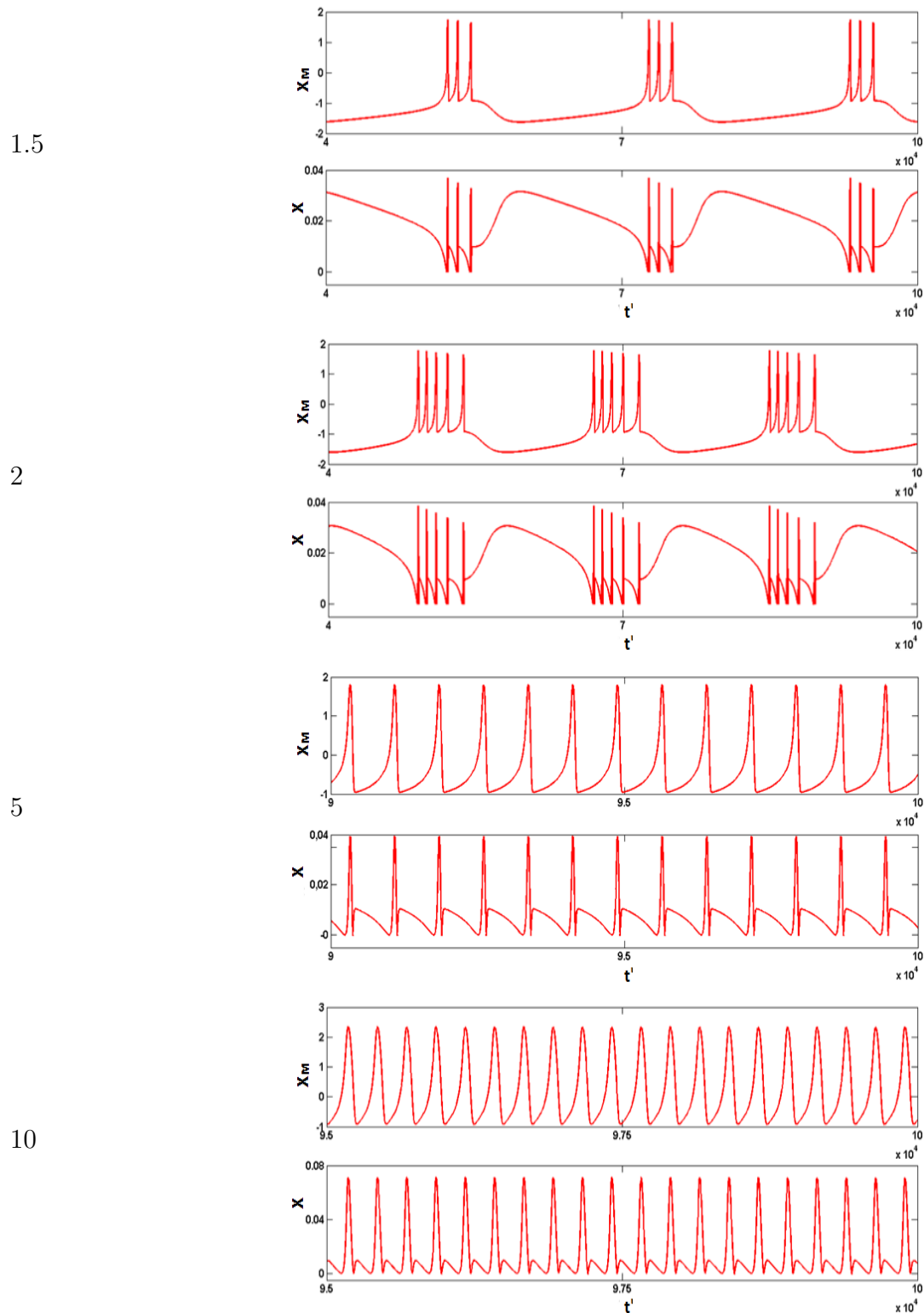


Figure 35: Time histories for different values of the applied DC current showing transition from bursting oscillations to spikes in both electrical oscillator and electromechanical system: $\alpha = 10^{-2}$, $r_r = 2.10 \times 10^{-3}$, $s_s = 4$, $X_0 = -8/5$.

As the square wave current amplitude varies, On Figure 36, it is found that in the region where in the continuous excitation leads to bursting oscillations under continuous square

wave excitation, the HR oscillator and the electromechanical device exhibit out of phase spikes. An interesting fact here is the downwards spikes of the mechanical displacement contrary to the upward behaviour seen in Figure 35.

injected current maximum $I_{I_{max}}$ Time histories of the HR oscillator and electromechanical system

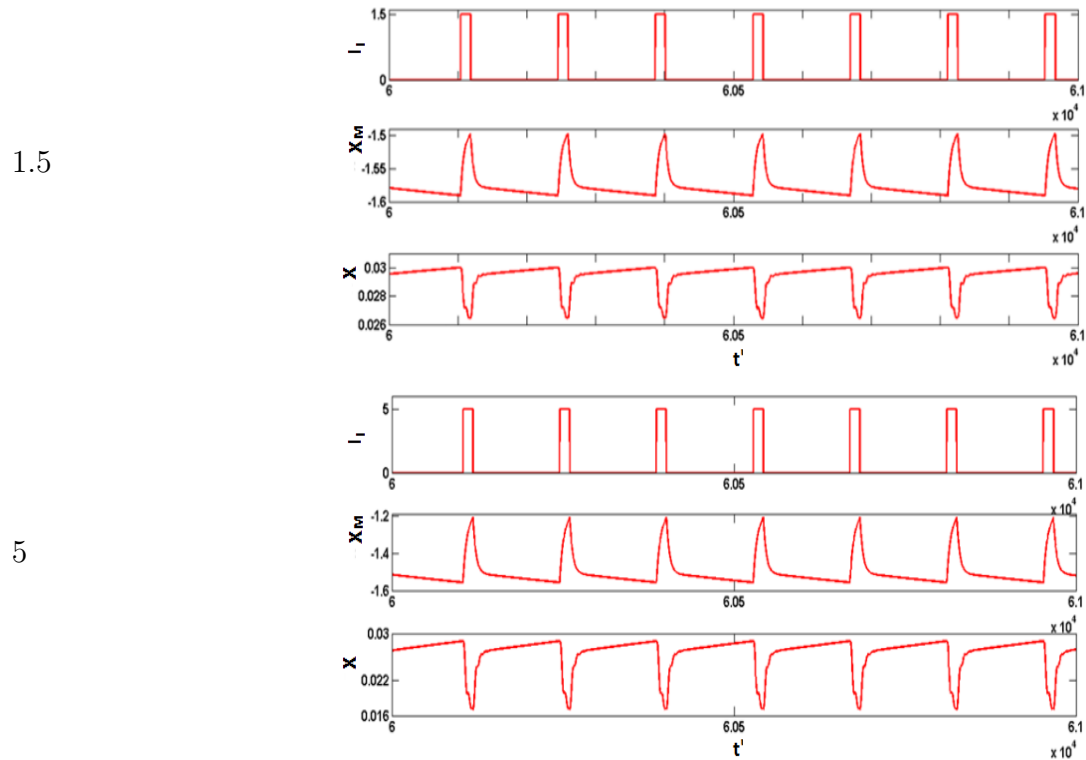


Figure 36: Time histories for different amplitudes of the square wave excitation showing the remaining spiking form in both the HR oscillator and the electromechanical system: $f = 0.5/f_p$, HR oscillator parameters of Figure 35.

At low frequency as the frequency changes, the square wave current excitation draws both the HR oscillator and electromechanical systems between two states(see Figure 37). But due to the proper rhythm of each system the transition is smoothed and both exhibit relaxation like oscillations. As the frequency increases, the HR oscillator switches between two states that come closer while the electromechanical system shows its own dynamics transitions from driven relaxation spikes, n-periodic (n being an integer) up to sinusoidal oscillations.

As the duty cycle increases for low frequency the driven relaxation oscillations become more observable, with the appearance of asymmetric and symmetric shapes.

This study has shown the transmission of spiking and bursting oscillations from an electronic Hindmarsh-Rose (HR) oscillator to our cardiac assist. Transitions from spikes,

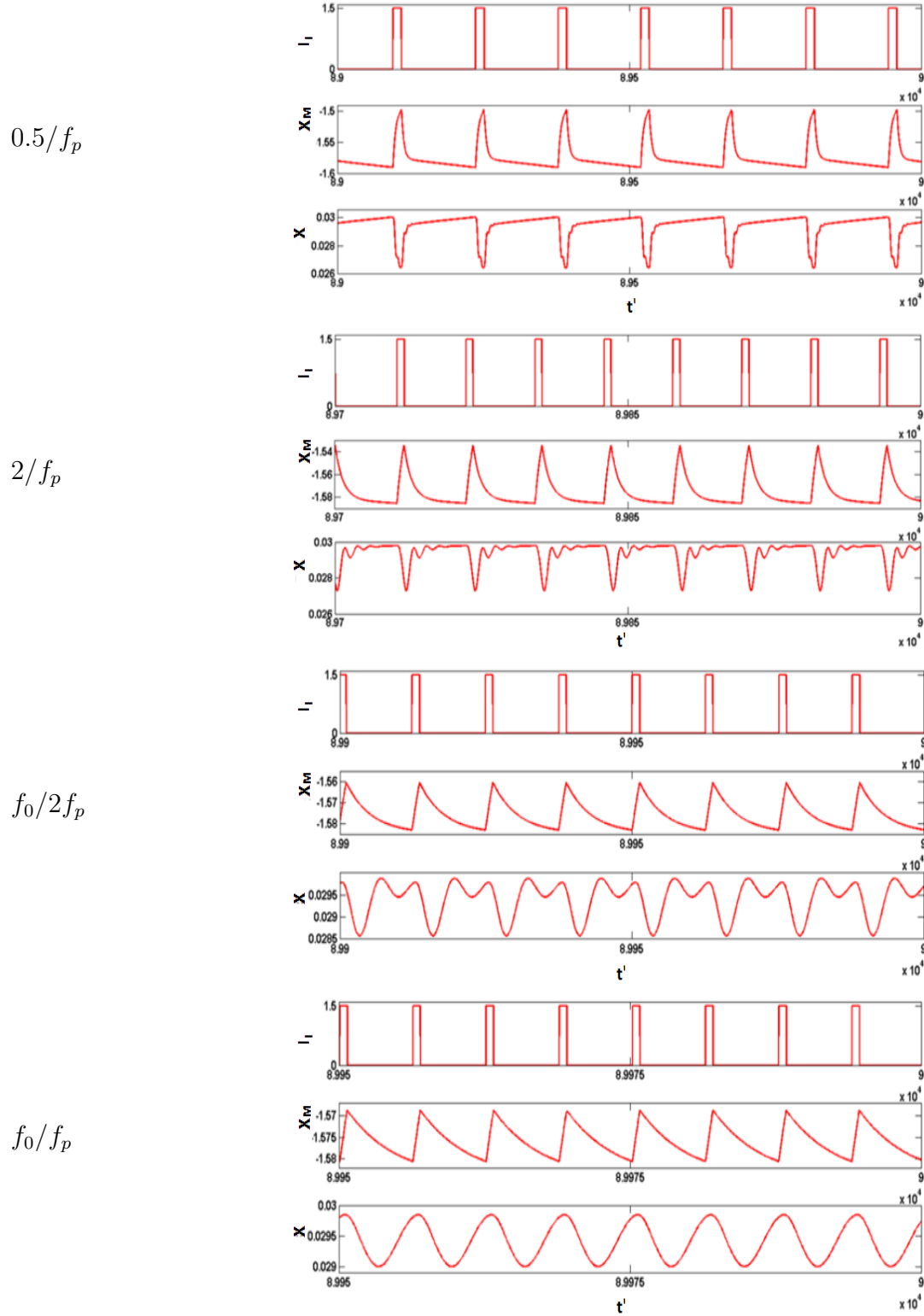


Figure 37: Time histories for different frequency values of square wave excitation showing the transition from driven distorted spikes to sinusoidal dynamics in the electromechanical system: $I_{I_{max}} = 1.5$, HR oscillator parameters of Figure 35.

bursting oscillations, relaxation spikes, multiperiodic and sinusoidal oscillations are found when the values of the parameters of the current (DC, or DC plus a square wave com-

ponent) activating the HR oscillator are varied. The HR oscillator is found to efficiently impose its bursting oscillations, spiking or driven relaxation oscillation shapes to the mechanical system at low frequency.

III-3-6- Analogical simulation of Van der Pol oscillator at low frequencies for pacemaking applications

Let us consider the following electronic circuit mounted with adder-integrator, inverter, integrator and multipliers. It is intended to pace an artificial heart at a basic frequency and to adapt the pumping function of our device to body needs, according to the sensed signal frequency $e_4(t)$. Following the approach of frequency servo-control (See III-3-2-) the signal $e_4(t)$ is obtained. Its breadboard implementation is shown on Figure 39.

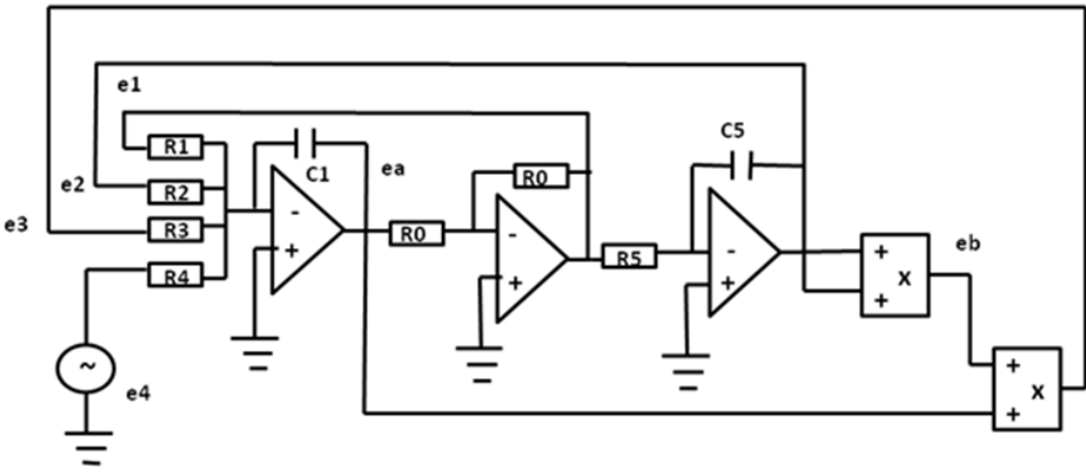


Figure 38: Analogical Van der Pol oscillator.

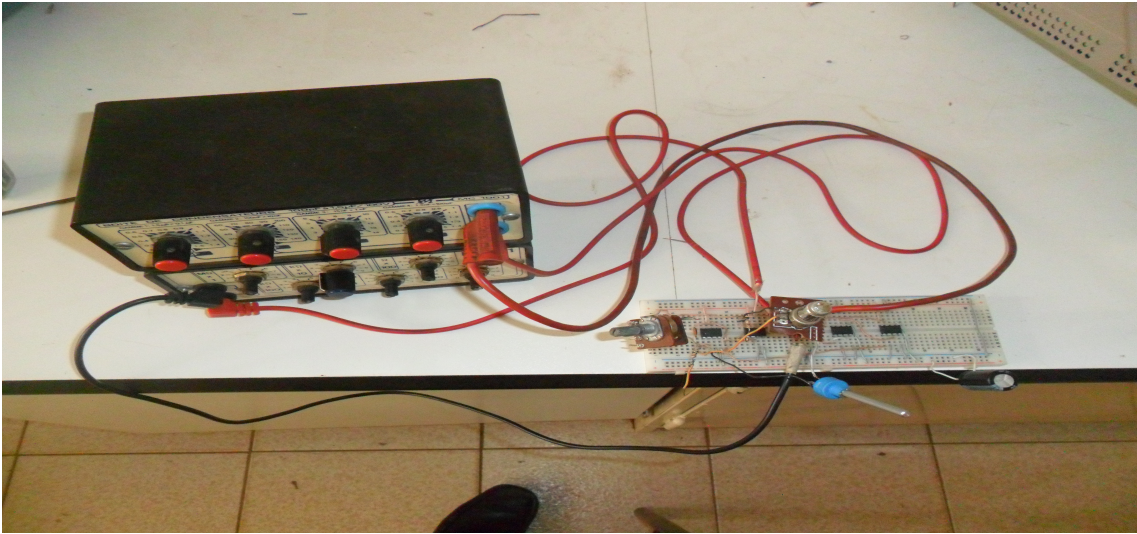


Figure 39: Breadboard implementation of the analogical Van der Pol oscillator.

Applying on it Kirchhoff's laws, we have the following equations:

$$\dot{u} = -\frac{1}{C_1} \int \left(\frac{e_1}{R_1} + \frac{e_2}{R_2} + \frac{e_3}{R_3} + \frac{e_4}{R_4} \right) dt \quad (47a)$$

$$e_a = \dot{u} \quad (47b)$$

$$e_1 = -\dot{u} \quad (47c)$$

$$e_2 = \frac{u}{R_5 C_5} \quad (47d)$$

$$e_b = \frac{e_2 \times e_2}{10} \quad (47e)$$

$$e_3 = \frac{e_a \times e_b}{10}. \quad (47f)$$

These equations can be written under the form

$$\ddot{u} - \frac{1}{R_1 C_1} \left(1 - \frac{R_1 u^2}{100 R_3 R_5^2 C_5^2} \right) \dot{u} + \frac{u}{R_2 R_5 C_1 C_5} = -\frac{e_4(t)}{R_4 C_1}. \quad (48)$$

Using the variable change $\tau = \zeta t$ and $u = u_0 U$ we have:

$$\ddot{U} - \frac{1}{\zeta R_1 C_1} \left(1 - \frac{R_1 u_0^2 U^2}{100 R_3 R_5^2 C_5^2} \right) \dot{U} + \frac{U}{R_2 R_5 C_1 C_5 \zeta^2} = -\frac{e_4(\tau)}{R_4 C_1 u_0 \zeta^2}. \quad (49)$$

Taking

$$\begin{aligned} \mu &= \frac{1}{\zeta R_1 C_1} \\ \frac{R_1 u_0^2}{100 R_3 R_5^2 C_5^2} &= 1 \\ \zeta_0^2 &= \frac{1}{R_2 R_5 C_1 C_5 \zeta^2} \end{aligned}$$

we obtain the Van der Pol equation

$$\ddot{U} - \mu(1 - U^2)\dot{U} + \zeta_0^2 U = -\frac{e_4(\tau)}{R_4 C_1 u_0 \zeta^2} \quad (51)$$

with $\zeta_0 = \frac{1}{\sqrt{R_2 R_5 C_1 C_5 \zeta^2}}$; $\mu = \frac{1}{\zeta R_1 C_1}$.

III-3-6-1- Free dynamics

The signal $e_4(t)$ is taken equal to zero. For two sets of components values, we have on Figure 40 analogical simulation giving times histories and phase diagram. The signal given by the y_1 probe is $e_2 = \frac{u}{R_5 C_5}$ and $e_a = \dot{u}$ is given by the probe y_2 . One observes qualitative similarity between numerical signals of Figure 41 and analogical ones of Figure 40, with a time reversal observed on analogical signals compare to numerical ones at the same

frequency. It is observed that low frequency affects electronic components, in such a way that the number of peaks of the analogical signal can be reproduced within the same time interval at the same frequency for a different value of the VDP nonlinearity coefficient, shifting the observed behaviour for higher values of the VDP nonlinearity coefficient.

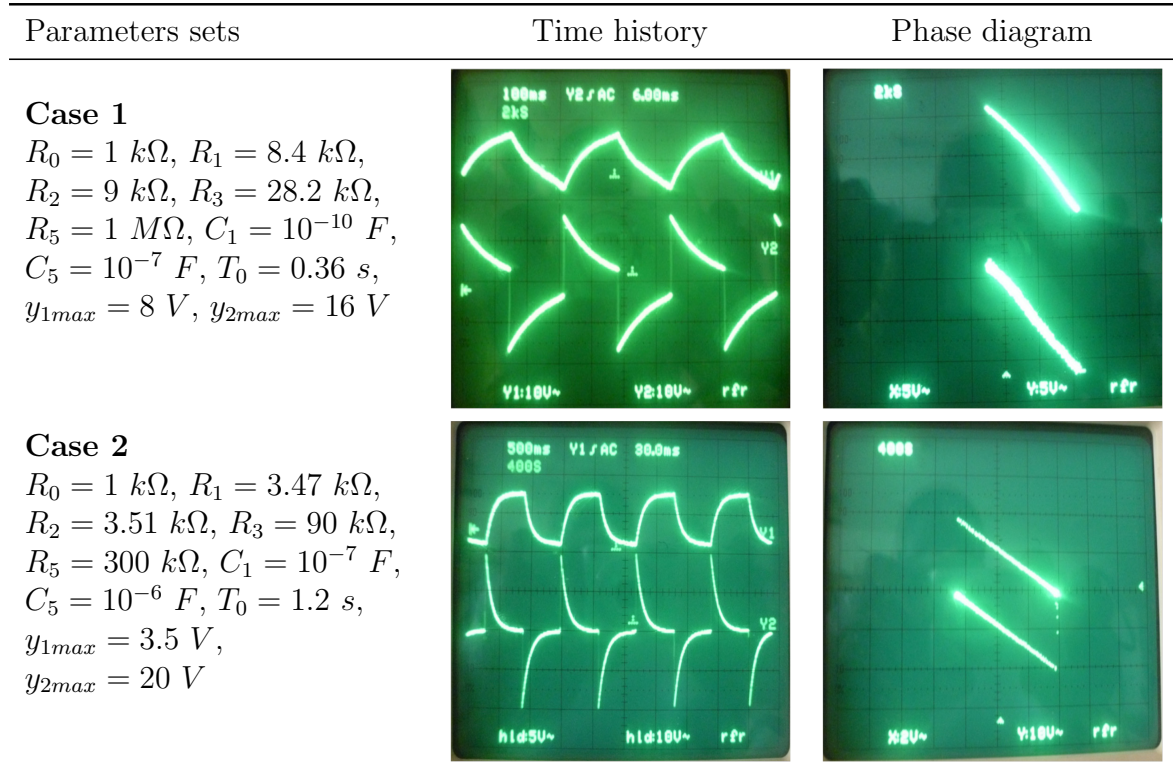


Figure 40: Low frequency signals of VDP oscillator and parameters sets.

Numerical results for comparison are shown in Figure 41. One should observe as the frequency is well defined, the number of peaks within the same time frame is linked to the nonlinearity coefficient hence, although the nonlinearity coefficient obtained for the analogical simulation are very high ($\mu = 6233$ when $T_0 = 0.36$ and $\mu = 154$ when $T_0 = 1.2$) a comparison can be done using the nonlinearity coefficient that gives the closest number of peaks within the same time frame (See Figure 41). Moreover the nonlinearity coefficient can be varied to obtain the same shape as on the analogical signal (See Figure 42).

As observation, the analogical simulation although not accurate at the level of nonlinearity coefficient, can allow the use of the oscillator as a VDP oscillator at low frequency.

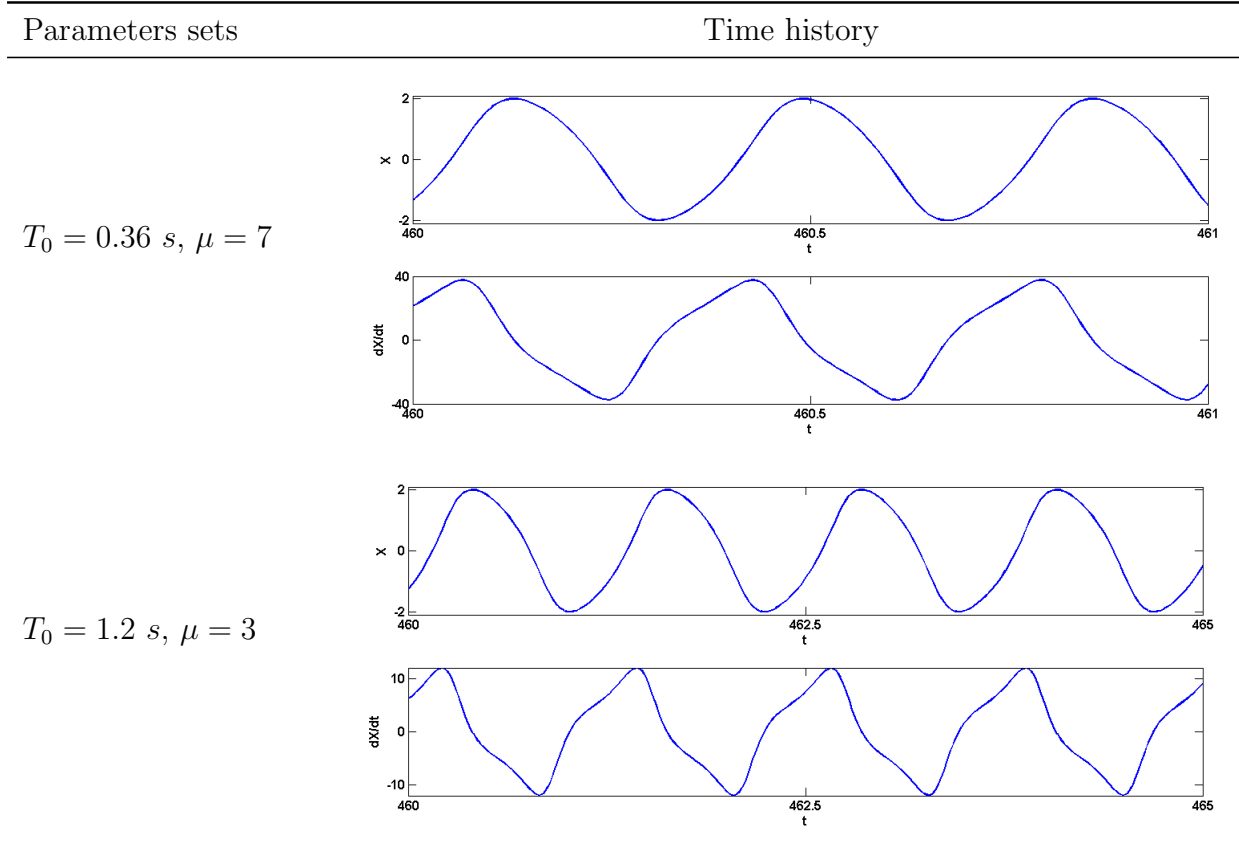


Figure 41: Numerical signals of VDP oscillator and parameters sets.

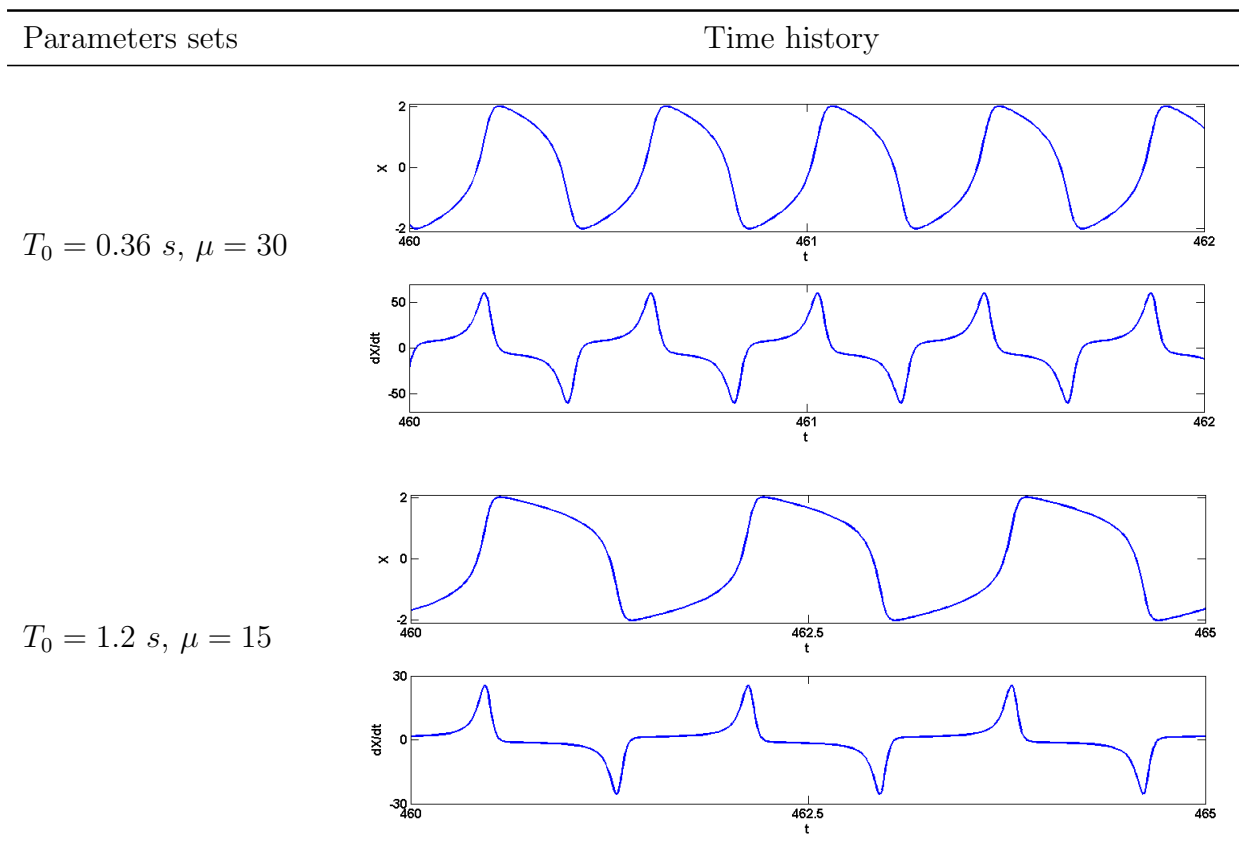


Figure 42: Closest numerical signals of VDP oscillator and parameters sets.

III-3-6-2- Excited dynamics

Using the servo-control approach of III-3-2-, the signal $e_4(t)$ is taken different from zero. To perform analogical simulations the duty cycle is equal to 50. Figure 43 show the free dynamics, the excitation signals and the resulting VDP signal under square wave excitation.

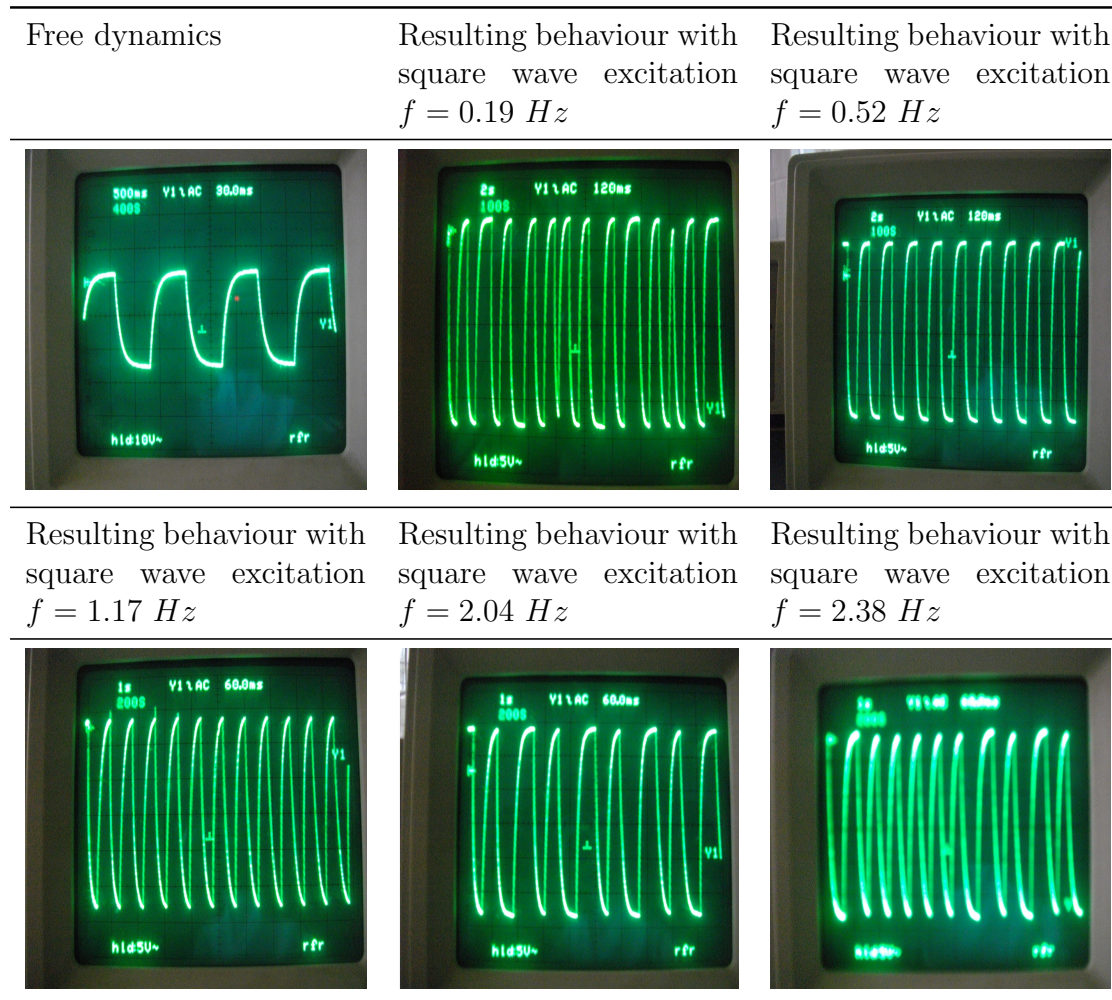


Figure 43: VDP oscillator under various square wave excitation.

Although the square wave signal generated by the low frequency generator is distorted, frequency modulation behaviour is similar to the one observe in III-3-4-3-, in the case of external frequency effects on the VDP oscillator where there is a coexistence of the free dynamics and an excited one.

It is worthy to note that some experiments with a preliminary prototype is underway, but as the device is a low impedance device, at low voltage the current called for the device to function well is important so that the low frequency generator available could not drive such a load. To reduce the power needs the ferromagnetic iron core taken from recycled transformers that has a relative magnetic permeability of about 1200, could be

replaced by material such as mumetal or superpermalloy having greater relative magnetic permeability.

III-3-7- Other applications of the device

As the proposed device can be used to adapt directly the rhythm of pumping to external fluctuation without invasive components with more flexibility, this strategy using fluid flow frequency servo-control can be extended to other positive displacement pumps to obtain an efficient, better and flexible response. Hence with sump pumps used in homes and draining pumps used to prevent overflows in sewers and floods, efficiency will be improved by fluid flow frequency servo-control as the incoming runoff water frequency increases, pumping frequency increases evacuating at the same rhythm water overflow.

In this sense sump and sewage pumps performances can be optimized when facing unsteadiness in residential areas, due to the influence of the environment. Since in case of high rainfall and snow melting, to avoid floods, pumps can be used. Their efficiency in floods avoidance can be optimized by their ability to adapt, to the rhythm of unsteady surface water runoff.

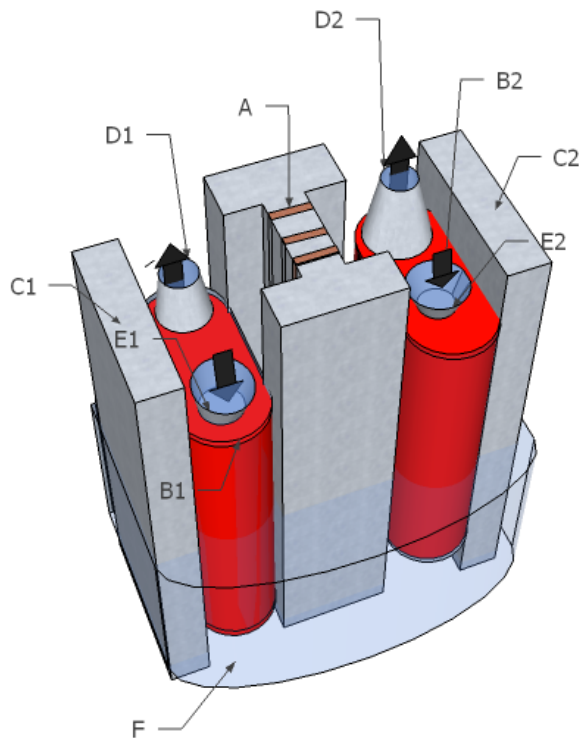
III-4- Biventricular heart based on ferromagnetic masses actuated by an electromagnet

Biventricular assist devices are used when both native right and left ventricle have defects, that means in the case where the need for an artificial heart is rushing to pump blood in both pulmonary and systemic circulation to prevent imminent death. The device we present here is intended to help in these critical cases.

III-4-1- Description of the device and mathematical model

III-4-1-1- Description of the BIVAD-TAH

On Figure 44 the device is made of two internal pockets, the left biocompatible elastic internal pocket and the right biocompatible elastic internal pocket. Between the two, is placed an electromagnet that send magnetic flux toward each of the ferromagnetic blades attached to each of the pocket in front of him. As a current flow in the electromagnet, magnetic lifting forces act on each of the blades therefore each of the blades is pulled toward the electromagnet compressing by the way the blood contained in each of the pocket. According to the form of the injected current the pumping process can be sustained.



- A: Electromagnet
- B1: Left biocompatible elastic internal blood pocket
- B2: Right biocompatible elastic internal blood pocket
- C1: Left ferromagnetic blade
- C2: Right ferromagnetic blade
- D1: Left outlet with valve
- D2: Right outlet with valve
- E1: Left inlet with valve
- E2: Right inlet with valve
- F: Biocompatible elastic external pocket

Figure 44: Isometric view of biventricular assist device (total artificial heart) model.

To obtain a BIVAD the device can be servo-controlled to the native heart by sensors. In this case the rhythm of the native heart could be passed to the BIVAD as in III-3-2- and III-3-3- To obtain a TAH the device should have associated to him a low frequency oscillator to command the pumping rhythm at rest with a servo-control to parasympathetic and sympathetic nerves, as in III-3-4- and III-3-5-.

III-4-1-2- Model of the BIVAD-TAH

The device of Figure 44 is also simplified for analysis under the form of Figure 45. The device shown on Figure 45 is made of two ferromagnetic blades of masses m_1 and m_2 fixed each on a spring and subjected to the action of an electromagnet under variable current and to damping. The electrical part is made of a circuit that has an inductor L (electromagnet inductance), a resistor (wiring resistance) supplied by a voltage source $u(t) = Ug(2\pi ft)$, t being the time, U the voltage amplitude, f the frequency, g the generative function.

The coupling between both parts is realized by the magnetic circuit, and in the mechanical part coupling between the two subsystems is made by the total flux shared. When a current flows through the coil of the electromagnet, it induces a magnetic flux in the core of the electromagnet, shared among the two magnetic subcircuits. Hence lifting forces attract each of the ferromagnetic masses toward the near electromagnet according to the signal at input.

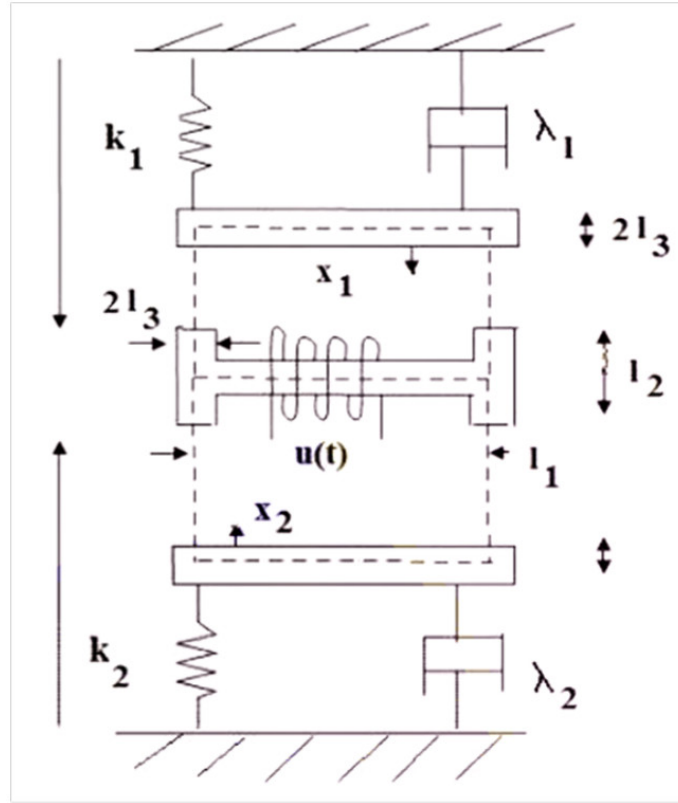


Figure 45: Simplification of BIVAD-TAH.

Using Hoppkinson's law in the mean magnetic circuit represented with dash-lines, assuming that magnetic circuit saturation is neglected, and ignoring leakage and fringing fluxes, the total flux flowing in the first and second magnetic circuits are respectively:

$$\Phi_1 = L_1 i = \frac{a \mu_0 \mu_r N^2 i}{2(l_1 + l_2 + l_3 + \mu_r e_1)} \quad (52)$$

$$\Phi_2 = L_2 i = \frac{a \mu_0 \mu_r N^2 i}{2(l_1 + l_2 + l_3 + \mu_r e_2)} \quad (53)$$

with $i(t)$ the current, a the cross section of the coil, $\mu_0 \mu_r$, the magnetic permeability of the electromagnet iron core. The mean circuit delineated by dash lines has the following dimensions: l_1, l_2, e_1 and e_2 with

$$e_1 = l_4 - l_0 - 2l_3 - x_1 \quad (54)$$

$$e_2 = l_4 - l_0 - 2l_3 - x_2 \quad (55)$$

e_1 , and e_2 being the gap between the free edge of the moving masses and the free edge of the proximal electromagnet, $2l_3$ is the ferromagnetic blade and the electromagnet thickness, l_0 the unload spring length, l_4 the distance between the fixed part of the spring and the free edge of the electromagnet that can be in contact with the moving blades, x_1 and x_2 are the displacement of the first and second mass respectively.

Using Ohm's law in the electrical circuit, one obtains

$$\frac{d\Phi}{dt} + \frac{\rho NP_m}{s} i = u(t) \quad (56)$$

where $\Phi = \Phi_1 + \Phi_2$ is the total flux shared, ρ is the wire resistivity, N the coil number of turns, P_m the coil mean perimeter, s the wire cross section. Hence the equation describing the electrical phenomena in the electrical part is (assuming no capacitor in the circuit) is:

$$\begin{aligned} & \left(\frac{a\mu_0\mu_r N^2}{2(l_1 + l_2 + l_3 + \mu_r(l_4 - l_0 - 2l_3 - x_1))} + \frac{a\mu_0\mu_r N^2}{2(l_1 + l_2 + l_3 + \mu_r(l_4 - l_0 - 2l_3 - x_2))} \right) \frac{di}{dt} + \\ & \frac{a\mu_0\mu_r^2 N^2 i}{2(l_1 + l_2 + l_3 + \mu_r(l_4 - l_0 - 2l_3 - x_1))^2} \frac{dx_1}{dt} + \frac{a\mu_0\mu_r^2 N^2 i}{2(l_1 + l_2 + l_3 + \mu_r(l_4 - l_0 - 2l_3 - x_2))^2} \frac{dx_2}{dt} + \\ & + \frac{\rho NP_m}{s} i = u(t). \end{aligned} \quad (57)$$

Taking the mechanical parts, their dynamics are described by the following equations

$$m_1 \frac{d^2 x_1}{dt^2} + \lambda_1 \frac{dx_1}{dt} + k_1 x_1 = \frac{1}{2} \frac{\partial W_{1mag}}{\partial x_1} \quad (58)$$

$$m_2 \frac{d^2 x_2}{dt^2} + \lambda_2 \frac{dx_2}{dt} + k_2 x_2 = \frac{1}{2} \frac{\partial W_{2mag}}{\partial x_2} \quad (59)$$

where m_1 and m_2 the respective masses of the first and second moving masses, λ_1 and λ_2 the damping coefficients affecting the movement of the first and second mass respectively, k_1 and k_2 the stiffness of the springs attached to the first and second mass respectively; $W_{1mag} = L_1(x)i^2$, $W_{2mag} = L_2(x)i^2$ the magnetic energy in the first and second magnetic circuit.

Replacing $L_1(x)$ and $L_2(x)$ by their expression derived from equation (52) and (53), one obtains

$$m_1 \frac{d^2 x_1}{dt^2} + \lambda_1 \frac{dx_1}{dt} + k_1 x_1 = \frac{a\mu_0\mu_r^2 N^2 i^2}{4(l_1 + l_2 + l_3 + \mu_r(l_4 - l_0 - 2l_3 - x_1))^2} \quad (60)$$

$$m_2 \frac{d^2 x_2}{dt^2} + \lambda_2 \frac{dx_2}{dt} + k_2 x_2 = \frac{a\mu_0\mu_r^2 N^2 i^2}{4(l_1 + l_2 + l_3 + \mu_r(l_4 - l_0 - 2l_3 - x_2))^2}. \quad (61)$$

Therefore the electromechanical system is described by the set of equations (57), (60) and (61). Introducing the normalization and change of variables, the equations of motion

(57), (60) and (61) are reduced to the following form:

$$\begin{aligned} \dot{I} + \frac{I}{(2 - X_1 - X_2)} \left(\frac{1 - X_2}{1 - X_1} \dot{X}_1 + \frac{1 - X_1}{1 - X_2} \dot{X}_2 \right) + AI(1 + p) \frac{(1 - X_1)(1 - X_2)}{(2 - X_1 - X_2)} \\ = EU_0(1 + p) \frac{(1 - X_1)(1 - X_2)}{(2 - X_1 - X_2)} g(2\pi f T_p \tau) \end{aligned} \quad (62a)$$

$$\ddot{X}_1 + F_1 \dot{X}_1 + \Omega_1^2 X_1 = G_1 \frac{p^2 I^2}{(1 + p)^3 (1 - X_1)^2} \quad (62b)$$

$$\ddot{X}_2 + F_2 \dot{X}_2 + \Omega_2^2 X_2 = G_2 \frac{p^2 I^2}{(1 + p)^3 (1 - X_2)^2} \quad (62c)$$

$$\begin{aligned} \text{with } X_1 = \frac{px_1}{(1+p)l_p}; \quad X_2 = \frac{px_2}{(1+p)l_p}; \quad I = \frac{i}{i_p}; \quad \tau = \frac{t}{T_p}; \quad U_0 = \frac{U}{u_p}; \\ l_p = l_4 - l_0 - 2l_3; \quad l_a = l_1 + l_2 + l_3; \quad i_p = \frac{2l_p T_p u_p}{a\mu_0}; \quad T_p^2 = \frac{m_1}{k_1}; \quad L_0 = \frac{a\mu_0 \mu_r N^2}{2l_a}; \\ p = \frac{\mu_r l_p}{l_a}; \quad A = \frac{\rho N P_m}{s L_0} T_p; \quad E = \frac{1}{N^2 p}; \quad F_1 = \frac{\lambda_1 T_p}{m_1}; \quad F_2 = \frac{\lambda_2 T_p}{m_2}; \\ \omega_0^2 = \frac{k_1}{m_1}; \quad \Omega_1^2 = 1; \quad \Omega_2^2 = \frac{m_1 k_2}{m_2 k_1}; \quad G_1 = \frac{L_0 T_p^2 i_p^2}{2m_1 l_p^2}; \quad G_2 = \frac{L_0 T_p^2 i_p^2}{2m_2 l_p^2}. \end{aligned}$$

Taking $\lambda_1 = \lambda_2 = \lambda$ and using the change of variables

$$\frac{k_1}{k_2} = \alpha \quad (63)$$

$$\frac{m_1}{m_2} = \beta \quad (64)$$

a more reduced form of equations (62) can be obtained, and the dynamics of our system is described by:

$$\begin{aligned} \dot{I} + \frac{I}{(2 - X_1 - X_2)} \left(\frac{1 - X_2}{1 - X_1} \dot{X}_1 + \frac{1 - X_1}{1 - X_2} \dot{X}_2 \right) + AI(1 + p) \frac{(1 - X_1)(1 - X_2)}{(2 - X_1 - X_2)} \\ = EU_0(1 + p) \frac{(1 - X_1)(1 - X_2)}{(2 - X_1 - X_2)} g(2\pi f T_p \tau) \end{aligned} \quad (65a)$$

$$\ddot{X}_1 + F_1 \dot{X}_1 + X_1 = G_1 \frac{p^2 I^2}{(1 + p)^3 (1 - X_1)^2} \quad (65b)$$

$$\ddot{X}_2 + \beta F_1 \dot{X}_2 + \frac{\beta}{\alpha} X_2 = \beta G_1 \frac{p^2 I^2}{(1 + p)^3 (1 - X_2)^2} \quad (65c)$$

with $F_2 = \beta F_1$; $\Omega_2^2 = \frac{\beta}{\alpha}$; $G_2 = \beta G_1$.

III-4-2- Dynamical behaviour of the device

III-4-2-1- Free vibration approach analysis

It is observed that the dynamics of a mass fixed on a spring and subjected to the action of an electromagnet in the case of linear electronic RL device can be given by:

$$\ddot{X} + F\dot{X} + \Omega^2 X = \frac{Gp^2 I^2}{(1+p)^3(1-X)^2}. \quad (66)$$

This system under sinusoidal signal has an equation similar to that giving the dynamics of a Micro-Electro-Mechanical System(MEMS) with a nonlinearity from capacitors as studied by Luo and Wang [74] in the absence of damping. Main results they obtained are the characteristic equilibrium points, natural frequency bands and responses, resonances conditions, chaotic motion in a certain frequency band.

To complete the study of our system in the case of the dynamics of the mechanical part, one can thus assume that a sinusoidal excitation on our system leads to a small influence of the mechanical part on the electrical part, hence we take in this sense a dimensionless current under the form $I(\tau) = I_0 \sin(2\pi f T_p \tau + \phi_I)$ where ϕ_I is the phase difference between the voltage and the current.

The equilibrium points satisfy the following equation

$$X^e(1 - X^e)^2 = Q_a \quad (67)$$

with

$$Q_0 = Q_2 = \frac{Gp^2 I_0^2}{2(1+p)^3}$$

$Q_a = Q_0$ for the first mass and $Q_a = \alpha Q_0$ for the second mass.

The eigenvalues derived from equation (67) are

$$\lambda_{1,2}^{(n)} = \pm \frac{F}{2} \sqrt{\frac{F^2}{4} + \frac{1}{\Omega_a^2} \left(\frac{2Q_a}{(1 - X_n^e)^3} - 1 \right)} \quad (68)$$

with $\Omega_a = 1$ for the first mass and $\Omega_a = \frac{\beta}{\alpha}$ for the second mass.

For stable equilibrium the maximum value of Q_a is given by $Q_a = Q_{amax} = 4/27$, $X_1^e = X_2^e = 1/3$, where possible vibration amplitude equal to zero. Following the results of Ref. [74], vibrations occur only for $Q_a < Q_{amax}$ and the $(2M : 1)$ resonance can be found (there is no chaotic motion near the resonant separatrix).

Applying the above analysis on the two mechanical systems, the following observations can be made:

- $\alpha < 1$, the first mechanical subsystem vibrations are quenched while the second one is still oscillating
- $\alpha = 1$, the two mechanical subsystems vibrations are quenched at the same time
- $\alpha > 1$, the second mechanical subsystem vibrations are quenched while the first one is still oscillating

III-4-2-2- Harmonic balance method approach

Assuming small dimensionless displacement and neglecting the influence of the mechanical part on the electrical part, one obtains equations (69)

$$\dot{I} + \frac{1}{2}AI(1+p) = \frac{1}{2}EU_0(1+p)\sin(w_p\tau) \quad (69a)$$

$$\ddot{X}_1 + F_1\dot{X}_1 + X_1 = G_1\frac{p^2I^2}{(1+p)^3} \quad (69b)$$

$$\ddot{X}_2 + \beta F_1\dot{X}_2 + \frac{\beta}{\alpha}X_2 = \beta G_1\frac{p^2I^2}{(1+p)^3}. \quad (69c)$$

Using the harmonic balance method to solve equations (69), the solution can be given as

$$I(\tau) = I_1\cos(w_p\tau) + I_2\sin(w_p\tau)$$

with

$$I_1 = \frac{-2w_pEU_0(1+p)}{4w_p^2 + A^2(1+p)^2} \quad (70)$$

$$I_2 = \frac{A(1+p)^2EU_0}{4w_p^2 + A^2(1+p)^2}. \quad (71)$$

The compact form gives

$$I(\tau) = I_0\sin(w_p\tau + \phi_I)$$

with

$$I_0 = \frac{EU_0(1+p)}{\sqrt{4w_p^2 + A^2(1+p)^2}} \quad (72)$$

with

$$\tan \phi_I = \frac{-2w_p}{A(1+p)}. \quad (73)$$

With these expressions of the electric current, the displacements of the mechanical parts are obtained as

$$X_1 = \frac{G_1 p^2 I_0^2}{2(1+p)^3} + \frac{G_1 I_0^2 p^2}{2(1+p)^3 \sqrt{1 + 4w_p^2(4w_p^2 + F_1^2 - 2)}} \sin(2w_p \tau + \phi_1) \quad (74)$$

$$X_2 = \frac{\alpha G_1 p^2 I_0^2}{2(1+p)^3} + \frac{\alpha \beta G_1 I_0^2 p^2}{2(1+p)^3 \sqrt{\beta^2 + 4\alpha w_p^2(4\alpha w_p^2 + \alpha \beta^2 F_1^2 - 2\beta)}} \sin(2w_p \tau + \phi_2). \quad (75)$$

The phase differences are given as:

$$\tan \phi_1 = \frac{(I_1^2 - I_2^2) - 4w_p(w_p I_1^2 - w_p I_2^2 + I_1 I_2 F_1)}{2(w_p F_1 (I_1^2 - I_2^2) - I_1 I_2 (4w_p^2 - 1))} \quad (76)$$

$$\tan \phi_2 = \frac{\beta(I_1^2 - I_2^2) - 4w_p \alpha (w_p I_1^2 - w_p I_2^2 + \beta I_1 I_2 F_1)}{2(\alpha \beta w_p F_1 (I_1^2 - I_2^2) - I_1 I_2 (4\alpha w_p^2 - \beta))}. \quad (77)$$

One should note that the mean positions of the masses given by equations (74) and (75) are different from the equilibrium points given by equations (67).

In the text A_1 and A_2 stand for the vibration amplitudes of the first and second masses respectively, X_1^m and X_2^m for the mean positions of the first and second masses respectively

Figures 46, 47, 48 and 49 show the variation of the amplitudes of the displacements, in terms of the frequency, the masses ratio, the stiffness coefficients ratio, and the voltage amplitude respectively. A good agreement is found and thus gives the domain of validity of such an approximation.

On Figure 46, one observes agreement on the resonance frequencies of both masses with a difference on quantitative aspects. On Figure 47, it is found that for both analytical and numerical results, as the value of the ratio between the stiffness coefficients increases from $\alpha = 1.00$, the amplitude of vibration of the second mass increases until $\alpha = 1.10$ where it is maximal. Above this value as the ratio increases, the vibration amplitudes of the second mass decreases monotonously, having the same amplitude as for $\alpha = 1.00$ at $\alpha = 1.23$.

We observe on Figure 48 that as the value of the ratio between the masses increases, on both analytical and numerical results, the vibration amplitude of the second mass decreases monotonously starting from the vibration amplitude of the first mass.

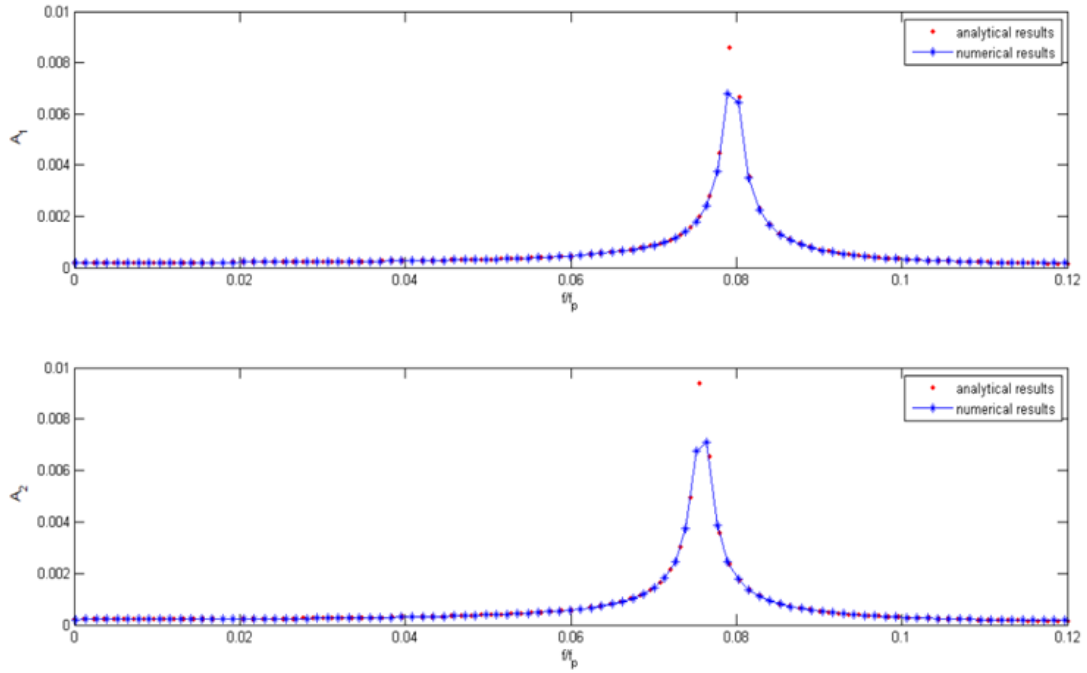


Figure 46: Variation of the amplitude of vibration in term of the frequency obtained from the analytical derivation and the numerical simulation for small displacement: $U_0 = 1.50 \times 10^{-1}$, $\alpha = 1.10$, $\beta = 1.00$ (sinusoidal power).

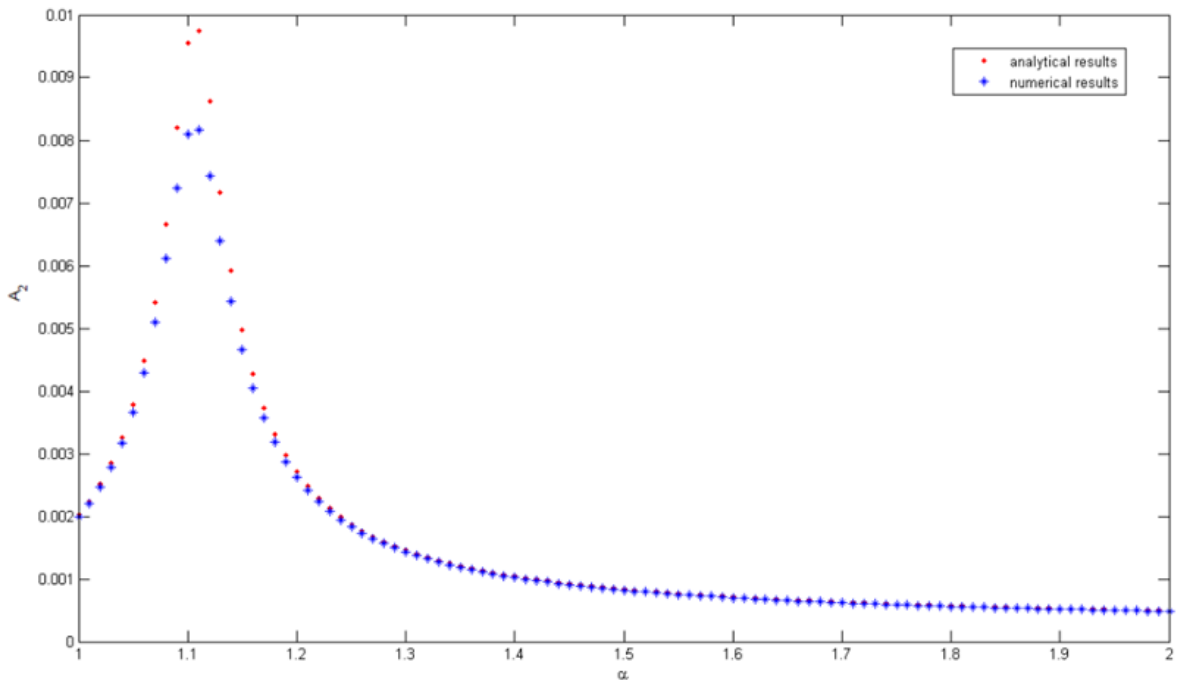


Figure 47: Variation of the amplitude of vibration of the second mass in term of the stiffness coefficients ratio obtained from the analytical derivation and the numerical simulation for small displacement: $f/f_p = 7.56 \times 10^{-2}$, $U_0 = 1.50 \times 10^{-1}$, $\beta = 1.00$.

It is observed on Figure 49 that as the applied voltage increases, the vibration amplitude increases and divergence between the analytical and numerical results is larger for the second mass. A good precision on the results is obtained for values of applied voltage for

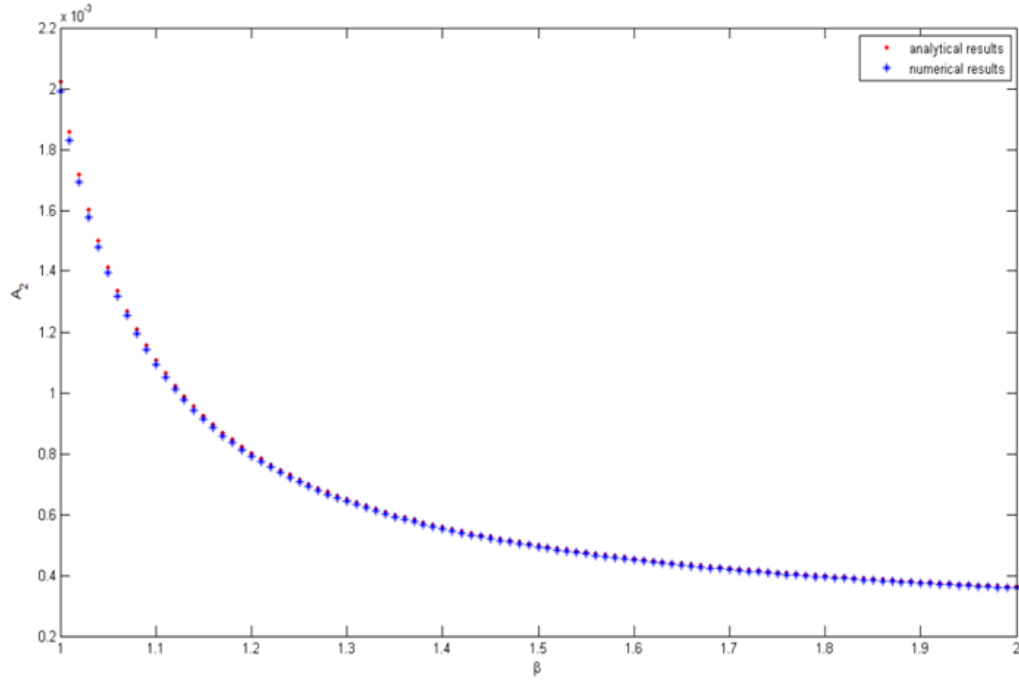


Figure 48: Variation of the amplitude of vibration of the second mass in term of the masses ratio obtained from the analytical derivation and the numerical simulation for small displacement: $f/f_p = 7.56 \times 10^{-2}$, $U_0 = 1.50 \times 10^{-1}$, $\alpha = 1.00$.

the first mass less than $U_0 = 0.8$ and $U_0 = 0.5$ for the second mass. Above 1.35 both masses are bound to the electromagnet as found from the numerical simulation.

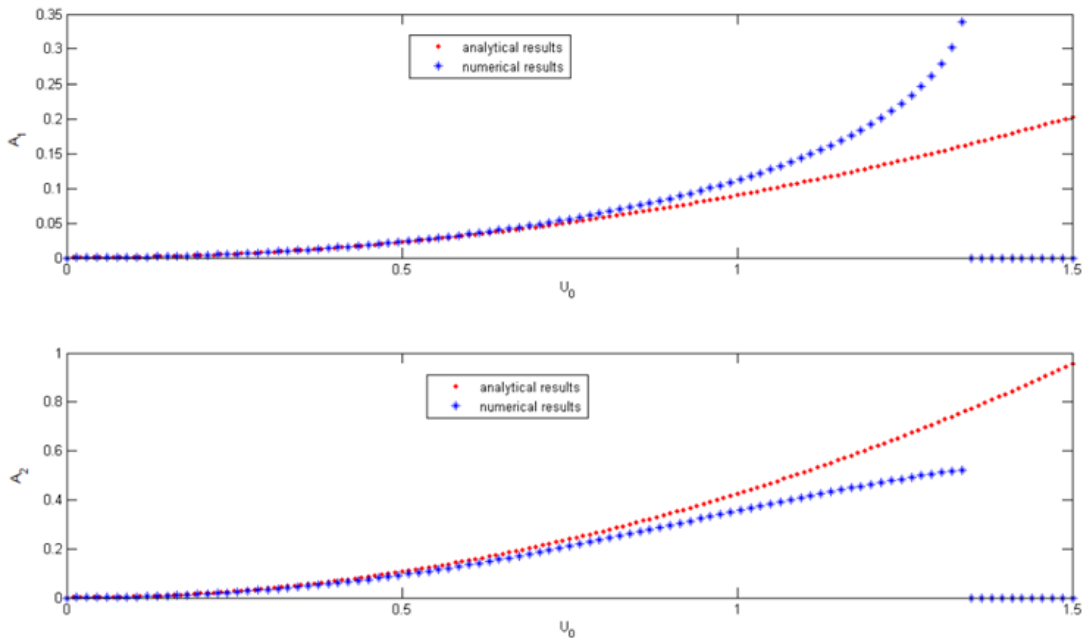


Figure 49: Variation of the amplitude of vibration in term of the voltage amplitude obtained from the analytical derivation and the numerical simulation for small displacement: $f/f_p = 7.56 \times 10^{-2}$, $\alpha = 1.10$, $\beta = 1.00$.

III-4-2-3- The resonant pull-in condition

Using the method used in Ref. [75] to obtain the resonant pull-in condition, on equations (65b) and (65c), taking into account that the potential energy curves determine the evolution of the whole system energy, one have pull-in in the mechanical systems when respective displacements reach or go beyond the considered unstable potential energy equilibrium points [76]. Taking the extreme point of the energy function under sinusoidal excitation $I = I_0 \sin(w_p \tau + \phi_I)$ we have as maximum potential energy responsible of the pull-in in the first and second mass respectively:

$$E_{p1} = \frac{1}{2}X_1^2 - \frac{G_1 p^2 I_0^2}{(1+p)^3(1-X_1)} \quad (78)$$

$$E_{p2} = \frac{\beta}{2\alpha}X_2^2 - \frac{\beta G_1 p^2 I_0^2}{(1+p)^3(1-X_2)}. \quad (79)$$

The equilibrium points of the potential energy are solution of the equation

$$X_p^e(1 - X_p^e)^2 = 2Q_a \quad (80)$$

with Q_a define as before.

Hence for the values of the unstable potential energy equilibrium point obtain as in Ref. [74] we have

$$X_{p1}^e = \frac{2}{3} + \Psi \sqrt[3]{\frac{b_1}{2} + \sqrt{\Delta_1}} + \Psi^2 \sqrt[3]{\frac{-b_1}{2} + \sqrt{\Delta_1}} \quad (81)$$

$$X_{p2}^e = \frac{2}{3} + \Psi \sqrt[3]{\frac{b_2}{2} + \sqrt{\Delta_1}} + \Psi^2 \sqrt[3]{\frac{-b_2}{2} + \sqrt{\Delta_2}} \quad (82)$$

where

$$\Delta_1 = \left(\frac{b_1}{2}\right)^2 + \left(\frac{p_1}{3}\right)^3; \Delta_2 = \left(\frac{b_2}{2}\right)^2 + \left(\frac{p_2}{3}\right)^3; p_1 = p_2 = -\frac{1}{3}; b_1 = \frac{2}{27} - 2Q_0;$$

$$b_2 = \frac{2}{27} - 2\alpha Q_0; \Psi = \frac{-1 + i\sqrt{3}}{2}; i = \sqrt{-1}.$$

Therefore one have as pull-in conditions

$$X_1 \geq X_{p1}^e \quad (83)$$

$$X_2 \geq X_{p2}^e. \quad (84)$$

When $\Delta_1 = 0$ or $\Delta_2 = 0$ the respective maximum displacement of the considered mass without pull-in, is reduced to $\frac{1}{3}$ the value obtain in the case of DC excitation.

Taking as parameters and natural frequency as in III-3-2-3- with $m_1 = 20 \text{ g}$, $k_1 = 100 \text{ N/m}$, $N = 80$, $A = 1.14 \times 10^{-1}$, $F_1 = 2.12 \times 10^{-2}$, $G_1 = 2.04 \times 10^{12}$, a numerical simulation is carried out using the fourth-order Runge-Kutta algorithm applied on the full equations (65).

III-4-2-4- Effects of the frequency

Figure 50a shows the variation of vibration amplitude of the mechanical part as the frequency varies, when $\alpha = 1.1$ and $\beta = 1$. Two resonances are found at $f_{r11} = 7.86 \times 10^{-2} f_p$ and $f_{r21} = 3.94 \times 10^{-2} f_p$ for the first mass, and also two resonances are found at $f_{r12} = 7.48 \times 10^{-2} f_p$ and $f_{r22} = 3.76 \times 10^{-2} f_p$ for the second mass. These two states correspond to two subharmonic resonances of the type $f_{01}/2$ and $f_{01}/4$, for the first mass and of the type $f_{02}/2$ and $f_{02}/4$, for the second mass. The displacement amplitudes at these points are respectively 4.06×10^{-1} , 1.4×10^{-2} for the first mass and 4.4×10^{-1} , 1.6×10^{-2} . As predicted, we observe that for $\alpha > 1$, the second mass has a higher amplitude dynamics.

Keeping the same parameters and taking $\alpha = 1$ and $\beta = 1.1$, we observe on Figure 50b that the resonances for the second mass are observed at $f_{r12} = 8.24 \times 10^{-2} f_p$ and $f_{r22} = 4.13 \times 10^{-2} f_p$ where the amplitudes are respectively 3.8×10^{-1} , 1.4×10^{-2} . Thus increasing only the ratio between the stiffness leads to a decrease of the subharmonics resonance frequencies for the second subsystem and an increase of the respective oscillations amplitudes. On the other side, increasing only the ratio between the masses leads to an increase of the subharmonics resonance frequencies for the second subsystem and a decrease of the respective oscillations amplitudes.

III-4-2-5- Effects of voltage amplitude

The frequency is taken equal to that of the subharmonic oscillation, that is $f_0/2$. It is observed on Figure 51 in the case where $\alpha = 1.00$ that the oscillation amplitude of the mechanical part increases monotonously till $U_0 = 1.10$ where it exhibits hysteresis between $U_0 = 1.10$ and $U_0 = 1.35$.

Between $U_0 = 1.35$ and $U_0 = 1.45$, high amplitudes vibrations are observed, and between $U_0 = 1.45$ and $U_0 = 1.70$, is obtained a zone where oscillations are sensitive to initial conditions. After $U_0 = 1.70$, the mass is bound to the electromagnet.

For some other values of $\alpha > 1$, one observes that the second mechanical oscillator has a higher amplitude dynamics. For $\alpha = 1.05$, hysteresis for the second mass is observed between $U_0 = 1.10$ and $U_0 = 1.23$, and the jump interval at hysteresis is smaller. The

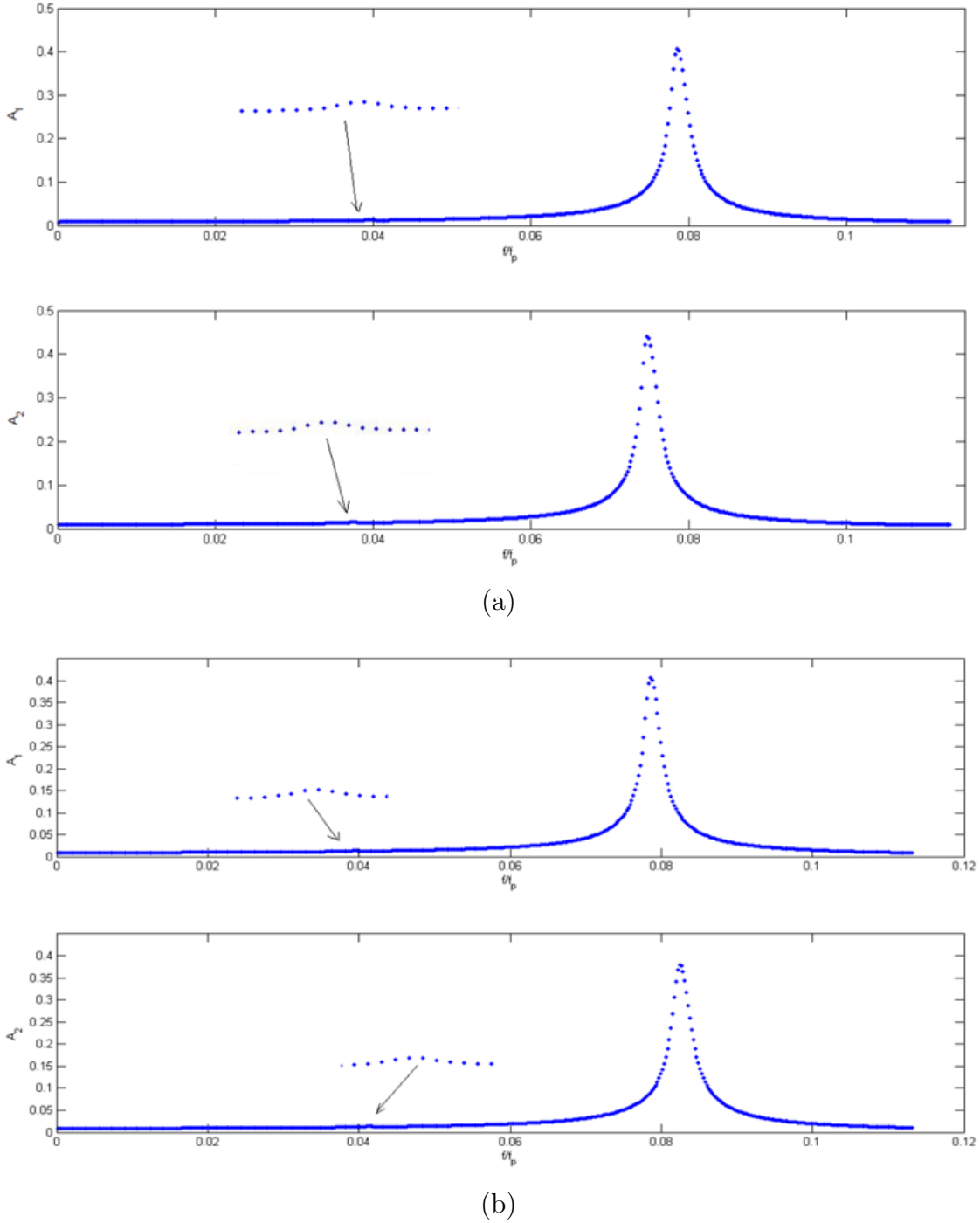
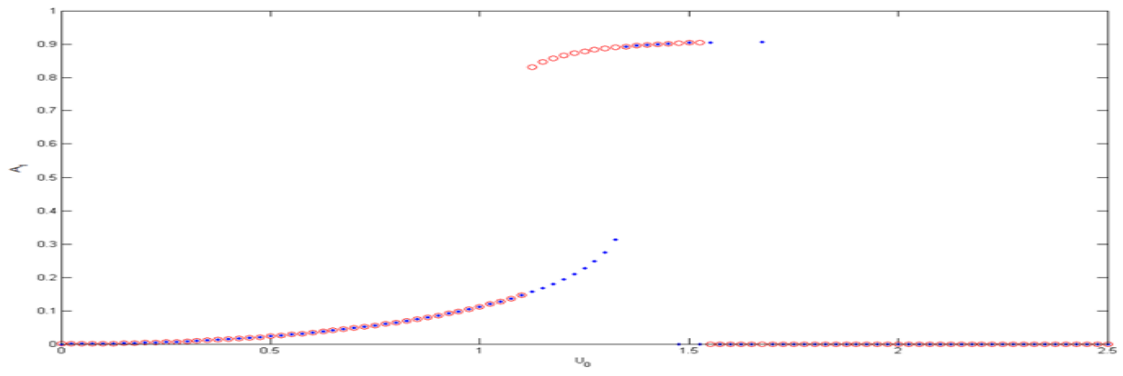


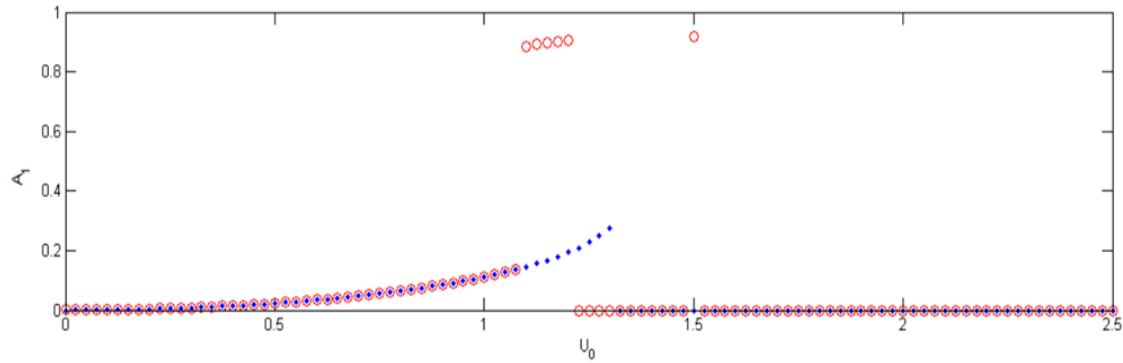
Figure 50: Amplitude-response curves of the mechanical oscillators versus f/f_p under sinusoidal voltage with enlargement around subharmonic resonances with $U_0 = 1.00$: (a) $\alpha = 1.10$, $\beta = 1.00$ (b) $\alpha = 1.00$, $\beta = 1.10$.

first mass also displays a hysteresis zone between $U_0 = 1.10$ and $U_0 = 1.23$. Between $U_0 = 1.23$ and $U_0 = 1.70$, both masses have oscillations sensitive to initial conditions, and after $U_0 = 1.70$ they are bound to the electromagnet.

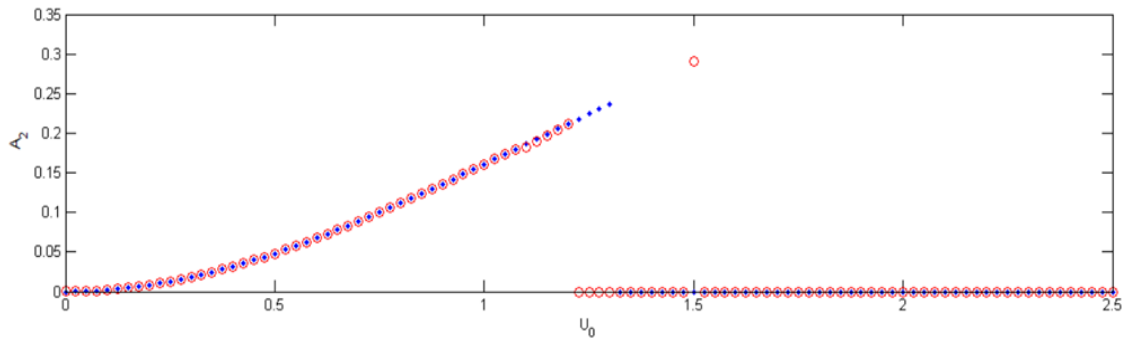
Looking at the effect of masses ratio on the mechanical vibration as U_0 changes, one observes on Figure 52 that increasing β leads to a decrease of vibration amplitudes of the



(a)



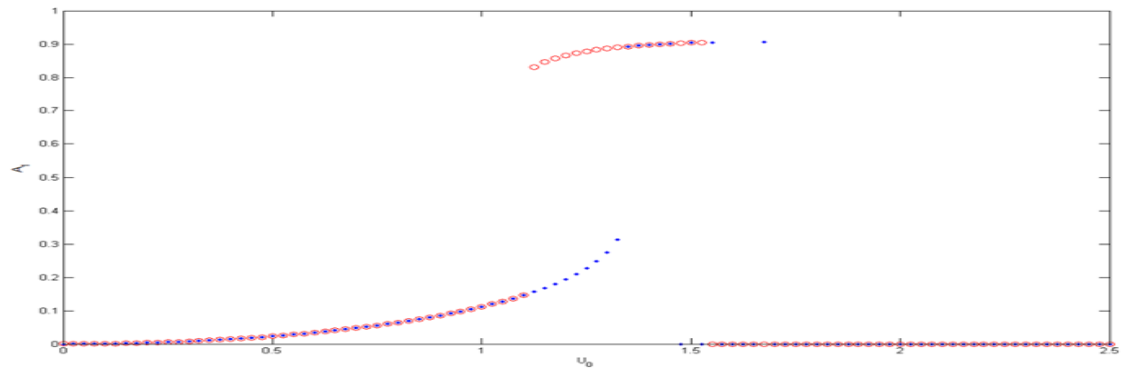
(b)



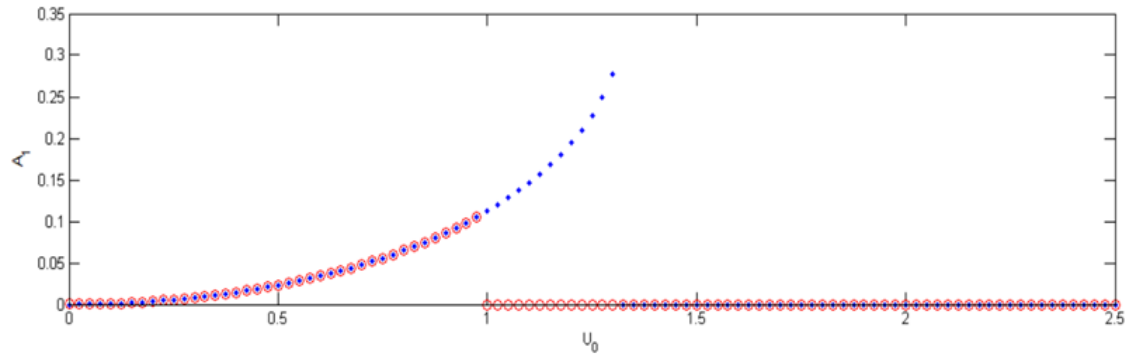
(c)

Figure 51: Amplitude-response curves of the mechanical oscillators versus U_0 under sinusoidal voltage for different values of stiffness coefficients ratio: $f/f_p = 7.56 \times 10^{-2}$, $\beta = 1.00$ (a) $\alpha = 1.00$ plot for the first mass; (b) $\alpha = 1.15$ plot for the first mass; (c) $\alpha = 1.15$ plot for the second mass.

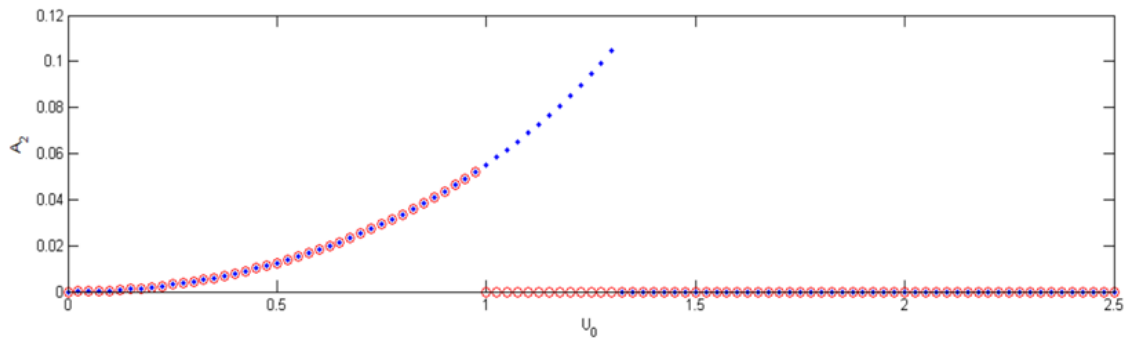
second mass. For $\beta = 1.10$, the hysteresis zone is between $U_0 = 0.97$ and $U_0 = 1.32$, with possible quenching of vibration of both masses. Above $U_0 = 1.32$, the masses are bound to the electromagnet.



(a)



(b)



(c)

Figure 52: Amplitude-response curves of the mechanical oscillators versus U_0 under sinusoidal voltage for different values of the masses ratio: $f/f_p = 7.56 \times 10^{-2}$, $\alpha = 1.00$ (a) $\beta = 1.00$ amplitude response of the first mass; (b) $\beta = 1.10$ amplitude response of the first mass; (c) $\beta = 1.10$ amplitude response of the second mass.

III-4-2-6- Effects of α and β

The frequency is taken equal to that of subharmonic oscillations $f_0/2$. On Figure 53, one observes that as the ratio between the stiffness coefficients of the first and the second mass increases, the vibration amplitudes of the second mass display a maximum at $\alpha = 1.10$ for $\beta = 1.00$

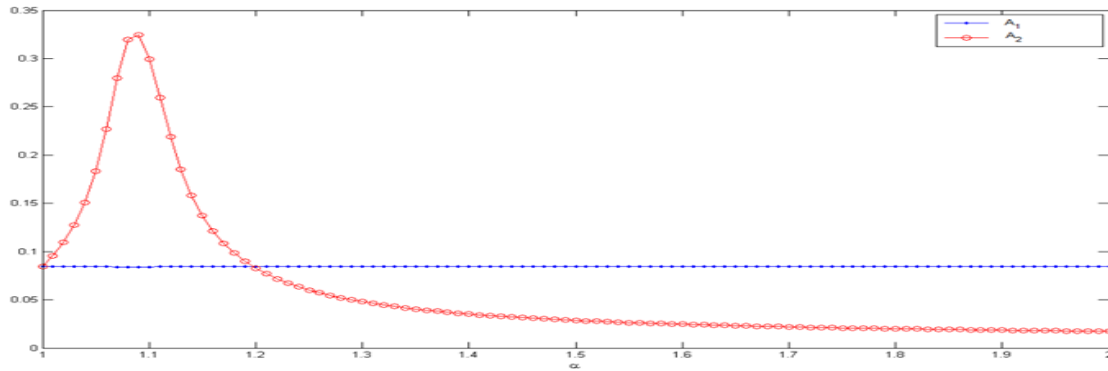


Figure 53: Amplitude-response curves of the mechanical oscillators versus the stiffness coefficient ratio under sinusoidal voltage: $f/f_p = 7.56 \times 10^{-2}, U_0 = 1.00, \beta = 1.00$.

At the same frequency, on Figure 54, as the ratio between the masses increases, the vibration amplitudes of the second mass decrease monotonously.

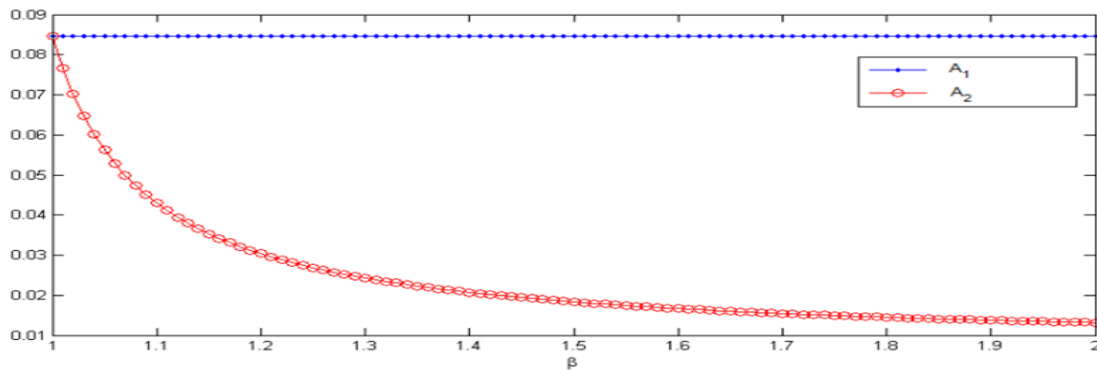


Figure 54: Amplitude-response curves of the mechanical oscillators versus the stiffness coefficient ratio under sinusoidal voltage: $f/f_p = 7.56 \times 10^{-2}, U_0 = 1.00, \alpha = 1.00$.

An analysis carried out on the system in case of triangle wave excitation has shown similar behaviour as in the case of sinusoidal excitation, as most of the energy of the triangle wave excitation is located at its first harmonics.

III-4-3- Dynamical behaviour of the device in the presence of square wave voltage

III-4-3-1- Dynamical behaviour in the presence of the square signal

Taking $g(2\pi f T_p \tau)$ in the form of a square wave, we assess the dynamics of the mechanical part, looking at the effects of frequency, voltage amplitude and that of phase difference.

IV-3-3-1-1-Effects of the frequency

Figure 55 shows the variation of the vibration amplitude of the mechanical part as the

frequency varies, when $\alpha = 1.1$ and $\beta = 1$. Various resonances are found at $f_{r11} = 7.81 \times 10^{-2} f_p$, $f_{r21} = 3.90 \times 10^{-2} f_p$, $f_{r31} = 2.60 \times 10^{-2} f_p$, $f_{r41} = 1.95 \times 10^{-2} f_p$ for the first mass, and $f_{r12} = 7.42 \times 10^{-2} f_p$, $f_{r22} = 3.72 \times 10^{-2} f_p$, $f_{r32} = 2.48 \times 10^{-2} f_p$, $f_{r42} = 1.85 \times 10^{-2} f_p$ for the second mass. These states correspond to subharmonic resonances of the type $f_0/2k$ (k a non-null integer) for the first mass and second mass.

With the same parameters and taking $\alpha = 1$ and $\beta = 1.1$, we observe that resonances for the second mass are observed at $f_{r12} = 8.19 \times 10^{-2} f_p$, $f_{r22} = 4.1 \times 10^{-2} f_p$, $f_{r32} = 2.72 \times 10^{-2} f_p$ and $f_{r42} = 1.64 \times 10^{-2} f_p$ where amplitudes are respectively 1.56×10^{-2} , 1.24×10^{-2} , 1.14×10^{-2} and 1.06×10^{-2} .

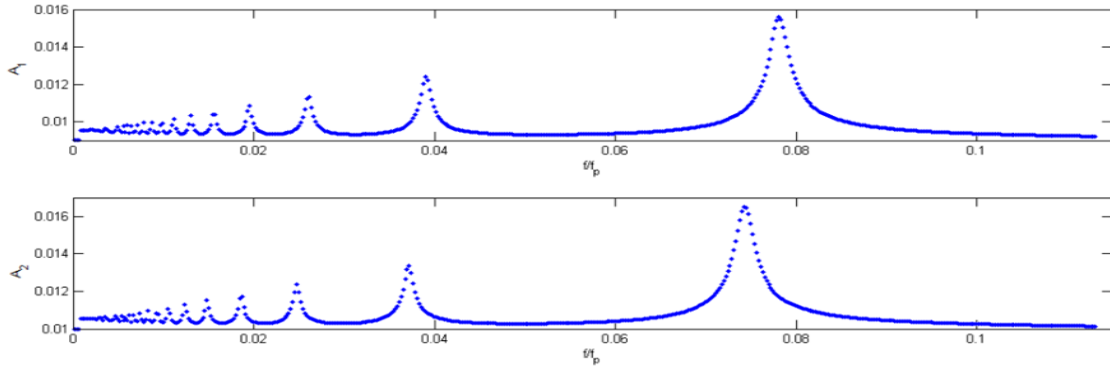


Figure 55: Amplitude-response curves of the mechanical oscillators versus f/f_p under a square wave voltage with parameters of Figure 50.

Compare to the first subsystem, increasing only the ratio between the stiffness of masses lead to a decrease of the subharmonics resonance frequencies for the second subsystem and an increase of the respective oscillations amplitudes. Increasing only the ratio between the masses leads to an increase of the subharmonics resonance frequencies for the second subsystem and a decrease of the respective oscillations amplitudes.

In order to have an idea on the evolution of the mechanical part, we plot on Figure 56 the time histories and phase diagram for some frequencies. We observe that as the frequency decreases, subharmonic oscillations are more present. And for low frequencies bursting which are alternating small and large amplitude excursion observed.

III-3-3-1-2-Effects of the voltage amplitude: hysteresis

While increasing the external voltage amplitude, it is observed that the current increases linearly, and on the mechanical part there is just an increase of displacement subsequently as shown on Figure 57. There is hysteresis for U_0 between 1.33 and $U_0 = 2.93$, with or without oscillations depending on the initial conditions. The moving mass is permanently bound to the electromagnet for U_0 larger than 2.93. Here the hysteresis shape is different from the one observed in the case of sinusoidal voltage excitation.

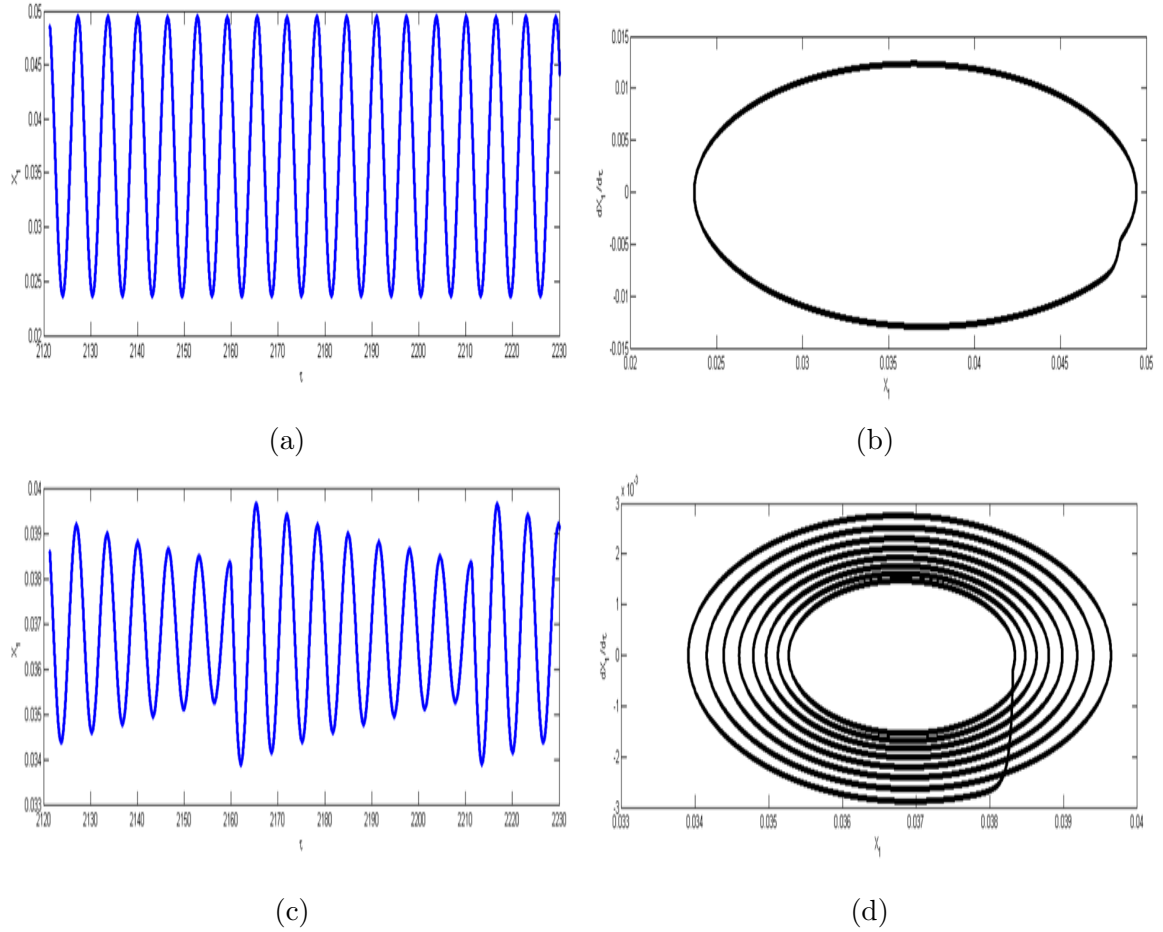


Figure 56: Time histories and phase diagrams of the first mass for different values of frequency in the case of excitation by a square wave: $U_0 = 1.40$, $\alpha = 1.00$, $\beta = 1.00$. (a) time history for $f/f_p = 7.56 \times 10^{-2}$, (b) phase diagram for $f/f_p = 7.56 \times 10^{-2}$; (c) time history for $f/f_p = 9.72 \times 10^{-3}$, (d) phase diagram for $f/f_p = 9.72 \times 10^{-3}$.

III-4-4- Other applications of the device

As an advantage of dual pumping such an approach could be extended in fluid flow pumping to multiply the number of pumps in usage for example for flood avoidance. The more the pumps in action to prevent floods, the more the efficiency of floods avoidance. Therefore many synchronized pumps can be used likewise with fluid flow frequency servo-control to optimize the time of reaction and the time of action when facing flood risks.

III-5- Conclusion

The basic device studied in this chapter presents as preliminary results the fact that pumping blood is possible with such a device based on the attraction of a ferromagnetic mass fixed on a spring and subjected to the action of an electromagnet under variable current. Some of the challenges that we attempted to solve open us the possibility to go further in order to build a complete artificial heart having a close behaviour as possible as the native heart not only with one ventricle but made of two pumping ventricles.

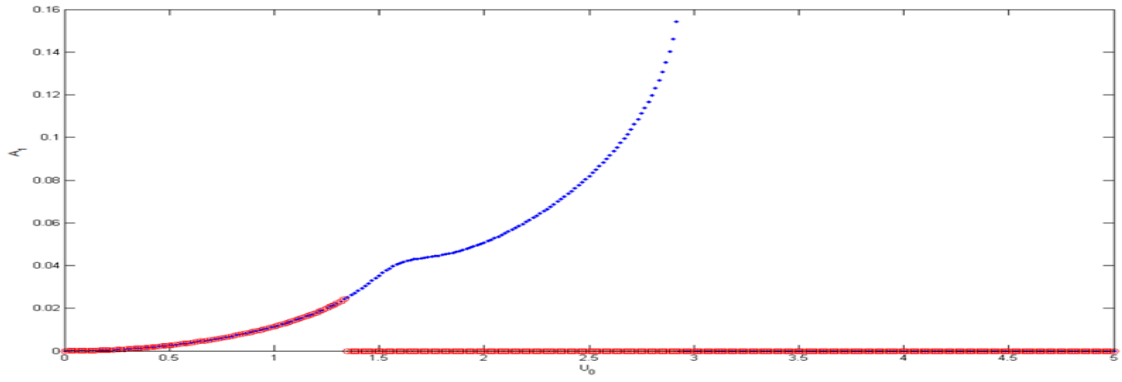


Figure 57: Amplitude-response curves of the mechanical oscillators versus U_0 under a square wave voltage: $f/f_p = 7.56 \times 10^{-2}, \alpha = 1.00, \beta = 1.00$.

Furthermore the biventricular CAD proposed in this chapter can serve as BIVAD or TAH, as it is possible to pump simultaneously a fluid like blood with a pulsatile behaviour with the two pumps. As each of the two pumps do not change significantly the dynamics of the other, each of the pumps can be considered as independent of the other. Hence the study done in Section II can be applicable to each pump. Therefore using an external oscillator pacing the pumps such as in III-3-4- and nerve servo-control such as in III-3-5- the device can perform the two ventricles pumping function with adaptation to body needs.

General Conclusion

In this thesis, a proposition of a new model of LVAD, BIVAD and TAH has been done, taking into account international specifications to obtain high beneficence and better life quality for patients suffering from end stage heart failure waiting for a transplant, an implant, or for heart recovery.

In the first chapter, we have presented different biological organs which can be replaced by an artificial device when they cannot be treated by classic means such as medication, physical and supportive therapies or surgery. Emphasis is put on how artificial organs are built and especially how other artificial hearts are implemented.

In the second chapter, the tools used for development and analysis have been presented. The specifications of LVAD have been presented to guide the development of the new model of LVAD, BIVAD and TAH. Analytical tools like harmonic balance method allowed obtaining small amplitude solutions, and Cardano's method to solve the third order polynomial equation coming out from equilibrium and instability studies. Furthermore the Fourth-order Runge-Kutta method is presented since it is used to solve numerically first-order coupled ODEs to access the time history, the phase diagram and the amplitude diagram of respective devices. Experimental materials used to perform analogical implementation for the analysis of natural or artificial pacemaking, with the effect of nerves excitation on our devices are introduced.

In the second section of the third chapter using international specifications, models of LVAD consisting of a ferromagnetic mass fixed on a spring and subjected to an electromagnet under variable current, blood flow frequency and pull-in servo-control are presented along with the adaptation approach to body needs through natural pacemaker pacing (that can be extended to artificial pacing) or nerves.

Basically, it is observed using the above analysis methods that as the internal or external parameters change, the devices can perform single pumping with subharmonic oscillation and hysteresis. Also the device possess an intrinsic instability called pull-in that has to be controlled to avoid sudden pumping arrest. The opportunity to adapt the pumping function to body needs through the blood flow frequency servo-control is also observed, allowing thus a better life quality for the patient who could receive such a pump. Moreover as the adaptation to body needs elicit unstationary and random flow it reduces thrombosis which are stationary clots in blood vessels and the type of pumping mechanism used reduces hemolysis as there is no high speed blood flow.

As the pumps do not use rotative parts, the pumping function can be made in all direction without the reducing gyroscopic effects of rotative parts and the translation

movement of the pumps coupled to pulsatile pumping tends to mimics the native heart pumping movement.

Another Application of such a system could be the use of the fluid flow frequency servo-control approach to pump runoff water at the rhythm they are appearing, to prevent floods.

The fourth section of the third chapter presents a BIVAD consisting of two ferromagnetic masses fixed on a spring and subjected to a common electromagnet under variable current for a dual pulsatile pumping. The TAH consisting of the model of BIVAD under an external oscillator are proposed and using the above analysis methods, the behaviour of devices is accessed under sinusoidal excitation or under square wave excitation inducing bursting like dynamics.

From the device specifications point of view, we succeed to avoid rotative parts, axis and pivots to avoid gyroscopic effects, using translation movement to meet the first requirement of our device specifications. The electromagnet lifting force actuates the pump in all orientations without physical link; this lifting force which is a field force, is used in both models of basic cardiac assist device, and biventricular heart, meeting thus the second requirement of our device specifications. An important result is that the mechanical system can show high stroke displacements (8/10 of the initial gap) in a heart like sequence without pull-in instability, under a 2V excitation by a VDP oscillator ; this shows that the third requirement of our device specification can be met in this condition while giving closest behaviour as the native heart. The fourth requirement of our device specification which is to achieve fluid flow frequency servo-control at low frequency, in order to reduce stationary flows, hemolysis and adaptation to body needs is met; in this sense when coupled to a section of blood vessel, although random frequency variations, the electrical sensed signal and the mechanical vibration possess common characteristic frequencies. Moreover, closest native heart behaviour is achieved, through pulsative pumping obtained with bursting oscillations and possible servo-control to nerves, native pacemaker to take into account body needs in pumping process depending on the device type.

This work leads to next steps and also opens some perspectives to obtain a high beneficence of devices. In this sense high beneficence can be obtained by the right choice of materials such as electromagnet core with higher relative magnetic permeability to reduce power needs and internal battery to increase autonomy and beyond all by the development of a new power amplifier with a reduce size, to drive the device by analogical oscillators or by biological signals sensed. As upcoming steps, one has to undertake a deep analysis for power reduction, turbulence studies, pressure control, other pulses types

excitations, real-time functioning, patent protection, market assessment, prototypes and technology demonstration, production of derived LVAD, BIVAD, TAH. Some prospective works could be to pay attention to precise tools of the device follow up and servo-control, energy harvest from the blood flow [80].

Other prospective works could be to adapt the pumping mechanism to pump large volume of fluid such as in high stroke displacement pumps that can be used in flood avoidance, concrete pumps or to use the movement of the ferromagnetic mass in industrial machine-tools.

Bibliography

- [1] **Hakim N**, *Artificial organs*, New Technique in Surgery Series, Springer, London, 183 (2009).
- [2] **Hench L L, Jones J R**, *Biomaterials, artificial organs and tissue engineering*, Woodhead Publishing Limited and CRC Press LLC, 284 (2005).
- [3] **Leprince P**, *Conception et modélisation d'actionneurs électroactifs innovants pour l'assistance circulatoire*, Docteur, Institut National Polytechnique de Toulouse, 161 (2005).
- [4] **Ambagtsheer F, Weimar W**, *A Criminological Perspective: Why Prohibition of Organ Trade Is Not Effective and How the Declaration of Istanbul Can Move Forward*, American Journal of Transplantation, 12, 571-575 (2011).
- [5] **World Health Organization**, *Fact sheet N° 317*, (2011).
- [6] **World Health Organization**, *Report 2010*, (2010).
- [7] **Kol G R**, *Arterial endoprosthesis: effects of blood flow and optimization*, PhD, University of Yaounde I, 77 (2010).
- [8] **Kol G R, Wofo P**, *The design of a reflectionless arterial prosthesis*, Journal of Biological Physics, 37, 51-60 (2011).
- [9] **Kol G R, Ntchantcho R, Wofo P**, *Effects of the wall stress-strain nonlinearity and viscoelasticity in a stented vessel*, Journal of Mechanics in Medecine and Biology, 10, 495-513 (2010).
- [10] **Perriard Y**, *Méthodologie de conception d'activateurs pour ventricule d'assistance cardiaque implantable*, Doctorat, Ecole Polytechnique Fédérale de Lausanne, 214 (1992).
- [11] **NHLBI**, *Request for Proposal RFP NHLBI 80-3. Development of an implantable integrated electrically powered left heart assist system* (1980).
- [12] **Longenbaker S**, *Mader's understanding human anatomy and physiology, 7th Edition*, McGraw-Hill, 492 (2011).

- [13] **World Health Organization**, *Global status report on noncommunicable diseases 2010*, Geneva, 176, (2011).
- [14] **Fuster V, Kelly B B**, *Promoting Cardiovascular Health in the Developing World: A Critical Challenge to Achieve Global Health*, National Academies Press, Washington DC, (2010).
- [15] **PNLMCVS**, *Programme National de Lutte contre les maladies cardiovasculaires au Sénégal (2007-2011)*.
- [16] **Dzudie A, Kenfack M, Monkam Y, Kingue S**, *Correspondance pour la Société Camerounaise de Cardiologie*, (2010).
- [17] **Mbewu A, Mbanya J-C**, *Disease and Mortality in Sub-Saharan Africa*, World Bank, Washington DC, 305-327 (2006).
- [18] **Kotto R M, Bouelet B A**, *Cardiovascular Diseases in Adults in Douala (Cameroon)*, *Cardiologie Tropicale*, 26, 61–64 (2000).
- [19] **Mbanya J-C, Minkoulou E, Salah J, Balkau B**, *The Prevalence of Hypertension in Rural and Urban Cameroon*, *International Journal of Epidemiology*, 27, 181–185 (1998).
- [20] **Jan J Z, Krzysztof G, Rafal B**, *Observations and modeling of unusual patterns in human heart rate variability*, *Acta Physica Polonica B*, 36, 1881–1895 (2005).
- [21] **Vladimir G I, Tijana T I**, *Complex nonlinearity: chaos, phase transitions, topology change and path integrals*, Springer-Verlag, Berlin (2008).
- [22] **Riehl C**, *Implementation eines präoperativen Risikoscores zur Abschätzung der Sterblichkeit nach Implantation eines ventrikulären mechanischen Assist-Systems*, Doctorat, Universitätsklinikum Münster, 114 (2009).
- [23] **Sami M, Katja M, Reijo L**, *Flexible Implantable Thin Film Neural Electrodes*, *Recent Advances in Biomedical Engineering*, Ganesh R Naik (2009).
- [24] **Kipke D R**, *Silicon-Substrate Intracortical Microelectrode Arrays for Long-Term Recording of Neuronal Spike Activity in Cerebral Cortex*, *IEEE Transactions on Neural Systems and Rehabilitation Engineering*, 11, 5(2003).
- [25] **Boppart S A, Wheeler B C, Wallace C S**, *A flexible perforated microelectrode array for extended neural recordings*, *IEEE Transactions on Biomedical Engineering*, 39, 37-42(1992).
- [26] **Cheung K C, Renaud P, Tanila H, Djupsund K**, *Flexible polyimide microelectrode array for in vivo recordings and current source density analysis*, *Biosensors and bioelectronics*, 22, 1783-1790(2007).

- [27] **de Haro C, Mas R, Abadal G, Muñoz J, Perez-Murano F, Domínguez C**, *Electrochemical platinum coatings for improving performance of implantable micro-electrode arrays*, *Biomaterials*, 23, 4515-4521(2002).
- [28] **González C, Rodríguez M**, *A flexible perforated microelectrode array probe for action potential recording in nerve and muscle tissues*, *Journal of Neuroscience Methods*, 72, 189-195(1997).
- [29] **Hollenberg B A, Richards C D, Richards R, Bahr D F, Rector D M**, *A MEMS fabricated flexible electrode array for recording surface field potentials*, *Journal of Neuroscience Methods*, 153, 147-153(2006).
- [30] **Pini F, McCarthy K**, *Capacitive instrumentation amplifier for low-power bio potential signal detection*, *Signals and Systems Conference (ISSC 2010)*, IET Irish , 54-58(2010).
- [31] **Gallot-Lavallee O**, *Electronique d'instrumentation I*, Université Joseph Fourier), Cours Magistraux, (2011).
- [32] **Millman J, Grabel A**, *Microelectronics*, McGraw-Hill, ()
- [33] **Williams J C, Rennaker R L, Kipke D R**, *Long-term neural recording characteristics of wire microelectrode arrays implanted in cerebral cortex*, *Brain Research Brain and Research Protocols*, 4, 303-313(1999).
- [34] **Polikov V S, Tresco P A, Reichert W M**, *Response of brain tissue to chronically implanted neural electrodes*, *Journal of Neuroscience Methods*, 148, 1-18(2005).
- [35] **Rousche P J, Normann R A**, *Chronic recording capability of the Utah Intracortical Electrode Array in cat sensory cortex*, *Journal of Neuroscience Methods* ,82, 1-15(1998).
- [36] **Griffith R W, Humphrey D R**, *Long-term gliosis around chronically implanted platinum electrodes in the Rhesus macaque motor cortex*, *Neuroscience Letters*,406, 81-86(2006).
- [37] **Gray C M**, *Tetrodes markedly improve the reliability and yield of multiple single-unit isolation from multi-unit recordings in cat striate cortex*, *Journal of Neuroscience Methods*,63, 12(1995).
- [38] **Zhong Y, Bellamkonda R V**, *Controlled release of anti-inflammatory agent a-MSH from neural implants*, *Journal of Controlled Release*, 106, 10(2006).
- [39] **He W**, *Nanoscale laminin coating modulates cortical scarring response around implanted silicon microelectrode arrays*, *Journal of Neural Engineering*, 3, 11(2006).

- [40] **He W, Bellamkonda R V**, *Nanoscale neuro-integrative coatings for neural implants*, *Biomaterials*, 26, 2983-2990(2005).
- [41] **Ludwig K A**, *Chronic neural recordings using silicon microelectrode arrays electrochemically deposited with a poly(3,4-ethylenedioxythiophene) (PEDOT) film*, *Journal of Neural Engineering*, 12(2006).
- [42] **Stauffer W R, Cui X**, *Polypyrrole doped with 2 peptide sequences from laminin*, *Biomaterials*, 27, 9(2006).
- [43] **Lu S**, *Receptor-Ligand-Based Specific Cell Adhesion on Solid Surfaces: Hippocampal Neuronal Cells on Bilinker Functionalized Glass*, *Nano Letters*, 6, 5(2006).
- [44] **Saneinejad S, Shoichet M S**, *Patterned glass surfaces direct cell adhesion and process outgrowth of primary neurons of the central nervous system*, *Journal of Biomedical Materials Research*, 42, 13-19(1998).
- [45] **Kennedy P R, Mirra S S, Bakay R A E**, *The Cone Electrode - Ultrastructural studies following long-term recording in rat and monkey cortex*, *Neuroscience Letters*, 142, 89-94(1992).
- [46] **Rathnasingham R**, *Characterization of Implantable Microfabricated Fluid Delivery Devices*, *IEEE Transactions on Biomedical Engineering*, 51, 8(2004).
- [47] **Polikov V S**, *In Vitro model of glial scarring around neuroelectrodes chronically implanted in the CNS*, *Biomaterials*, 27, 9(2006).
- [48] **Subbaroyan J**, *A finite-element model of the mechanical effects of implantable microelectrodes in the cerebral cortex*, *Journal of Neural Engineering*, 2, 11(2005).
- [49] **Russo A P**, *Microfabricated Plastic Devices from Silicon using Soft Intermediates*, *Biomedical Microdevices*, 4, 7(2002).
- [50] **Keough E M, Mackey W C, Connolly R, et al**, *The interaction of blood components with PDMS (polydimethylsiloxane) and LDPE (low-density polyethylene) in a baboon ex vivo arteriovenous shunt model*, *Journal of Biomedical Material Research*, 19, 577-587 (1985).
- [51] **Campbell E J, O'Byrne V, Stratford P W, et al**, *Biocompatible surfaces using methacryloylphosphorylcholine laurylmethacrylate copolymer*, *Asaio Journal*, 40, 853-857 (1994).
- [52] **Hayashi C**, *Nonlinear Oscillations in physical systems*, Mc-Graw-Hill, New York, (1964).

- [53] **Gilmore R J, Steer M B**, *Nonlinear circuit analysis using the method of harmonic balance—A review of the art. Part I. Introductory concept*, International Journal of Microwave and Millimeter-Wave Computer-Aided Engineering,1, 22–37 (1991).
- [54] **Nakhla M S, Vlach J**, *A piecewise harmonic balance technique for determination of periodic response of nonlinear systems*, IEEE Transactions on Circuits and Systems, (1976).
- [55] **Maas S A**, *Nonlinear microwave and RF circuits*, Artech House, (2003).
- [56] **Saunders M L , Birkhoff G**, *Algebra (3rd ed.)*, American Mathematical Society, 626 (1999).
- [57] **Hoffman J D**, *Numerical Methods for Engineers and Scientists*, Marcel Dekker, New-York, 372-373 (2001).
- [58] **Van Der Pol B, Van Der Mark J**, *The heartbeat considered as a relaxation oscillator and an electrical model of the heart*, Philosophical Magazine, 6, 763-775 (1928).
- [59] **Gois S R F S M, Savi M A** , *An analysis of heart rhythm dynamics using a three-coupled oscillator model*, Chaos, Solitons and Fractals, 41, 2553-2565 (2009).
- [60] **Hindmarsh J L, Rose R M** , *A model of neural bursting using three coupled first order differential*, Philosophical Transaction of the Royal Society of London, 221, 87-102 (1984).
- [61] **Rabinovich M I, Abarbanel H D I, Huerta R, Elson R, Selverston A** , *Self-regularization of Chaos in Neural Systems: Experimental and Theoretical Results*, IEEE Transactions on Circuits and Systems, 44, 997-1005 (1997).
- [62] **Tao R, Huang K**, *Reducing blood viscosity with magnetic fields*, Physical Review E, 84, 1-5 (2011).
- [63] **Schenck J F**, *Safety of Strong, Static Magnetic Fields*, Journal of Magnetic Resonance Imaging, 12, 2–19 (2000).
- [64] **Stronati L, Testa A, Villani P, Marino C, Lovisolo G A, Conti D, Russo F, Fresegna A M, Cordelli E**, *Absence of genotoxicity in human blood cells exposed to 50 Hz magnetic fields as assessed by comet assay, chromosome aberration, micronucleus, and sister chromatid exchange analyses*, Bioelectromagnetics, 25, 41-48 (2004).
- [65] **Haken H**, *Advanced Synergetics*, Springer, Berlin, Heidelberg (1985).
- [66] **Nicolis G, Prigogine I**, *Self-Organization in Non-Equilibrium Systems*, Wiley, New York (1977).

- [67] **Feistel R, Ebeling W**, *Evolution of Complex Systems*, Kluwer, Dordrecht (1989).
- [68] **Garcia-Ojalvo J, Sancho J M**, *Noise in Spatially Extended Systems*, Springer, New York (1999).
- [69] **Anishchenko V, Astakhov V V, Neiman A B, Vadivasova T, Schimansky-Geier L**, *Nonlinear Dynamics of Chaotic and Stochastic Systems*, Springer, Berlin–Heidelberg–New York (2002).
- [70] **Han X, Bi Q**, *Bursting oscillations in Duffing’s equation with slowly changing external forcing*, *Communications in Nonlinear Science and Numerical Simulation*, 16, 4146–4152 (2011).
- [71] **Izhikevich E M**, *Dynamical systems in neuroscience: the geometry of excitability and bursting*, MIT Press, Cambridge, 522 (2007).
- [72] **Izhikevich E M**, *Neural excitability, spiking and bursting*, *International Journal of Bifurcation and Chaos*, 10, 1171–1266 (2000).
- [73] **Graeme J G**, *Designing with operational amplifier: applications alternatives*, McGraw-Hill, 59-60 (2010).
- [74] **Luo A C J, Wang F Y**, *Chaotic motion in a micro-electro-mechanical system with nonlinearity from capacitors*, *Communications in Nonlinear Science and Numerical Simulation*, 7, 31-49 (2002).
- [75] **Fargas-Marques A, Shkel A M**, *On electrostatic actuation beyond snapping condition*, *Proceedings of Eurosensors XIX, Spain*, 600-603 (2005).
- [76] **Fargas-Marques A, Casals-Terre J, Shkel A M**, *Resonant pull-in condition in parallel-plate electrostatic actuators*, *Journal Microelectromechanical systems*, 16, 1044 – 1053 (2007).
- [77] **Simo H, Woafu P**, *Bifurcation structure of a Van der Pol oscillator subjected to nonsinusoidal periodic excitation*, *International Journal of Bifurcation and Chaos*, 22, 1250003: 1-8 (2012).
- [78] **Rabinovich M I, Abarbanel H D I, Huerta R, Elson R, Selverston A**, *Self-regularization of Chaos in Neural Systems: Experimental and Theoretical Results*, *IEEE Transactions on Circuits and Systems*, 44, 997-1005 (1997).
- [79] **Gonzalez-Miranda J M**, *Observation of a continuous interior crisis in the Hindmarsh-Rose neuron model*, *Chaos*, 13, 845-852 (2003).
- [80] **Karami M A, Inman D J**, *Powering pacemakers from heartbeat vibrations using linear and nonlinear energy harvesters*, *Applied Physics Letters*, 100, 042901-042904 (2012).

Publications

Published

Abobda L T, Woafu P, *Ferromagnetic mass fixed on a spring and subjected to an electromagnet powered by self-sustained oscillators*, European Physical Journal Special Topics, 223, 2885–2895 (2014)

Abobda L T, Woafu P, *Subharmonic and bursting oscillations of a ferromagnetic mass fixed on a spring and subjected to an AC electromagnet*, Communications in Non-linear Science and Numerical Simulation, 17, 3082-3091(2012)

Submitted

Abobda L T, Woafu P, *Modeling, mathematical and numerical studies of a new biventricular artificial heart powered by an electromagnet subjected to sinusoidal and square voltages*, International Journal of Artificial Life research

Abobda L T, Woafu P, *Fluid flow frequency and pull-in servo-control of the vibration of a ferromagnetic mass fixed on a spring and subjected to an electromagnet*, Control Theory and Technology

Ferromagnetic mass fixed on a spring and subjected to an electromagnet powered by self-sustained oscillators

L.T. Abobda and P. Woaf^a

Laboratory of Modelling and Simulation in Engineering, Biomimetics and Prototypes, and TWAS Research Unit, Faculty of Science, University of Yaounde I, PO Box 812, Yaounde, Cameroon

Received 30 June 2014 / Received in final form 17 October 2014
Published online 10 December 2014

Abstract. The study of a ferromagnetic mass, fixed on a spring and subjected to an electromagnet powered by a Van der Pol (VDP) oscillator and by a Hindmarsh-Rose (HR) oscillator is performed, to serve as an electromechanical devices, but also to mimic the action of a natural pacemaker and nerves on a cardiac assist device or artificial heart. The excitation with the VDP oscillator shows in the mechanical part the transition from harmonic, periodic, biperiodic up to bursting oscillations, high displacement without pull-in instability in the free dynamics regime. Under DC plus square wave excitation, there is a coexistence of the bursting oscillations of the free dynamics and the one of the modulated dynamics. Considering the action of a HR oscillator, it is found transition from spikes, bursting oscillations, relaxation spikes, multiperiodic and sinusoidal oscillations under DC or DC plus square wave excitation. These electrical behaviors are transferred to the mechanical part which can then adopt spiking or bursting dynamics as the HR oscillator. For this electromechanical model, the VDP oscillator is more efficient than the HR oscillator to induce pulsatile pumping function with higher amplitude and to react to external influences without pull-in.

1 Introduction

Self-sustained oscillators are systems that exhibit the property to transform directly continuous energy to a periodic form. One of the most studied self-sustained oscillators is the Van der Pol oscillator (VDP oscillator). Its special feature is that, it can be a harmonic oscillator and becomes a relaxation oscillator, under the increase of one parameter. It is useful for the modulation of some devices and to model biological systems [1–8].

One self-sustained system among others that can be modeled by the VDP oscillator is the heart pacemaker [9, 10]. In an open environment and due to external influence, the pacemaker can see its frequency change under the effects of parasympathetic and sympathetic innervations of the heart, ranging from 28 beats per minute

^a e-mail: pwoaf01@yahoo.fr

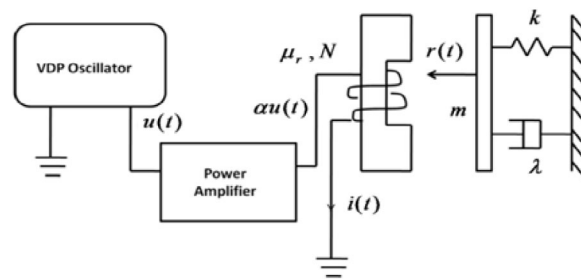


Fig. 1. Synoptic diagram of the electromechanical system made of a ferromagnetic mass fixed on a spring and subjected to an electromagnet powered by a VDP electronic oscillator.

up to 200 beats per minute to adapt to body needs, according to the age or the training [11,12].

One of the most challenging issues in such research is to obtain hybrid systems, which can take over after a failure of the biological system, with the constraint to behave like the native system. Among other biological inspired devices, we can cite cardiac assist devices that could take over a cardiac failure, as it is one of the most studied with severe requirements [6,7]. Moreover, biological inspired devices are gaining more interest in many engineering and scientific fields. In this line, artificial organs, artificial members, bioinspired robots are under active research. The aim is to reproduce the behaviors of biological systems observed in nature with the ambition to copy their dynamics in electromechanical and mechatronic systems such as robots and actuators or for bio-engineering [6,13–17].

One of the interesting models describing neurons behaviors is the Hindmarsh-Rose (HR) model. It can exhibit spike, bursting and chaos under the effects of an injected bias current acting as the principal bifurcation parameter [18,19]. Recent studies in the field of nano-electromechanical systems, micro-electromechanical systems and macro-electromechanical systems focus on variable capacitor and variable inductor actuators, and their technological applications [20–22].

In this work we consider a pump made of a ferromagnetic mass fixed on a spring subjected to an electromagnet first powered by a VDP oscillator and then by a HR electric oscillator. The system can act as an electromechanical device for robotic uses or as artificial heart subjected to the action of the pacemaker (Van der Pol oscillator) or of the nervous systems.

Section 2 deals with the description of the device and the analysis of its dynamical states and behaviors when it is powered by a Van der Pol oscillator. In Sect. 3, the same study is carried out when the excitation comes from the Hindmarsh-Rose electronic oscillator. Section 4 concludes the paper.

2 Dynamical behavior of the system powered by the Van der Pol oscillator

2.1 Description of the system

Let us consider a ferromagnetic mass with mass m , fixed on a spring with spring coefficient k , and subjected to the attraction of a N turns coil electromagnet fed by a Van der Pol oscillator (Fig. 1). The moving ferromagnetic mass has permeability μ_r like the N turns electromagnet. The power amplifier is used to adapt the power to displacement amplitude needs. This model can be a simplification after modal

projection of an elastic pocket containing a fluid (for instance blood) on which, on a side is fixed a ferromagnetic mass and besides this mass is fixed an electromagnet commanding the movement of the mass and thus the fluid pumping function.

With the model of [22], the electromechanical system is governed by Eqs. (1) and (2)

$$\frac{a\mu_0\mu_r N^2}{2(l_a + \mu_r(l_p - r))} \frac{di}{dt} + \frac{a\mu_0\mu_r^2 N^2 i}{2(l_a + \mu_r(l_p - r))^2} \frac{dr}{dt} + \frac{\rho N P_m}{s} i = \alpha u(t) \quad (1)$$

$$m \frac{d^2 r}{dt^2} + \lambda \frac{dr}{dt} + kr = \frac{a\mu_0\mu_r^2 N^2 i^2}{4(l_a + \mu_r(l_p - r))^2}. \quad (2)$$

The electromechanical system is excited by the potential u of the Van der Pol oscillator [4]. This potential is governed by the following equation

$$\frac{d^2 u}{dt^2} - \epsilon \omega_r (1 - u^2) \frac{du}{dt} + \omega_r^2 u = \omega_r^2 v(t) \quad (3)$$

with ω_r its natural frequency and ϵ the VDP nonlinear coefficient. $v(t)$ is an external electric input.

In the dimensionless form, the electromechanical system is governed by the set of equations:

$$\ddot{U} - \epsilon \omega_r T_p (1 - U^2) \dot{U} + \omega_r^2 T_p^2 U = \omega_r^2 T_p^2 V(\tau) \quad (4)$$

$$\dot{I} + \frac{\dot{R}I}{(1 - R)} + AI(1 - R) = E\alpha U(1 - R) \quad (5)$$

$$\ddot{R} + F\dot{R} + R = G \frac{I^2}{(1 - R)^2} \quad (6)$$

where the dots refer to the derivation with respect to the dimensionless time τ given below, α the voltage gain. The non dimensional coefficients are given as:

$$R = \frac{pr}{(1 + p)l_p}; \quad U = \frac{u}{u_p}; \quad V = \frac{v}{u_p}; \quad I = \frac{i}{i_p}; \quad \tau = \frac{t}{T_p}; \quad L_0 = \frac{a\mu_0\mu_r N^2}{2l_a};$$

$$i_p = \frac{2l_p T_p u_p}{a\mu_0}; \quad p = \frac{\mu_r l_p}{l_a}; \quad A = (1 + p) \frac{\rho N P_m T_p}{s L_0}; \quad E = \frac{1 + p}{pN}; \quad F = \frac{\lambda T_p}{m};$$

$$\omega_0^2 = \frac{k}{m}; \quad T_p = \sqrt{\frac{m}{k}}; \quad G_1 = \frac{L_0 T_p^2 i_p^2 p^2}{2m l_p^2 (1 + p)^3}.$$

The only equilibrium point of the electromechanical system is ($U = 0, \dot{U} = 0, I = 0, R = 0, \dot{R} = 0$). The eigenvalues of the Jacobian evaluated at the equilibrium point, are given by $(\epsilon \pm \sqrt{\epsilon^2 - 4})T_p \omega_r / 2, (-F \pm \sqrt{F^2 - 4})/2, -A$. Thus the equilibrium point is unstable for $\epsilon > 0$.

As the VDP oscillator dynamics under weak nonlinear coefficient tends toward the harmonic form [1], some analytical results of the dynamical behavior of this resonator under the VDP oscillator at weak nonlinear coefficient, can be obtained in Ref. [22] under harmonic excitation.

The set of Eqs. (4), (5) and (6) is solved using the fourth-order Runge-Kutta algorithm.

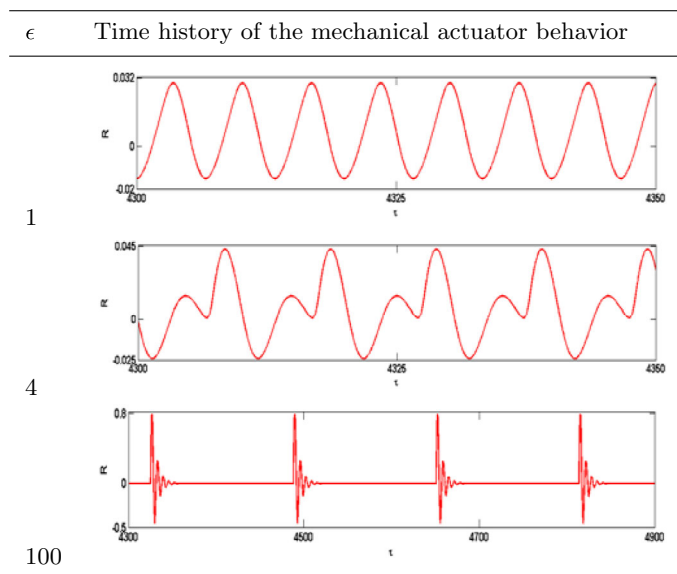


Fig. 2. Time histories of the mechanical part for different values of the VDP nonlinearity coefficient ϵ : $\alpha = 10^{-2}$, $\omega_r = \omega_0/2$.

2.2 Dynamical states and behaviors of the electromechanical device without external excitations

For numerical simulations the parameters of the electromechanical system are taken as follows. The fixed parameters are $f_p = \frac{1}{T_p} = 70.71$ Hz, $f_0 = \frac{\omega_0}{2\pi} = 0.16 f_p$, $l_p = 3 \times 10^{-2}$ m. The reference parameters are $u_p = 1.00$ Volt, $i_p = 6.75 \times 10^6$ A while the calculated parameters are $G = 3.37 \times 10^9$, $p = 600 \text{ m A}^{-1}$, $A = 68.89$, $E = 1.25 \times 10^{-2}$, $F = 3.54 \times 10^{-1}$.

The external voltage applied to the VDP oscillator is first set to zero and we analyze the effects of the nonlinearity coefficient ϵ and that of the frequency ω_r of the VDP oscillator on the evolution of the electromechanical system. An increase of the nonlinearity coefficient ϵ results in a progressive transformation of the behavior of the mechanical actuator behavior from harmonic oscillation into bi-periodic and bursting oscillations with an increase of the amplitude and a decrease of the frequency (see Fig. 2). One observes also that as the nonlinear coefficient increases, the frequency of oscillation decreases, the maximal value of current amplification to obtain oscillation without pull-in decreases and the frequency of the bursting oscillation is equal to the double of the frequency of the VDP oscillator (not plotted). The bursting oscillations observed here are similar to those found in Ref. [22] and can also allow high pulsatile pumping in heartbeat like sequence. Decreasing the frequency ω_r , it is found a reduction of the amplitude of vibration of the mechanical actuator, a refinement of the bursting shape leading to a simple pulse with disappearance of negative displacement in low frequencies (Fig. 3).

These results show that in order to build an artificial heart with this electromechanical system where the VDP oscillator serves as an autonomous pacemaker, the larger the nonlinear coefficient, the better the pulsatile pumping function is achieved. The same fact appears for low frequencies of the VDP oscillator.

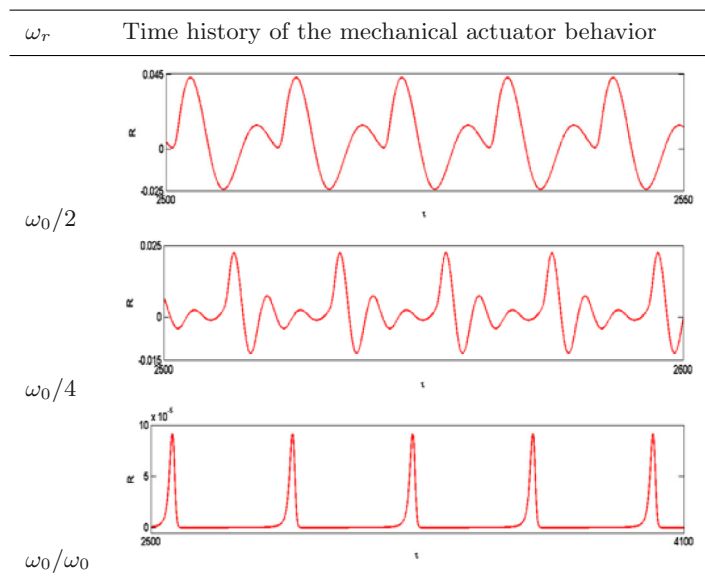


Fig. 3. Time histories of the mechanical part for different values of the VDP oscillator frequency ω_r : $\alpha = 10^{-2}$, $\epsilon = 4$.

2.3 Effects of the parameters of the external excitation

The external influence is taken into account by a DC plus square wave external voltage applied on the VDP oscillator. This voltage is taken on a continuous square wave form. The DC plus square wave signal is consistent with the analogical to digital conversion of the electrical sensed signal acting on the native pacemaker or an artificial pacemaker under a nerve signal sensed and converted. The conversion is to reduce noises on the original sensed signal. Some results of the behavior of the VDP oscillator under square wave can be found in Ref. [3].

As the frequency of the external applied voltage changes, the periodicities of the electrical and mechanical part are equal. The dynamics of the electrical and mechanical parts are modulated by the applied voltage (see the time histories in Fig. 4). So there is a coexistence of the free dynamics and a modulated dynamics in both electrical and mechanical parts. As the applied voltage frequency increases, the free dynamics vanishes leading to a sort of frequency entrainment. As the amplitude of the applied voltage increases, the displacement of the mechanical part decreases because of the dispersion of the energy at higher harmonics. Moreover the free dynamics of the electrical and mechanical parts are quenched progressively (Fig. 5). As the duty cycle increases (not plotted), the free dynamics of the electrical and mechanical displacement are quenched progressively. One also observes modulated dynamics.

One can conclude that in this case where the artificial pacemaker commanding pumping function is under nerve excitation converted under DC plus square wave voltage, there is a coexistence of dynamics. Indeed as membrane potential exhibits a time in low state (quiescence) greater than the one in up state (bursting or peak), after membrane potential signal conversion under digital form, there is a preponderance of the free dynamics of the electromechanical system modulated by the dynamics of the membrane potential, increasing thus the number of efficient beats of the artificial heart within the same time frame.

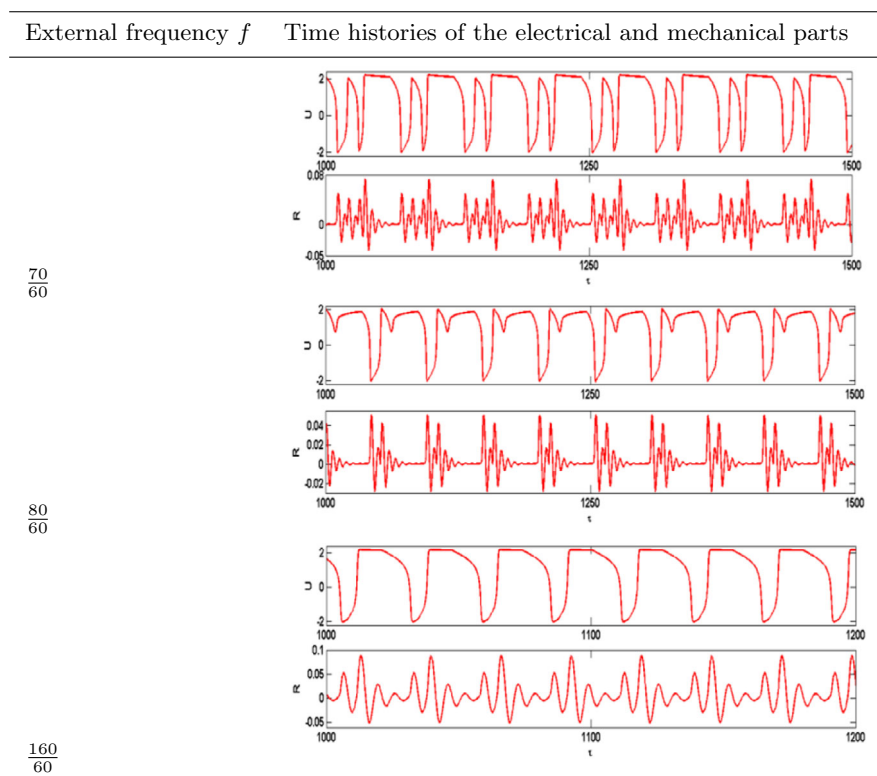


Fig. 4. Time histories of the response of the VDP oscillator and that of the mechanical part as the applied voltage frequency increases for $\alpha = 10^{-2}$, $\epsilon = 4$, $\omega_r = \omega_0/2$, $V_{max} = 2$, $d = 50$.

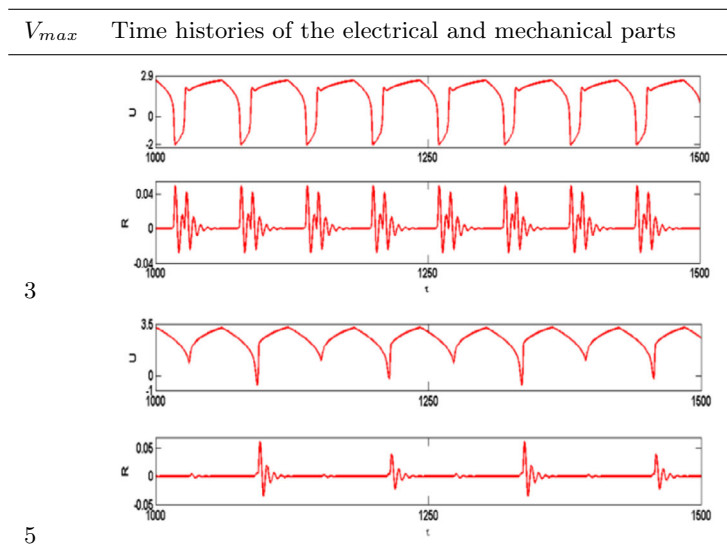


Fig. 5. Time histories of the response of the VDP oscillator and that of the mechanical part as the applied voltage amplitude increases for $\alpha = 10^{-2}$, $\epsilon = 4$, $\omega_r = \omega_0/2$, $f = \frac{70}{60}$, $d = 50$.

3 Dynamical behaviors in presence of a Hindmarsh-Rose electrical oscillator

Let us now consider the system in Fig. 1 where the VDP electronic oscillator is replaced by a Hindmarsh-Rose electronic oscillator. The dynamical evolution of the membrane potential of the three dimensional HR oscillator is given by [23].

$$\frac{dx}{dt} = -x^3 + 3x^2 + y + I_i - z \quad (7)$$

$$\frac{dy}{dt} = 1 - 5x^2 - y \quad (8)$$

$$\frac{dz}{dt} = r_r(s_s(x - x_0) - z) \quad (9)$$

where x stands for the membrane potential of the neuron, y the rapid current through the membrane and z the slow current through the membrane, I_i the external applied current. The dimensionless equations governing the dynamics of the whole system are thus

$$\dot{X} = T_p(-X^3 + 3X^2 + X + I_I - Z) \quad (10)$$

$$\dot{Y} = T_p(1 - 5X^2 - Y) \quad (11)$$

$$\dot{Z} = T_p r_r(s_s(X - X_0) - Z) \quad (12)$$

$$\dot{I} + \frac{\dot{R}I}{(1-R)} + AI(1-R) = E\alpha X(1-R) \quad (13)$$

$$\ddot{R} + F\dot{R} + \Omega^2 R = G \frac{I^2}{(1-R)^2} \quad (14)$$

with the new dimensionless parameters given by $X = \frac{x}{x_r}$; $Y = \frac{y}{y_r}$; $Z = \frac{z}{z_r}$; $I_I = \frac{I_i}{I_r}$. With the parameters of Ref. [18], the dynamics of the HR oscillator is well studied by Gonzalez-Miranda [19]. The values of the new reference parameters are: $x_r = 1$, $y_r = 1$, $z_r = 1$, $I_r = 1$.

The only equilibrium point is ($X = -0.9487$, $Y = -3.5001$, $Z = 2.6052$, $I = -\frac{0.9487E\alpha}{A}$, $R = R_0$, $\dot{R} = 0$) with $R_0 = \frac{20}{3} + B + \frac{1}{B}$;

$$B = \frac{10^4 A \Omega}{\left[3 \left((-\Omega A^2 \times 10^{12} + 1.2150 \times 10^{13} G \alpha^2 E^2 + 300 E \alpha) \right. \right. \\ \left. \left. \times \sqrt{-1.3500 \times 10^{10} G (2\Omega A^2 \times 10^{10} - 1.2150 \times 10^{11} G \alpha^2 E^2)} \right) A \Omega^2 \right]^{1/3}}$$

and the eigenvalues equal to $-\frac{1.8000 G \alpha^2 E^2 + A^2 R_0^2 (R_0 - 3) + A^2 (3R_0 - 1)}{A^2 (R_0 - 1)^3}$, $-T_p$, $A(R_0 - 1)$, $-0.0032T_p$, $-7.3911T_p$, 1 . This equilibrium point is unstable since the real part of at least one eigenvalue is positive.

 I_I Time histories of the HR oscillator and electromechanical system

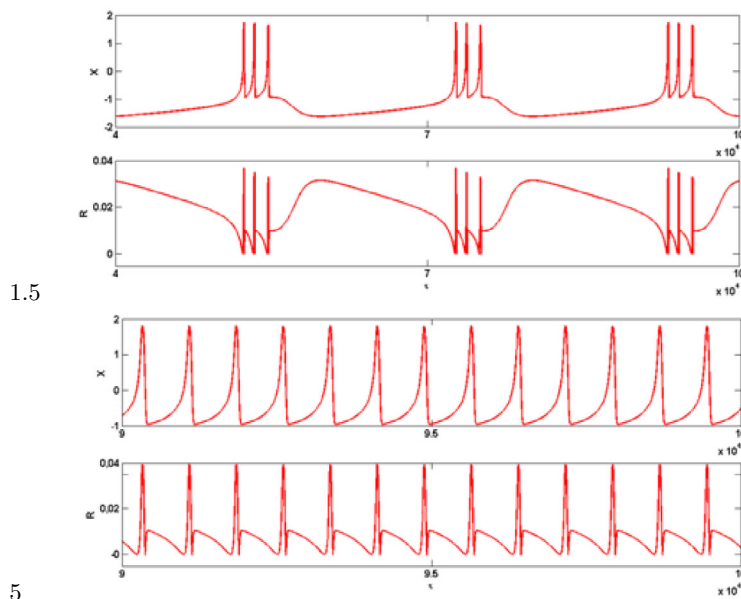


Fig. 6. Time histories for different values of the applied DC current showing transition from bursting to spikes in both electrical oscillator and electromechanical system $\alpha = 10^{-2}$, $r_r = 2.10 \times 10^{-3}$, $s_s = 4$, $X_0 = -8/5$.

3.1 Effects of the value of a direct current

The selected choice of the applied DC current I_I is taken outside of the parameter set [3.135, 3.150], [3.222, 3.319] giving a chaotic dynamics of the HR oscillator where chaos to chaos transition occurs, with a continuous interior crisis [19]. Indeed the chaos to chaos transition here is a sudden and continuous size change of the chaotic attractor observed at the transition between the spiking and bursting dynamics [19]. This parameters choice is performed according to the will of reproducing all the observed membrane potential behaviors in the mechanical resonator.

As the continuous injected current increases, the HR oscillator exhibits square-wave bursts which are progressively transformed into spikes. These electrical signals are transferred in the mechanical part (see Fig. 6). The number of bursts of the HR oscillator and that of the electromechanical device increase with an increase of displacement amplitude as the value of the DC current increases.

With the choice of external current taken inside of the parameter set [3.135, 3.150], [3.222, 3.319] giving a chaotic dynamics, the chaotic bursting sequence of the HR oscillator is also reproduced in the mechanical system (not plotted).

The main results here are that the HR oscillator transfers its dynamical behavior to the mechanical resonator, generating bursting oscillations. This indicates how our model of artificial or natural heart reacts when submitted to the action of bursting signals coming from the nervous systems.

3.2 Effects of the parameters of square wave current

In order to control the frequency of the oscillator and thus the one of the electromechanical system, the injected current is taken on a square wave signal form, as

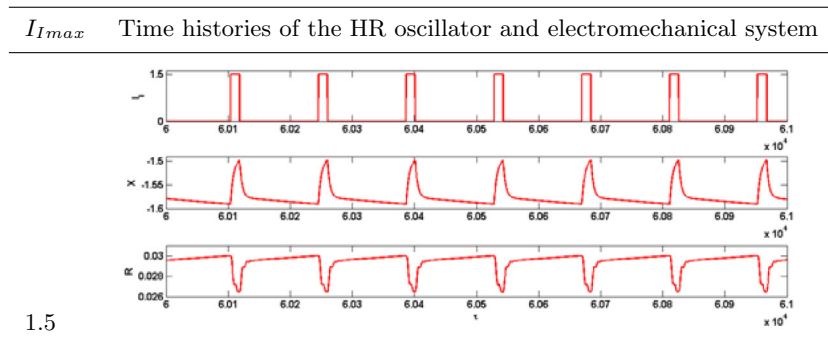


Fig. 7. Time histories for different amplitudes of the square wave excitation showing the remaining spiking form in both the HR oscillator and the electromechanical system: $f = 0.5/f_p$, HR oscillator parameters of Fig. 6.

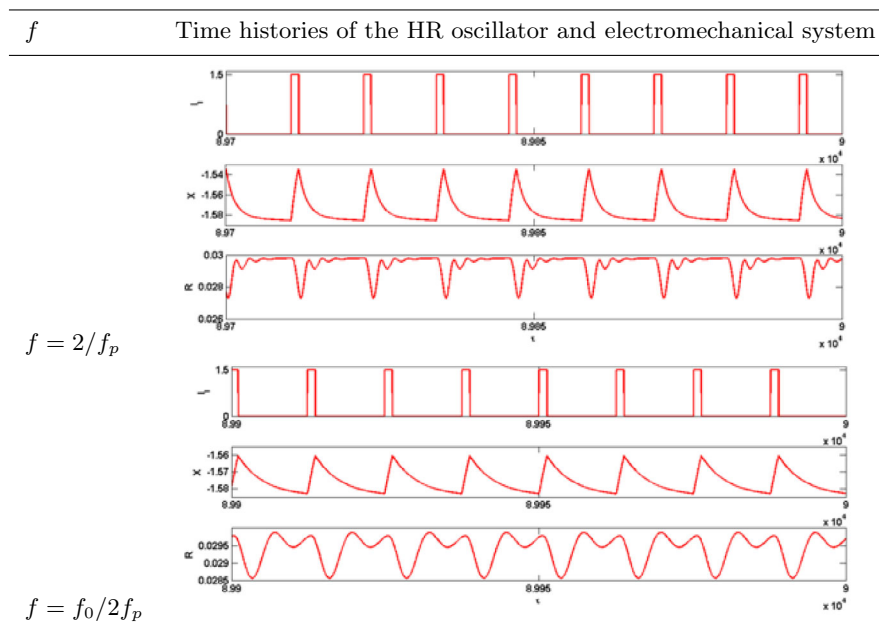


Fig. 8. Time histories for different amplitudes of the square wave excitation showing the remaining spiking form in both the HR oscillator and the electromechanical system: $I_{I_{max}} 1.5$, HR oscillator parameters of Fig. 6.

it can easily allow the analysis the effects of amplitude, periodicity and duty cycle. Hereafter the duty cycle of the square wave current is taken at 10%.

In Fig. 7, it appears that in the region where the bursting dynamics under continuous square wave excitation, the HR oscillator and the electromechanical device exhibit out of phase spikes. An interesting fact here is the downwards spikes of the mechanical displacement contrary to the upward behavior seen in Fig. 6. This dynamics is observed for I_I taken up to 10. Figure 8 shows the effects of the frequency on the dynamical behavior of the system. At low frequency, the square wave current excitation draws both the HR oscillator and electromechanical systems between two states. But due to the proper rhythm of each system, the transition is smoothed and

both exhibit relaxation like oscillations. As the frequency increases, the HR oscillator switches between two states that come closer while the electromechanical system shows its own dynamical transitions from driven relaxation spikes, period- n (n being an integer) up to period-1 sinusoidal oscillations. As the duty cycle increases for low frequency the driven relaxation oscillations become more observable with the appearance of asymmetric and symmetric shapes.

4 Conclusion

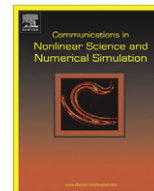
A ferromagnetic mass fixed on a spring subjected to an electromagnet powered first by a Van der Pol (VDP) oscillator and then by a Hindmarsh-Rose electrical oscillator has been studied. The mechanical system under the free VDP oscillator excitation mode shows a transition from harmonic, periodic, biperiodic up to bursting oscillations. When the VDP oscillator is submitted to an external continuous square wave excitation, there is a coexistence of a free dynamics and a modulated dynamics. As the external applied voltage modulates the dynamics of the mechanical part, the periodicities of the applied voltage, electrical part and mechanical part are equal with some distortions occurring in the electromechanical system. The pulsatile shape of the mechanical system under the VDP oscillator is like the dynamics of the myocardial muscle subjected to the natural pacemaker. In the case of the system powered by the HR oscillator, one finds the transitions from spikes, bursting oscillations, relaxation spikes, multiperiodic and sinusoidal oscillations when the values of the parameters of the current (DC or DC plus a square wave component) activating the HR oscillator are varied. The HR oscillator is found to efficiently imposes its bursting, spiking or driven relaxation oscillation shape to the mechanical system at low frequency.

This work has been supported by the Humboldt Foundation, Germany.

References

1. M. Tsatsos, *Theoretical and Numerical Study of the Van der Pol equation* (Aristotle University, Thessaloniki, 2006)
2. R. Mettin, U. Parlitz, W. Lauterborn, *Int. J. Bif. Chaos* **3**, 1529 (1993)
3. H. Simo, P. Wofo, *Int. J. Bif. Chaos* **22**, 1250003 (2012)
4. S.L. Mc Murrin, J.J. Tattersall, *Contemp. Math.* **208**, 265 (1997)
5. C.A. Kitio Kwiimy, B. Nana, P. Wofo, *J. Sound Vib.* **329**, 3137 (2010)
6. H. Simo, P. Wofo, *Mech. Res. Commun.* **38**, 537 (2011)
7. D.B. Forger, M.E. Jewett, R.E. Kronauer, *J. Biol. Rhythms* **14**, 533 (1999)
8. P.F. Rowat, A.I. Selverston, *J. Neurophys.* **70**, 1030 (1993)
9. B. Van Der Pol, *J. Van Der Mark, Philos. Mag.* **6**, 763 (1928)
10. S.R.F.S.M. Gois, M.A Savi, *Chaos, Soliton Fract.* **41**, 2553 (2009)
11. D.M. Sacknoff, G.W. Gleim, N. Stachenfeld, N.L. Coplan, *Am. Heart J.* **127**, 1275 (1994)
12. K. Umetani, D.H. Singer, R. McCraty, M. Atkinson, *J. Am. Coll. Cardiol.* **31**, 593 (1998)
13. M. Gawlikowski, T. Pustelny, R. Kustos, *Eur. Phys. J. Special Topics* **154**, 65 (2008)
14. T. Pustelny, P. Struk1, Z. Nawrat, M. Gawlikowski, *Eur. Phys. J. Special Topics* **154**, 175 (2008)
15. X. Han, Q. Bi, *Commun. Nonlinear Sci. Numer. Simul.* **16**, 4146 (2011)
16. E.A. Rose, A.C. Gelijns, A.J. Moskowitz, D.F. Heitjan, L.W. Stevenson, W. Dembitsky, J.W. Long, D.D. Aschein, A.R. Tierney, R.G. Levitan, J.T. Watson, P. Meier, *New. Engl. J. Med.* **345**, 1435 (2001)
17. M.C. Oz, M. Argenziano, K.A. Catanese, M.T. Gardocki, D.J. Goldstein, R.C. Ashton, A.C. Gelijns, E.A. Rose, H.R. Levin, *Circ.* **95**, 1844 (1997)

18. M.I. Rabinovich, H.D.I. Abarbanel, R. Huerta, R. Elson, A. Selverston, *IEEE Trans. Circ. Syst.* **44**, 997 (1997)
19. J.-M Gonzalez-Miranda, *Chaos* **13**, 845 (2003)
20. C.T. Leondes, *MEMS/NEMS: Handbook Techniques and Applications. Manufacturing Methods* (Springer, New York, 2006)
21. J.A. Pelesko, D.H. Bernstein, *Modeling MEMS and NEMS* (Chapman and Hall/CRC, 2003)
22. L.T. Abobda, P. Wofo, *Commun. Nonlinear Sci. Numer. Simulat.* **17**, 3082 (2012)
23. J.L. Hindmarsh, R.M. Rose, *Proc. R. Soc. Lond.* **221**, 87 (1984)



Subharmonic and bursting oscillations of a ferromagnetic mass fixed on a spring and subjected to an AC electromagnet

L.T. Abobda, P. Wofo*

Laboratory of Modelling and Simulation in Engineering, Biomimetics and Prototypes, Faculty of Science, University of Yaoundé I, P.O. Box 812, Yaoundé, Cameroon
 TWAS Research Unit, Faculty of Science, University of Yaoundé I, P.O. Box 812, Yaoundé, Cameroon

ARTICLE INFO

Article history:

Received 6 April 2011

Received in revised form 29 September 2011

Accepted 26 October 2011

Available online 11 November 2011

Keywords:

Electromechanical systems

Subharmonic oscillations

Bursting phenomena

ABSTRACT

This paper considers the dynamics of an electromechanical system consisting of a ferromagnetic mass fixed on a spring and subjected to an AC electromagnet. Subharmonic and bursting oscillations are found and their shape analyzed when one varies the viscous damping coefficient, the number of turns of the coil, the frequency and amplitude of the AC voltage. Pulse packages patterns and sharp burstings are observed in the motion of the mechanical part.

© 2011 Elsevier B.V. All rights reserved.

1. Introduction

Electromechanical systems transform electrical energy into mechanical form and vice versa; in these systems the dynamics is due to the interaction between an electrical part and a mechanical part. According to the coupling, various main classes are often considered: coil electromechanical devices, movable plate capacitive electromechanical systems, piezo-electromechanical devices, moving magnetic electromechanical systems and moving ferromagnetic mass electromechanical systems [1].

In the literature, these systems have been widely studied under sinusoidal excitation and self-sustained electrical circuits, with and without nonlinearities taking into account. And as general behaviors, resonances, anti-resonances, hysteresis, harmonic, sub and super-harmonic oscillations, multi-stability and transitions to chaos have been observed from theoretical and experimental investigations [2–8].

Recent studies on the dynamics of oscillators have shown that bursting oscillations, which consist of alternating small and large amplitude excursion, can appear in several systems according to the following mechanism: periodical jump between two stable nodes [9] or a periodical jump between one stable node and a limit cycle [10]. Bursting oscillations are found in various fields of sciences: neurosciences, biochemistry, chemistry and physics [9–11].

An interesting topic of research is the analysis of the behavior of electromechanical systems in which the electrical or the electronic component delivers bursting oscillations. This is interesting not only from the practical point of view for the automation of processes in industries, but also in the field of artificial organs for the cardiovascular system. Indeed, the cardiac electrical activities behave like bursts. These bursts are responsible for the mechanical response of the cardiac membrane [12].

* Corresponding author at: Laboratory of Modelling and Simulation in Engineering, Biomimetics and Prototypes, Faculty of Science, University of Yaoundé I, P.O. Box 812, Yaoundé, Cameroon.

E-mail address: pwofo1@yahoo.fr (P. Wofo).

This work deals with such a topic, by considering the dynamical behavior of a system consisting of a ferromagnetic mass fixed on a spring and subjected to the action of an electromagnet. Section 2 describes the electromechanical system. Section 3 discusses the dynamical behavior in the case where the electrical/electronic circuit has linear components. In Section 4, considering that the uncoupled electronic circuit is in a state where it delivers bursting oscillations, an analysis of the response of the mechanical part magnetically coupled to the electronic part is analyzed and discussed. Conclusion appears in Section 5.

2. Description of the electromechanical system and equations

The device shown on Fig. 1 is a ferromagnetic beam of mass m fixed to a spring and subjected to the action of an electromagnet under variable current. In the first step at the study, the electrical part is made of a circuit that has an inductor L (electromagnet inductance), a resistor (wiring resistance) and is powered by a voltage source $u(t) = U \sin(2\pi ft)$, U and f being respectively the amplitude and frequency, and t the time. The mechanical part consists of a ferromagnetic mass, fixed to a spring and subjected to damping. In the second step at the study we add to the electrical circuit a capacitor having non-linear charge–voltage characteristics. The coupling between both parts is realized by the magnetic circuit. When a current flows through the coil of the electromagnet, it induces a magnetic flux in the core of the electromagnet. Hence a lifting force attracts the ferromagnetic mass toward the electromagnet according to the signal at input (see Fig. 1).

In order to derive the dynamics of the mass under the magnetic lifting force, we use the Hopkinson’s law which is the magnetic analogue of Ohm’s law for magnetic circuits. In this law, the reluctance plays the role of the resistance in an electrical circuit although it does not dissipate magnetic energy, the magnetic flux plays the role of current intensity, and the magnetomotive force plays the role of the voltage.

Considering the mean magnetic circuit represented with dash-line in Fig. 1, assuming that magnetic circuit saturation is neglected, and ignoring leakage and fringing fluxes, Hopkinson’s law in gives

$$Ni = R(x)\phi \tag{1}$$

where N is the number of turns of the coil, i the current flowing in the coil, $R(x)$ the reluctance of the magnetic circuit, x the displacement of the mass, and ϕ the magnetic flux. The reluctance is given as

$$R(x) = \frac{2l_1 + 2l_2 + 2l_3}{\mu_0\mu_r a} + \frac{2e}{\mu_0 a} \tag{2}$$

where a is the cross section of the iron core, $\mu_0\mu_r$ is the magnetic permeability of the electromagnet iron core and e is the gap between the moving ferromagnetic mass and the free edge of the electromagnet. The mean circuit delineated by dash lines has the following dimensions:

$$l_1 = L_1 - 2l_3 \tag{3}$$

$$l_2 = L_2 - l_3 \tag{4}$$

$$e = l_4 - l_0 - 2l_3 - x \tag{5}$$

L_1 is the external length of the electromagnet, L_2 is the external width of the electromagnet, $2l_3$ is the ferromagnetic blade and electromagnet thickness, l_0 the unload spring length, l_4 the distance between the fixed part of the spring and the free edge of the electromagnet that can be in contact with the moving blade.

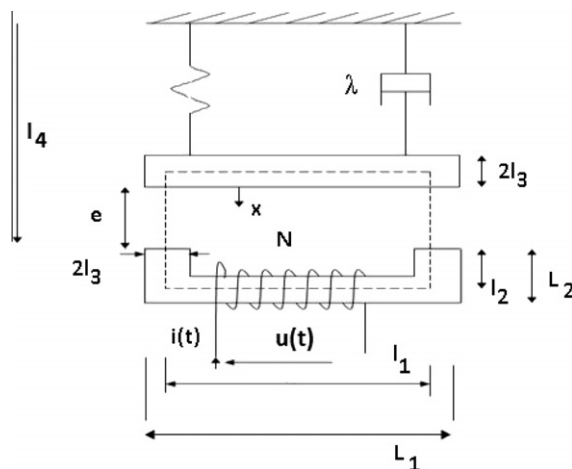


Fig. 1. The electromechanical system made of a ferromagnetic mass fixed on a spring and subjected to an AC electromagnet.

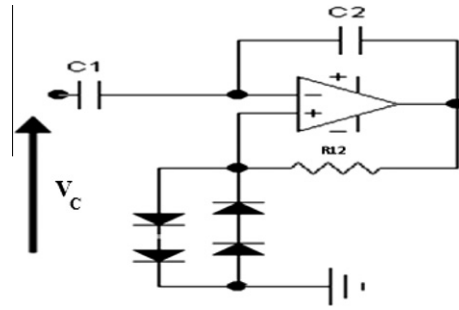


Fig. 2. Non-linear capacitor made of diodes, operational amplifier, resistor and linear capacitors.

The total flux flowing in the whole coil is

$$\Phi = N\phi = Li = \frac{a\mu_0\mu_r N^2 i}{2(l_1 + l_2 + l_3 + \mu_r e)} \tag{6}$$

Using Ohm’s law in the electrical circuit, one obtains

$$\frac{d\Phi}{dt} + \frac{\rho NP_m}{s} i = u(t) \tag{7}$$

where ρ is the wire resistivity, P_m the mean perimeter, s the wire cross section, $u(t)$ the applied voltage. Hence, the equation describing the electric phenomena in the electrical part is (assuming no capacitor in the circuit)

$$\frac{a\mu_0\mu_r N^2}{2(l_1 + l_2 + l_3 + \mu_r(l_4 - l_0 - 2l_3 - x))} \frac{di}{dt} + \frac{a\mu_0\mu_r^2 N^2 i}{2(l_1 + l_2 + l_3 + \mu_r(l_4 - l_0 - 2l_3 - x))^2} \frac{dx}{dt} + \frac{\rho NP_m}{s} i = u(t) \tag{8}$$

Taking the mechanical part, its dynamics is described by the following equation

$$m \frac{d^2x}{dt^2} + \lambda \frac{dx}{dt} + kx = \frac{\partial W_{mag}}{\partial x} \tag{9}$$

where λ the damping coefficient, k the spring stiffness and $W_{mag} = L(x)i^2/2$ is the magnetic energy of the coil. Replacing $L(x)$ by its expression derived from Eq. (6), one obtains

$$m \frac{d^2x}{dt^2} + \lambda \frac{dx}{dt} + kx = \frac{a\mu_0\mu_r^2 N^2 i^2}{4(l_1 + l_2 + l_3 + \mu_r(l_4 - l_0 - 2l_3 - x))^2} \tag{10}$$

Therefore the electromechanical system is described by the set of Eqs. (8) and (10).

Introducing the normalization and change of variables, equations of motion (8) and (10) are reduced to the following form

$$\dot{I} + \frac{p\dot{X}I}{(1 + p(1 - X))} + A_1 I(1 + p(1 - X)) = E_1 \cdot U_0(1 + p(1 - X)) \cdot \sin(2\pi f T_1 \tau) \tag{11a}$$

$$\ddot{X} + F_1 \dot{X} + \Omega_1^2 X = G_1 \frac{pI^2}{(1 + p(1 - X))^2} \tag{11b}$$

with

$$X = \frac{x}{l_p}; I = \frac{i}{i_p}; \tau = \frac{t}{T_1}; U_0 = \frac{U}{u_{p1}}; L_0 = \frac{a\mu_0\mu_r N^2}{2l_a}; i_p = \frac{2l_p T_1 u_{p1}}{a\mu_0}; p = \frac{\mu_r l_p}{l_a}; A_1 = \frac{\rho NP_m}{sL_0} T_1; E_1 = \frac{1}{N^2 p}; F_1 = \frac{\lambda T_1}{m}; \omega_0^2 = \frac{k}{m}; T_1 = \sqrt{\frac{m}{k}}; \Omega_1^2 = 1; G_1 = \frac{2L_0 m u_{p1}^2}{a^2 k^2 \mu_0^2}$$

The dot over a dynamical variable stands for the time derivative.

We also consider the system with a nonlinear capacitor in the electrical circuit. The capacitor is constructed from the electronic components as it appears in Fig. 2. The voltage across the whole block of Fig. 2 is

$$V_c = V_1 + V_2 \tag{12}$$

where $V_1 = q/C_1$ is the voltage across the capacitor C_1 and V_2 is the voltage across the diodes network. Using the Kirchooff’s law, one can find that the current I_{12} flowing in the resistor R_{12} is

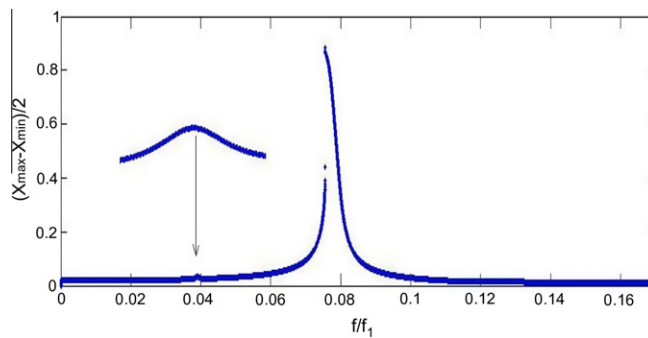


Fig. 3. Amplitude-response curve of the mechanical oscillator versus f/f_1 in the sinusoidal regime with enlargement shown around $f/f_1 \approx 0.04$: $N = 80$, $U_0 = 1.40$, $A_1 = 1.14 \times 10^{-1}$, $F_1 = 2.12 \times 10^{-2}$, $G_1 = 2.04 \times 10^{12}$.

$$I_{12} = \frac{-q}{R_{12}C_2} \tag{13}$$

This current is equal to the difference (node law) of the current I_+ flowing downward in the left branch of the diodes network and the one I_- flowing upwards in the other branch. These currents are given as

$$I_{\pm} = \frac{i_0}{2} \left(\exp\left(\frac{\pm V_2}{nV_0}\right) - 1 \right) \tag{14}$$

where V_0 and n are constants related to the type and number of diodes. From Eqs. (13) and (14), it comes that

$$V_2 = nV_0 \sinh^{-1}\left(\frac{-q}{R_{12}i_0C_2}\right) \tag{15}$$

Therefore, the charge–voltage characteristics is obtained as

$$V_c = \frac{q}{C_1} + nV_0 \sinh^{-1}\left(\frac{-q}{R_{12}i_0C_2}\right) \tag{16}$$

In the case of small voltage V_c or small charge in the capacitor, V_c can be expanded till the third order to give

$$V_c = a_1q + a_3q^3 \tag{17}$$

with

$$a_1 = V_0n \left(\frac{1}{nC_1V_0} - \frac{1}{C_2R_{12}i_0} \right) \quad \text{and} \quad a_2 = \frac{V_0n}{6C_2^3R_{12}^3i_0^3}$$

It is assumed in this work that $\frac{1}{C_1} - \frac{nV_0}{C_2R_{12}i_0} < 0$, consequently $a_1 < 0$ and $a_3 > 0$, to obtain a Duffing electrical nonlinearity with a double well potential system. With this capacitor in the circuit, the electromechanical system is now described by the following dimensionless equations

$$\begin{aligned} \ddot{Q} + \frac{p\dot{X}\dot{Q}}{(1+p(1-X))} + A_2\dot{Q}(1+p(1-X)) + B_2(1+p(1-X))Q + C_2(1+p(1-X))Q^3 \\ = E_2 \cdot U_0(1+p(1-X)) \cdot \sin(2\pi fT_2\tau') \end{aligned} \tag{18a}$$

$$\ddot{X} + F_2\dot{X} + \Omega_2^2X = G_2 \frac{p\dot{Q}^2}{(1+p(1-X))^2} \tag{18b}$$

with $Q = \frac{q}{Q_p}$; $U_0 = \frac{U}{u_{p2}}$; $\tau' = \frac{t}{T_2}$; $A_2 = \frac{\rho N F_m}{s l_0} T_2$; $B_2 = \frac{a_1}{l_0} T_2^2$; $C_2 = \frac{a_2}{l_0} Q_p^2 T_2^2$; $E_2 = \frac{u_{p2} T_2^2}{l_0 Q_p}$; $F_2 = \frac{\gamma T_2}{m}$; $\Omega_2^2 = \omega_0^2 T_2^2$; $G_2 = \frac{l_0 Q_p^2}{2m p^2}$

One should note that Eqs. (11) and (18) are not defined for $X = 1$. At this point the ferromagnetic mass is permanently bound to the electromagnet, and there is no motion for the mechanical part. The times references T_1 and T_2 , as well as the voltage references u_{p1} and u_{p2} , are chosen different. The dimensionless time is τ' in Eq. (18). In the manuscript, Eqs. (11) and (18) are solved numerically, using the fourth-order Runge–Kutta algorithm. In case of system with noise, an appropriate Euler algorithm is used [13].

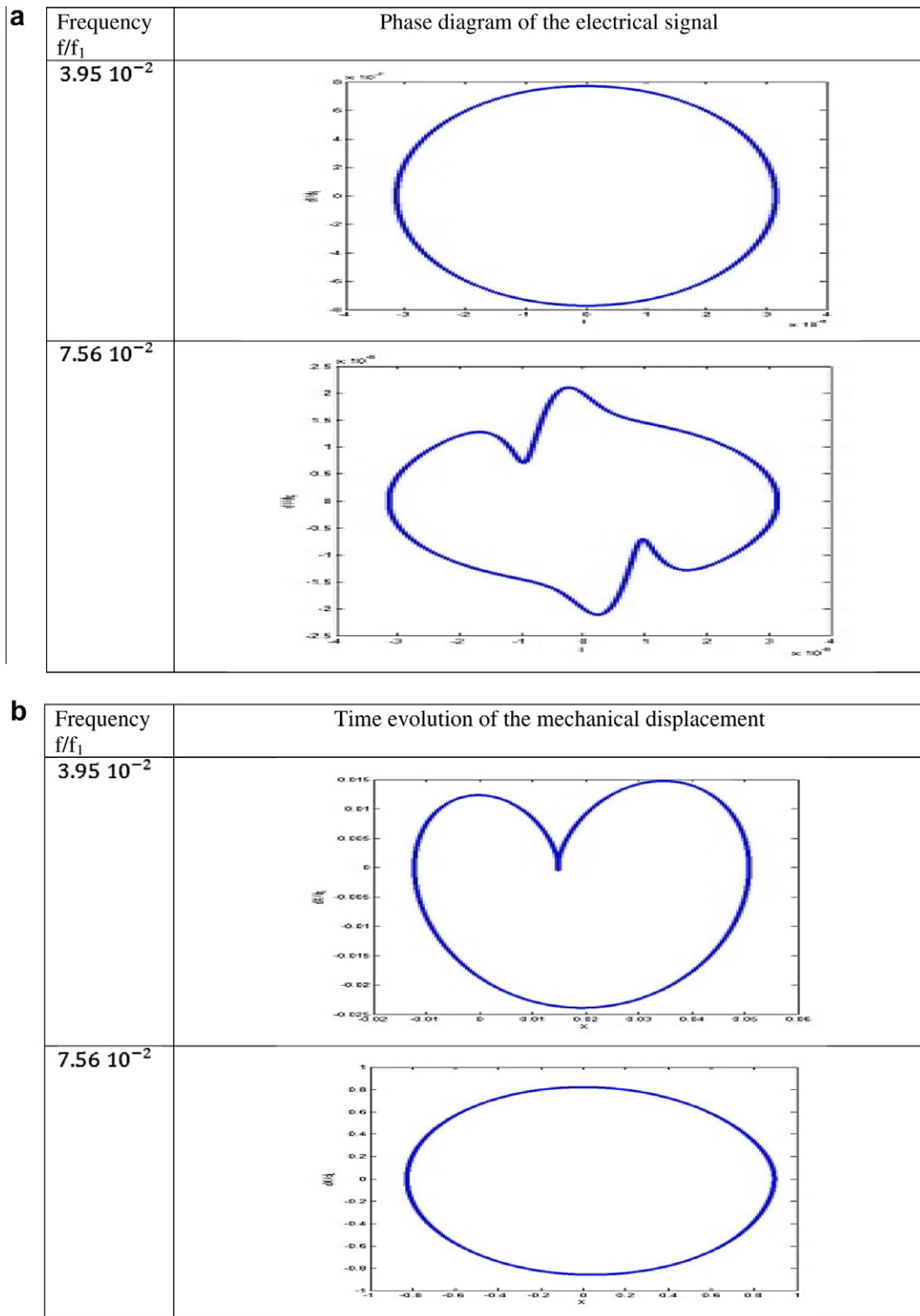


Fig. 4. Some time histories and phase diagrams of the electrical signal (a) and mechanical displacement (b), with parameters of Fig. 3 in the sinusoidal regime.

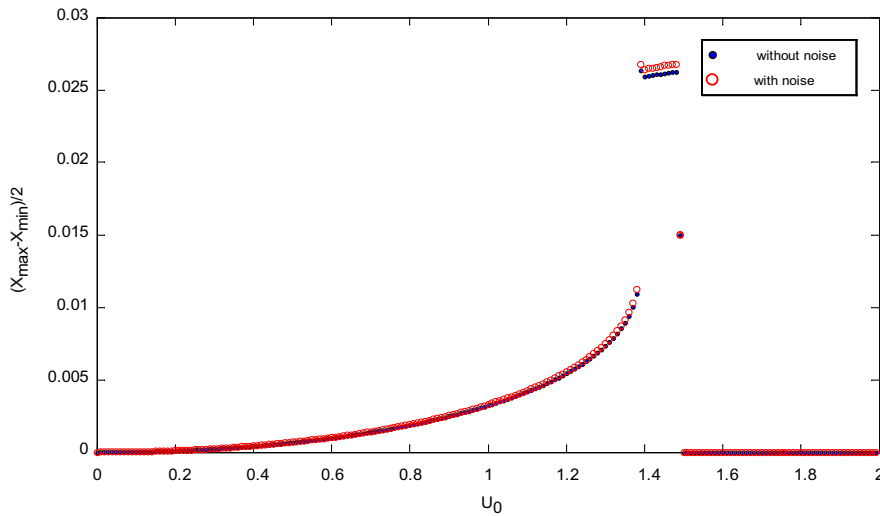


Fig. 5. Amplitude-response curve of the mechanical oscillator versus U_0 in the sinusoidal regime, without and with white noise of maximal amplitude of a tenth the applied voltage: $N = 80$, $f/f_1 = 7.56 \times 10^{-2}$, $A_1 = 1.14 \times 10^{-1}$, $F_1 = 2.12 \times 10^{-2}$, $G_1 = 2.04 \times 10^{12}$.

3. Dynamical behaviors in the case of linear RL circuit

This section deals with the analysis of the dynamical behavior of the device when the electrical circuit is constituted with the inductor and the resistor. In particular, the effects of the amplitude and frequency of the AC voltage are analyzed as they affect the amplitude of vibration and give rise to subharmonic oscillations. The results of the numerical simulation will be complemented with a mathematical analysis in the case of small displacement.

The values of the dimensionless parameters are given as $f_1 = \frac{1}{T_1} = 70.71$ Hz, $u_{p1} = 1.00$ V, $l_p = 3.00 \times 10^{-2}$ m, $i_p = 6.75 \times 10^6$ A, $p = 600$ m/A, the natural frequency of the mechanical part is given as $f_0 = 0.16f_1$.

3.1. Effects of the frequency

Fig. 3 shows the variation of the amplitude of vibration of the mechanical part as the frequency f varies. Two resonances are found at $f_{r1} = 7.56 \times 10^{-2}f_1$ and $f_{r2} = 3.95 \times 10^{-2}f_1$. These two states correspond to two subharmonic resonances of the type $f_0/2$ and $f_0/4$. One can also observe a sort of jump of amplitude around $f \simeq 0.075f_1$. Fig. 4 shows some representatives of phase portraits of the electrical and mechanical parts for two values of the frequency. At the subharmonic resonance $f_0/4$, there is a distortion on the sinusoidal movement of the mechanical part, with an inflection point and an asymmetry on the displacement. Around this frequency, the inflection point is shifted down for frequency values less than $f_0/4$, and shifted up for frequency values greater than $f_0/4$. At the subharmonic resonance $f_0/2$, an important distortion of the current is observed. This is due to the current induced by the high value of the mechanical displacement. Here, there is symmetry on the behavior of both current and displacement.

3.2. Effects of the voltage amplitude and white noise

For this analysis, the frequency is taken equal to that of the subharmonic frequency $f_0/2$. We have found that the current oscillations amplitude increases linearly as U_0 increases. In Fig. 5, the amplitude of vibration of the mechanical part also increases monotonously till $U_0 = 1.39$ where it exhibits a jump. The mechanical part oscillates with almost constant amplitude for $1.39 \leq U_0 \leq 1.48$. Above $U_0 = 1.48$, the mechanical part is bound to the electromagnet.

In the presence of additive white noise, the system is governed by the following equations:

$$\dot{I} + \frac{p\dot{X}I}{(1+p(1-X))} + A_1I(1+p(1-X)) = E_1 \cdot (1+p(1-X)) \cdot U_0(\sin(2\pi fT_1\tau) + \varepsilon(\tau)) \tag{19a}$$

$$\ddot{X} + F_1\dot{X} + \Omega_1^2X = G_1 \frac{pI^2}{(1+p(1-X))^2} \tag{19b}$$

with

$$\langle \varepsilon(\tau) \cdot \varepsilon(\tau') \rangle = d\delta(\tau - \tau') \quad \text{and} \quad \langle \varepsilon_1(\tau) \cdot \varepsilon_2(\tau') \rangle = 0$$

where d is taken here as been equal to 0.1. The numerical simulation of Eqs. (19), with a noise of maximal magnitude value equal to the tenth of the applied voltage, shows that despite the increase of the amplitude in the region of high amplitudes (after the jump), the behavior of the amplitude variation is qualitatively the same as in the case of system without noise (see Fig. 5).

To end this part devoted to the presentation of the results from the numerical simulation of Eqs. (11), we note that by increasing the number N of turns of the coil, a decrease of the oscillations amplitude of both current and displacement is found.

3.3. Analytical approach of the amplitude curves

Assuming small current and displacement, the set of Eqs. (11) can be reduced to

$$\dot{I} + A_1 I(1 + p) = E_1 \cdot U_0(1 + p) \cdot \sin(2\pi f T_1 \tau) \tag{20a}$$

$$\ddot{X} + F_1 \dot{X} + \Omega_1^2 X = G_1 \frac{pI^2}{(1 + p)^2} \tag{20b}$$

The solution of Eq. (20a) can be written as

$$I = I_1 \cos(w_{p1} \tau) + I_2 \sin(w_{p1} \tau) \tag{21}$$

with

$$I_1 = -\frac{w_{p1} U_0 (b_0 + 1)}{w_{p1}^2 N^2 + A_1^2 (b_0 + 1)^2} \quad \text{and} \quad I_2 = \frac{A_1 U_0 (b_0 + 1)^2}{N(w_{p1}^2 N^2 + A_1^2 (b_0 + 1)^2)}$$

Eq. (21) can also be written as

$$I = I_m \sin(w_{p1} \tau + \phi_I) \tag{22a}$$

with

$$I_m = \frac{U_0 (b_0 + 1)}{N \sqrt{w_{p1}^2 N^2 + A_1^2 (b_0 + 1)^2}}, \tag{22b}$$

$$\text{tg}(\phi_I) = -\frac{N w_{p1}}{A_1 (b_0 + 1)}, \tag{22c}$$

$$w_{p1} = 2\pi f T_1 \quad \text{and} \quad b_0 = 1/p.$$

Substitution of (22a)–(22c) in (20b) leads to:

$$X = X_0 + X_m \sin(2w_{p1} \tau + \pi + \phi_X) \tag{23a}$$

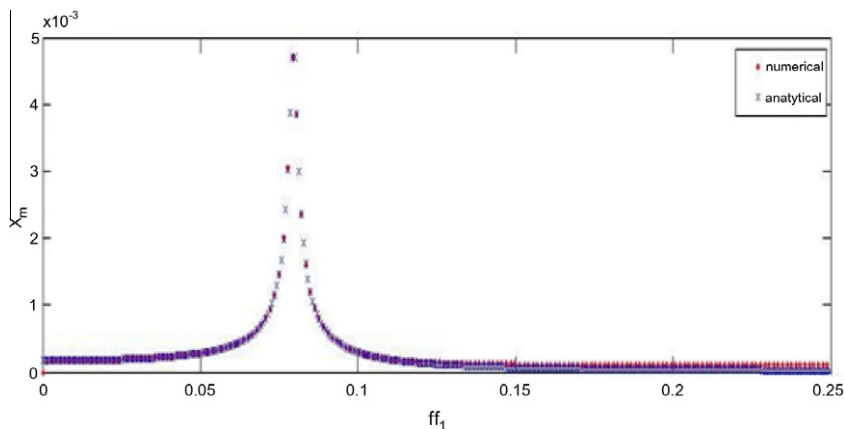


Fig. 6. Variation of the amplitude of vibration obtained from the analytical derivation and the numerical simulation for small displacement, in the sinusoidal regime with other parameters of Fig. 3 and $U_0 = 0.14$.

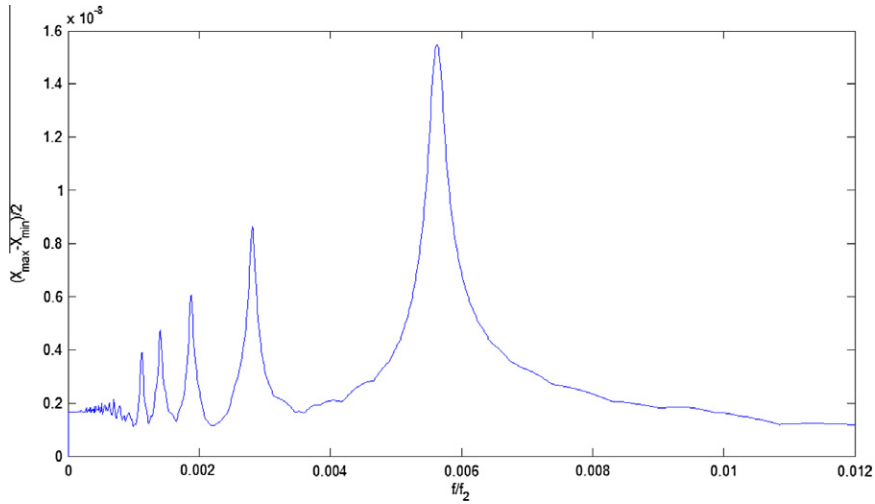


Fig. 7. Amplitude-response curve of the mechanical oscillator versus f/f_2 in the bursting regime: $N = 3 \times 10^2$, $U_0 = 8.00 \times 10^{-6}$, $A_2 = 2.16 \times 10^{-3}$, $B_2 = 4.78 \times 10^{-3}$, $C_2 = 2.84 \times 10^{-4}$, $E_2 = 8.84 \times 10^2$, $F_2 = 1.50 \times 10^{-3}$, $\Omega_2^2 = 5.00 \times 10^{-3}$, $G_2 = 1.88 \times 10^{-6}$.

with

$$X_0 = \frac{G_1 N^2 I_m^2}{2(b_0 + 1)^2 \sqrt{16w_{p1}^4 + 4F_1^2 w_{p1}^2 - 8w_{p1}^2 + 1}}, \tag{23b}$$

$$X_m = \frac{G_1 N^2 I_m^2}{2(b_0 + 1)^2 \sqrt{16w_{p1}^4 + 4F_1^2 w_{p1}^2 - 8w_{p1}^2 + 1}}, \tag{23c}$$

$$tg(\varphi_X) = \frac{I_2^2 - I_1^2 - 4w_{p1}^2(I_2^2 - I_1^2) + 4I_1 I_2 F_1 w_{p1}}{2(F_1 w_{p1}(I_2^2 - I_1^2) + I_1 I_2(4w_{p1}^2 - 1))} \tag{23d}$$

I_1 and I_2 are given by Eq. (21). Fig. 6 shows the variation of X_m in terms of the frequency. A good agreement is found between the analytical and the numerical results.

4. Bursting vibrations in the case of nonlinear electrical circuit component

As we noted in the introduction, bursting oscillations have been observed recently in double-well Duffing oscillator [9]. This phenomenon is considered here in order to find out how the burstings in the electrical circuit impact on the vibration of the mechanical part. An appropriate choice of the coefficients of Eqs. (18) is done as $T_2 = 10^{-3}$ s, $u_{p2} = 10^2$ V, $Q_p = 10^{-6}$ C. The control parameters are the frequency and amplitude of the AC voltage, the number of turns of the coil and the viscous damping. Again, the fourth order Runge–Kutta algorithm is used to solve Eqs. (18).

Fig. 7 shows the maximal amplitude-response curve of the mechanical part in the bursting regime in terms of the frequency. It appears the following subharmonic resonances $f_0/2, f_0/4, f_0/6, f_0/8$ and subharmonic antiresonances at $f_0/3, f_0/5, f_0/7, f_0/9$.

As concerns the effects of U_0 on the phenomenon, it has been found that the increase of U_0 leads to a sort of sinusoidal modulation, and the appearance of one more burst within the same time frame. This modulation is clearly visible on the mechanical part where instead of having a pattern of vibration with decreasing amplitude, the amplitude first increases, and then decreases.

The analysis of the effects of the number of turns in the coil shows the appearance of the decreasing behavior of the bursting amplitude in the electrical part. The pulse package behavior of the mechanical part is characterized by an increase of amplitude.

The effects of the last control parameter considered in this work are represented in Fig. 8. This Figure shows that the value of the viscous coefficient has an interesting impact on the shape of burstings. Indeed, the mechanical oscillations in the pattern decrease quickly as the viscous coefficient increases. This is obviously the consequence of the well-known exponential decrease of mechanical vibration due to viscous damping. Hence, sharp bursting oscillations of the mechanical part are made more visible when the viscous damping increases.

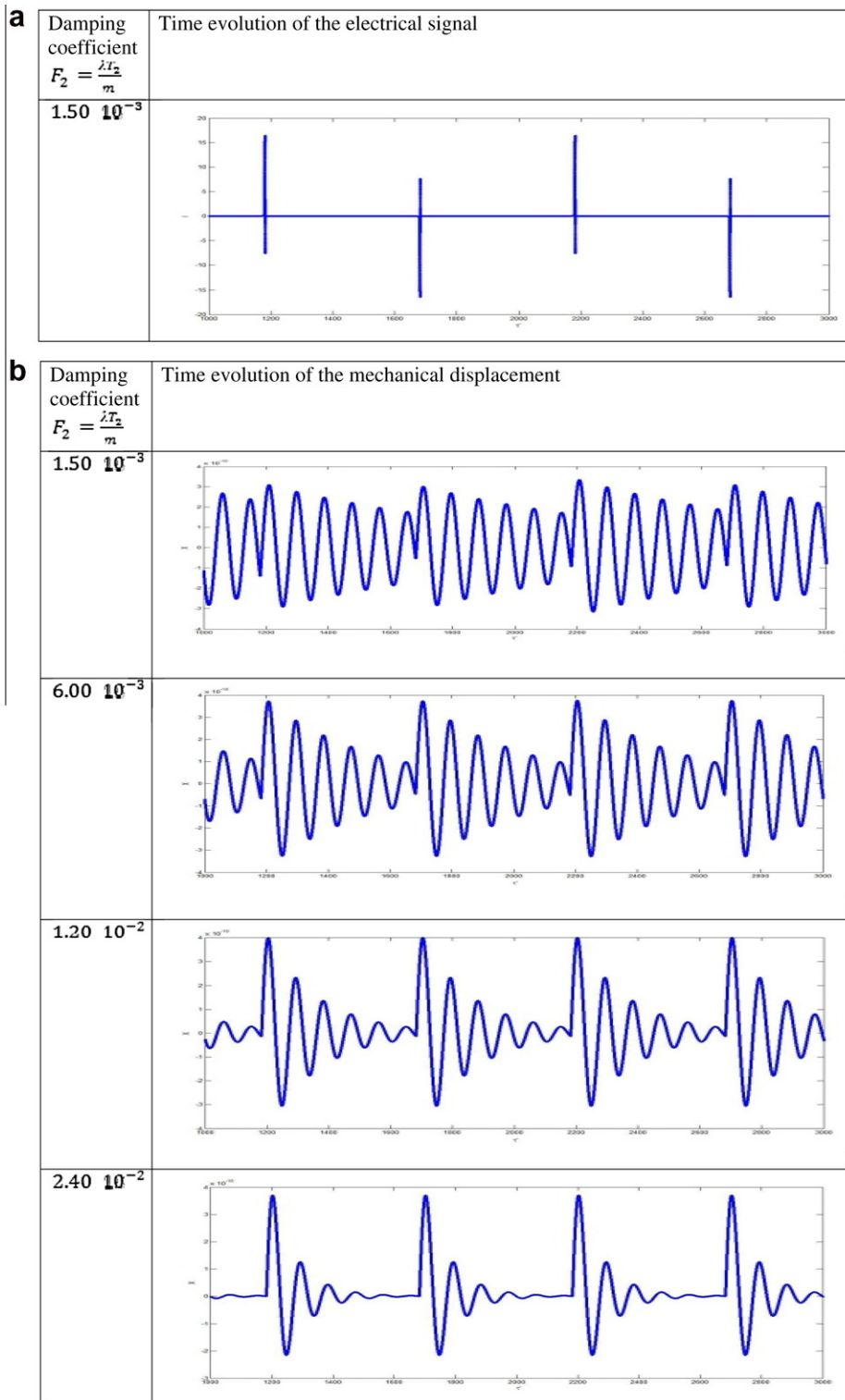


Fig. 8. Evolutions of the electrical signal (a) and mechanical displacement (b) as the damping increases in the bursting regime. $U_0 = 8.00 \times 10^{-6}$, $f_1 = 1.00 \times 10^{-3}$, $N = 80$, $A_2 = 8.10 \times 10^{-3}$, $B_2 = 6.72 \times 10^{-2}$, $C_2 = 3.99 \times 10^{-3}$, $E_2 = 12433.98$, $G_2 = 1.34 \times 10^{-7}$.

5. Conclusion

In this paper, we have considered the study of a ferromagnetic mass fixed on a spring and subjected to the action of an electromagnet in the case of electrical/electronic linear component without a capacitor, and in the case where the electronic circuit is nonlinear and delivers bursting oscillations. The effects of the frequency, external voltage amplitude, number of turns and damping have been discussed. Subharmonic and bursting oscillations have been observed in the periodic displacement of the mechanical part. The bursting behavior is modulated by the logarithm decrease of natural oscillations with the coexistence of resonances and anti-resonances and the appearance of sharp bursting when the coefficient of viscous damping increases.

It should be interesting in future works to look at hysteresis in the system in case of electrical/electronic linear component, since the effect of external voltage has shown a jump of mechanical vibration amplitude. In order to have bursting in the electrical part, the electrical system has been chosen to possess two stable equilibrium points where it can jump periodically. With the limitation of analytical study of bursting, and some bursting mechanism presented in [10], it would be interesting to study the case where the bursting behavior occurs in a system having one stable node and a strange attractor. Moreover, an experimental investigation of the phenomenon analyzed in this work could add new information for the applications in engineering and bio-engineering.

Acknowledgements

This work has been supported by The Academy of sciences for the Developing World (TWAS) under the research Grant No. 08-032LDC/PHYS/AF/AC.

References

- [1] Preumont A. *Mechatronics, dynamics of electromechanical and piezoelectric systems*. Netherlands: Springer; 2006.
- [2] Yamapi R, Woafu P. *Nonlinear electromechanical devices: dynamics and measurement, effect and control*. Nova Science Publishers; 2009.
- [3] Kitio Kwuimy CA, Woafu P. Experimental realization and simulations a self-sustained macro electromechanical system. *Mech Res Commun* 2010;37:106–10.
- [4] Kitio Kwuimy CA, Nana B, Woafu P. Experimental bifurcations and chaos in a modified self-sustained macro electromechanical system. *J Sound Vib* 2010;329:3137–48.
- [5] Kitio Kwuimy CA, Woafu P. Dynamics of a self-sustained electromechanical system with flexible arm and cubic coupling. *Commun Nonlinear Sci Numer Simul* 2007;12:1504–17.
- [6] Awrejcewicz J, Dzyubak L, Lamarque C-H. Modelling of hysteresis using Masing–Bouc–Wen’s framework and search of conditions for the chaotic responses. *Commun Nonlinear Sci Numer Simul* 2008;13:935–58.
- [7] Awrejcewicz J, Supel B, Lamarque C-H, Kudra G, Wasilewski G, Olejnik P. Numerical and experimental study of regular and chaotic motion of triple physical pendulum. *Int J Bifurcat Chaos* 2008;18:2883–915.
- [8] Awrejcewicz J, Kudra G, Wasilewski G. Chaotic zones in triple pendulum dynamics observed experimentally and numerically. *Appl Mech Mater* 2008;9:1–17.
- [9] Han X, Bi Q. Bursting oscillations in duffing’s equation with slowly changing external forcing. *Commun Nonlinear Sci Numer Simul* 2011;16:4146–52.
- [10] Izhikevich EM. *Dynamical systems in neuroscience: the geometry of excitability and bursting*. Cambridge: MIT Press; 2007.
- [11] Izhikevich EM. Neural excitability, spiking and bursting. *Int J Bifurcat Chaos* 2000;10:1171–266.
- [12] Nikerson DP, Smith NP, Hunter PJ. A model of cardiac cellular electromechanics. *Phil Trans R Soc Lon A* 2001;359:1159–72.
- [13] San Miguel M, Toral R. Stochastic effects in physical systems, Instituto Mediterraneo de Estudio Avanzados IMEDEA; 1984.